STUDIES IN THE FLOW OF GRANULAR MATERIALS

Thesis by

Tanh Van Nguyen

In Partial Fulfillment of the Requirements

for the Degree of

Doctor of Philosophy

California Institute of Technology

Pasadena, California 91125

1980

(Submitted September 4, 1979)

ACKNOWLEDGMENTS

The author wishes to express his deepest appreciation to Professor Christopher Brennen for his patient guidance and support throughout this investigation. The advice and suggestions which he made have greatly contributed to the results presented in this thesis.

He wishes to express his most sincere thanks to Professor R. H. Sabersky for his encouragement and support. At times when things were not progressing well, his understanding was most gratefully appreciated. He would like to thank Professor S. B. Savage for the opportunities to discuss with him on the topics of the research. Thanks are due to Mr. Fred Mac Donald and Mr. Elmer Szombathy for their assistance in the construction of the experimental apparatus. A note of appreciation goes to Charles Campbell for his assistance with the experiments. The author would like to thank Susan Berkley for her meticulous typing and organization of the manuscript.

The research presented in this thesis was sponsored by the National Science Foundation and the Union Carbide Company. The generosity of their contribution is gratefully acknowledged.

Finally, the author dedicates this thesis to his parents who have devoted their lives to their children's education.

ABSTRACT

A number of problems related to the flow of cohesionless granular materials in hoppers are investigated.

An approximate solution to the flow of granular materials in a conical hopper is presented. The material is modeled as a rigid-perfectly plastic continuum which satisfies the Mohr-Coulomb yield condition. Unknown geometries of the upper and lower free surfaces are determined from the stress-free conditions. The results are compared to those based on different constitutive postulates as well as to experimental observations. The computed mass flow rate and wall stress compare well with the experimental measurements made with small and full size hoppers.

The flow field in a hopper with a vertical bin is observed to gain a better understanding of the details of the flow field. The observations seem to correspond to the recent results obtained by other investigators using X-ray radiography.

The funnel flow regime in hoppers is studied in detail. The different types of flow which exist are identified and classified. The possibility of having a transition from one type of flow into another one is recorded as a function of the material properties and hopper geometry. Finally, the boundary between the moving and stagnant material is studied as a function of the hopper geometry. Other parameters such as the effect of the hopper thickness and wall roughness on the flow field are also studied.

TABLE OF CONTENTS

TABLE OF CONTENTS (CONTINUED)

TABLE OF CONTENTS (CONTINUED)

NOMENCLATURE

A	=	Integration constant
b	=	Hopper thickness
C	=	Integration constant
D	=	Exit opening
D'	=	Reduced exit diameter
E	=	Young's modulus
F	=	Modified Froude number
ff	=	Critical flow factor
ff_a	=	Actual flow factor
f_c	=	Unconsolidated strength of the material
G	=	Shear modulus = $E/2(1+\nu_1)$
g	=	Gravitational acceleration
H	=	Height of material in vertical bin
K	=	Ratio of stress in vertical direction to stress in horizontal direction
k	=	$(1+\sin\varphi)/(1-\sin\varphi)$
k_1	=	Width of empty annulus around exit diameter
q	=	Integration constant
Q	=	Mass flow rate
Q_B	=	Force in vertical direction in vertical bin
Q_H	=	Force in vertical direction in hopper
r_1, r_2	=	The lower and upper radius of hopper
r	=	Radial position in spherical and polar coordinate systems

NOMENCLATURE (CONTINUED)

S	=	Distance from edge of exit opening to merge point
u_x, u_y, u, v	=	Velocity components
U	=	Integration constant
W	=	Width of vertical bin
X, Y	=	Dimensionless coordinates of funnel boundary
x	=	Depth of material in vertical bin measured from free surface
y_0	=	Critical height of material in vertical bin at transition
α	=	Hopper wall angle
β	=	Angle of approach of funnel
γ_w	=	Value of stress angle along hopper wall
δ	=	Wall friction angle
Γ	=	Lower free surface near hopper exit
ϵ	=	Distance between free surface and circumferential surface
ϵ_1	=	$(\tan \delta)^{1/2}$
$\mathring{\epsilon}_x, \mathring{\epsilon}_y, \mathring{\epsilon}_{xy}$	=	Components of strain rate tensor
λ	=	$2(1+m)K \tan \delta$
$\varkappa$	=	Constant value of σ_0
ν	=	Angle of dilatation of the material
ν_1	=	Poisson ratio
μ_w	=	Coefficient of friction along hopper wall
φ	=	Internal friction angle
Φ	=	Stress function
ρ	=	Bulk density

NOMENCLATURE (CONTINUED)

θ	=	Angular position of spherical and polar coordinate systems
θ_w	=	Hopper wall angle
ω	=	Dimensionless parameter
Ω	=	Rotation of material
ψ	=	Angle between major principal stress direction
σ	=	Mean stress = $(\sigma_r+\sigma_\theta)/2$
$\sigma_r, \sigma_\theta, \sigma_\alpha, \sigma_{r\theta}$	=	Components of stress tensor

LIST OF FIGURES

LIST OF FIGURES (CONTINUED)

LIST OF FIGURES (CONTINUED)

LIST OF FIGURES (CONTINUED)

LIST OF FIGURES (CONTINUED)

CHAPTER 1

INTRODUCTION

1.1 BACKGROUND

The granular material being investigated in this study has a solid phase which is composed of discrete particles in direct contact with each other and an interstitial fluid in the pore volume between the particles. The internal forces come from Coulomb friction between the particles and the deformation of the material results from the relative displacement of the particles. The interstitial fluid is frequently air and its effect on the material behavior can be neglected under some circumstances to be described later.

Granular materials occur in a great number of processes in industry. The mining industry handles millions of tons of raw material in granular form each day (Pariseau [67]). In the chemical and pharmaceutical industries, most of the products in the final or intermediate processes are in granular form. This is also true for the agricultural and food industries which have to store and transport their crops in bulk form. The requirement to build larger and more energy efficient handling equipment necessitates a better understanding of the behavior of the material.

Considering the importance of granular materials in industry, it might be expected that there would be a well developed level of knowledge of the mechanics of such flows. This is not however the case. Until recently, the work done in the field was more or less based on

trial and error. As pointed out by Wieghardt [110], "The dynamics of granular materials has failed to attract general interest to the same degree as fluid dynamics, although first papers were written by well-known hydrodynamicists such as Hagen (1852) and Reynolds (1885)". Similar thoughts were shared by Brown and Richards in their book on powder mechanics [11]. The difference in the state of knowledge is particularly evident when one considers the amount of attention which has been given to similar fields such as soil mechanics and fluidized beds.

The early work in granular materials concerned the flow in bins and hoppers. Quasistatic flows in which inertia is neglected were investigated, the constitutive relations of the material being rate independent. In these studies, the main objectives were to predict the stress pattern on the bin walls to prevent structural failures (Theimer [101]) and to predict the discharge of material from the hopper. In 1895, Janssen developed an expression for the stress in the material in a vertical bin and showed that it is independent of the height of the material in the bin if it is sufficiently large. This result is still in use today to obtain a lower bound on the wall stress in bins (Cowin [14]). The early investigations of the discharge of granular materials from bins and hoppers relied on the empirical correlation of experimental data to obtain an expression of the flow rate. The resulting correlations vary widely since they depend on the individual experimental conditions and the assumptions made by the investigators (Deming and Mehring [20], Rose and Tanaka [79], Beverloo et al [2], McDougall and Knowles [58], Fowler and Glastonbury [29]). These experimental observations

showed that the mass flow rate was independent of the head of the material in the hopper if this head was large enough. The important questions in the design and operation of hoppers were not answered until the investigations conducted by Jenike at the University of Utah in the early 1960's [40], [42]. Jenike applied the principles of plasticity to study the mechanics of bulk solids as they flow in hoppers and other devices. He classified hoppers into the mass flow type where the whole mass of material in the hopper is moving and the funnel flow type where stagnant material appears in the flow field. Conditions on the hopper geometry are given so that funnel flow and arching of the material over the exit diameter can be avoided.

Since the pioneering work of Jenike, a number of analytical and experimental studies have been conducted with the objective of understanding the mechanics of the granular material as it is deforming continuously. Concepts of plasticity and continuum mechanics have been used to describe the deformation of the material (Shield [91], Jenike and Shield [39], Takagi [98], Spencer [93], Mehrabadi and Cowin [61], De Josselin De Jong [19]). Analytical solutions of the complete equations of the flow were presented by Savage [82], [86], Williams [111], Brennen and Pearce [9] and recent experimental observations by Cuttress and Pulfer [17], Blair-Fish and Bransby [3] and Lee et al [55] revealed a new picture of the kinematics of deformation of materials in hoppers.

Other investigators have been concerned with the flow in chutes and channels where the velocities are generally much higher. Much less is known about

the mechanics of deformation in this flow regime. Some experiments have been conducted to study a specific type of flow (Wolf et al [112], Choda et al [12], Augenstein et al [1]) and others have been conducted to study the mechanics of the material (Roberts [75], Savage [84], [85], Takahashi [99]. The analytical models used to describe the material in this flow regime introduce the void fraction of the material as an extra unknown and the constitutive relations depend on the rate of deformation of the material. Goodman and Cowin [32] presented such a continuum model and applied it to some simple flow conditions. The model has been used by Passman et al [68], [69] and Jenkins [49] and similar models have been recently proposed by Savage [85] and Jenkins and Cowin [50]. It is however fair to say that there is no universally accepted form for the constitutive laws at the present time.

1.2. CONSTITUTIVE POSTULATES

Under quasi-static flow conditions, the granular material is usually modeled as a rigid-perfectly plastic continuum which satisfies the Coulomb yield condition. The material will deform by shear when the shear stress on a given plane is equal to the product of the normal stress and a coefficient of friction which is a material property. Drucker and Prager [25] and Shield [89] considered the Coulomb yield function to be the plastic potential and used the associative flow rule to obtain the necessary relations between the stress and the displacement fields. The resulting constitutive relations, however, give a displacement field which requires the material volume to increase during deformation. This is contradictory to the known experimental observations that underconsolidated soil contracts during deformation (Scott [88]).

Thus, the associative flow rule does not seem to describe the yielding behavior of the material very well. Drucker et al [26] considered the material to be of the work hardening type and introduced the dependence of the yield function on the hydrostatic stress. Jenike and Shield [39] further developed this yield condition; the size of the yield surface was varied depending on the hydrostatic stress. Thus material properties such as the internal friction angle, the bulk density and the cohesion are direct functions of the hydrostatic stress. This Jenike-Shield model is used in the present investigation to describe the yielding of the materials which are undergoing continuous and large deformation.

Since the associative flow rule does not describe the deformation of granular materials very well, a second constitutive postulate is used to relate the velocity to the stress field. This has been done indirectly by considering the characteristic directions or the principal directions of stress and strain rate or by defining a mode of deformation of the material along its characteristics. In analogy to the constitutive relations of isotropic solids and fluids (Fung [30]), a number of investigators have proposed that the principal directions of stress and strain rate coincide (Jenike [40], Shield [91], Pariseau [66]). Despite its simplicity, such a condition may not, however, be valid for granular materials undergoing plane deformation as has been shown experimentally by Drescher and De Josselin De Jong [22] and Drescher [23]. Mandl and Luque [60] reviewed the various flow rules of granular materials and proposed a theory based on the non-coaxiality of the principal directions. De Josselin De Jong [19] and other investigators claimed that the deviation angle between the principal directions can be any value between $-\varphi/2$ and $\varphi/2$ where φ is the internal friction angle of

the material.

A second group of investigators fix the direction of the stress and strain rate characteristics; under these conditions the solution gives the orientation of the principal directions of stress and strain rate (Takagi [98]). For a material with an angle of dilatation ν and an internal friction angle φ, the characteristics of stress and strain rate are oriented at angles $\pm(\pi/4 - \varphi/2)$ and $\pm(\pi/4 - \nu/2)$ from their respective principal directions.

Another group of investigators proposed that the material deforms by sliding along the stress characteristics. It is also allowed to rotate during the deformation (De Josselin De Jong [19], Spencer [93]). This model does not require that the principal directions of stress and strain rate are coincident while their characteristic directions have to coincide. Similar models for compressible materials are proposed by Spencer and Kingston [94] and Mehrabadi and Cowin [61]. In the present investigation, both the St. Venant principle (coincidence of the principal directions of stress and strain rate) and the Spencer model are used as constitutive postulates.

The final constitutive relation concerns the compressibility of the bulk material during large and continuous deformation. This is related indirectly to the flow rules discussed above. It is known that, at large deformation, the material will reach a critical state where further deformation will not change its void fraction (Schofield and Wroth [87], Roscoe [78]). The density of the material is therefore constant at critical state and this concept has been used to describe the behavior of granular materials which undergo large and continuous deformation. Jenike et al [41] and Jenike and Shield [39] have verified

from their experimental data that this assumption is valid and it is a common practice to use the critical void ratio to describe the behavior of the granular materials. The angle of dilatation of the material is then equal to 0 and the characteristic of strain rates form an angle $\pi/2$ while the characteristics of stress are at an angle $\pi/2+\phi$ from each other. Recently, Cuttress and Pulfer [17], Blair-Fish and Bransby [3] and Lee et al [55] observed from radiographs of the flow field that the void ratio is not uniformly distributed but varies depending on the state of deformation of the material in the hopper. In the present investigation, we use the concept that the material is flowing at a constant void ratio equal to its critical value; the density is then uniform in the flow field of the hopper.

1.3. TOPICS OF THE INVESTIGATION

A number of problems related to the flow of granular materials in hoppers are considered. Chapter 2 presents an approximate solution to the flow of granular materials in conical hoppers. The solution presents a good test of the constitutive relations since the material in the flow field undergoes continuous deformation and plug flow does not occur. The analytical results are also of practical interest since bins and hoppers are the most common devices used to store and handle granular materials. The results will be compared to experimental measurements made by other investigators in full size experiments. The approximate solution is based on an expansion scheme with modified boundary conditions being introduced for the free surfaces of the hopper.

Chapter 3 presents an experimental investigation of the flow field in a two-dimensional hopper. The objective of the investigation is to

gain a better understanding of the details of the flow field. The experimental observations address the question of symmetry and steadiness of the flow field and the kinematics of the material deformation. A qualitative indication of the wall stress at the transition corner between the hopper and the vertical walls of a bin is recorded; this stress is observed to fluctuate with time in some materials while it is steady with other materials.

Finally Chapter 4 addresses the question of funnel flow in hoppers. A systematic observation of the flow field is conducted at various hopper geometries. The different flow regimes which are present are identified and the transition from one flow regime to the other is also studied. The boundary between the moving and stagnant material is observed and its variation with the hopper geometry is documented.

CHAPTER 2

GRAVITY FLOW OF GRANULAR MATERIALS IN CONICAL HOPPERS

2.1 INTRODUCTION

The problem being studied concerns the gravity flow of granular materials in conical hoppers. Since hoppers and bins are widely used in the storage and handling of granular materials, a reliable prediction of the mass flow rate and wall stress pattern would be of great practical interest. From an analytical point of view, the problem provides a good test of the constitutive postulates of the material. With a converging flow field, the material is forced to deform as it flows and the tendency of the material to move as a plug is avoided. The solution will reflect the observed phenomena in hopper flow such as the fact that the flow rate is independent of the head of the material in the hopper and the fact that the stress field is in a passive state. However, the validity of the solution is restricted to a range of hopper angles for which mass flow is present in the hopper.

A listing of the constitutive postulates is presented first; it will be followed by a review of the studies which have been done in the past. The present solution will be presented in the last section of the chapter.

2.2 CONSTITUTIVE POSTULATES

Since the material is modeled as a rigid-plastic continuum which satisfies the Coulomb yield condition, the stress state at all points in the flow field will satisfy the condition

$$\sigma_{sn} \leq \sigma_{nn} \tan\varphi'$$

where σ_{sn} is the shear stress on a given plane

σ_{nn} is the normal stress at the point

φ' is the friction angle of the material.

The angle φ' is equal to the material internal friction angle φ when it is deforming within itself while it is equal to the wall friction angle δ when the material is sliding along a solid boundary.

In a cartesian coordinate system, the Coulomb yield condition is written as

$$\left(\frac{\sigma_x - \sigma_y}{2}\right)^2 + \sigma_{xy}^2 \leq \left(\frac{\sigma_x + \sigma_y}{2}\right)^2 \sin^2\varphi \qquad (2.1)$$

The equality sign represents the condition when the material starts to yield.

The second constitutive postulate which will be used to relate the stress and velocity fields can be either the St. Venant principle (coincidence of the principal directions) or the double sliding model proposed by Spencer [93] and De Josselin De Jong [19]. The St. Venant principle is written in a cartesian coordinate system as

$$\frac{\sigma_x - \sigma_y}{\sigma_{xy}} = \frac{\dot{\epsilon}_x - \dot{\epsilon}_y}{\dot{\epsilon}_{xy}} \qquad (2.2)$$

where σ_{ij} are the components of the stress tensor

$\dot{\epsilon}_{ij}$ are the components of the strain rate tensor.

The validity of this condition has been questioned by a number of investigators as discussed in Chapter 1. The various models proposed by previous authors differ on the issue of whether the principal directions coincide or whether the stress and velocity characteristics coincide. The model proposed by Spencer [93], which is motivated by the work of De Josselin De Jong, introduced the concept that the material deforms by sliding along the stress characteristics. This is called the double sliding, free rotating model (De Josselin De Jong [19]). A consequence of this model is that the characteristics coincide; it does not however require that St. Venant principle is satisfied. The following relation is obtained between the stresses and strain rate components

$$\sin 2\psi\,(\dot{\epsilon}^{\circ}_{x} - \dot{\epsilon}^{\circ}_{y}) - 2\cos 2\psi\,\dot{\epsilon}^{\circ}_{xy} + \sin\varphi\left(\frac{\partial u_y}{\partial x} - \frac{\partial u_x}{\partial y} - 2\Omega\right) = 0 \qquad (2.3)$$

where ψ is the stress angle in the Sokolovskii's expressions for the stresses (Eq. (2.13)). The definition of the rotation Ω is not well defined. Spencer [93] claimed that $\Omega = D\psi/Dt$ but other investigators (Mandel [59], Drescher and De Josselin De Jong [22]) did not agree with him. This model of deformation of granular materials have been used by a number of investigators to study some flow problems in hoppers and chutes (Pemberton [70], Morrison and Richmond [62], Morrison [63]). It is also used in the present solution in order to compare the results with those utilizing the relation (2.2).

Finally, the continuum model includes the condition that the material deforms at constant density. While this condition is not valid for incipient deformation, it describes the material behavior when it is undergoing large and continuous deformation. In hopper flow, the

condition in the lower part of the hopper near the exit is critical to the solution of the flow field. It has been observed that in this area near the exit, the approximation of constant density is fairly reasonable. The continuity equation is then written as

$$\frac{\partial u_x}{\partial x} + \frac{\partial u_y}{\partial y} = 0 \qquad (2.4)$$

These constitutive postulates are solved with the equations of motion to determine the velocity (u_x, u_y) and the three stress components $(\sigma_x, \sigma_y, \sigma_{xy})$.

A review of the past work done on the subject is presented in the next section and the solution obtained in the present study will be discussed.

2.3 REVIEW OF PAST WORK

A large number of investigations have examined the flow of granular materials in hoppers. In the early days, attention was directed toward developing an empirical expression of the mass flow rate from experimental data. A number of experimental studies of the flow rate were available (Deming and Mehring [20], Rose and Tanaka [79]) and some empirical relations of the mass flow rate were obtained (Beverloo [2], Fowler and Glastonburry [29]).

In a book on the mechanics of powders, Brown and Richards [11] discussed the various effects of hopper geometry and material properties on the mass flow rate. The discharge of granular materials from the hopper is found to be independent of the head of the material in the hopper if this head is sufficiently large. It is also independent of the width of the vertical bin. Some effects of the shape of the particles

can be observed especially when the roughness of the hopper walls is increased.

From dimensional analysis, the mass flow rate Q is found to depend on the gravitational acceleration g, the bulk density ρ and the exit diameter D in the following manner:

$$Q \propto \rho \sqrt{g} D^{5/2} \tag{2.5}$$

This gives a dimensionless parameter similar to the Froude number $4Q/\pi\rho\sqrt{g}D^{5/2}$ which is a constant when the material is flowing in a hopper with a given half wall angle θ_w. Brown and Richards [11] extrapolated their experimental data and found a limiting value of D for which the mass flow Q is equal to zero. This is obviously due to the discrete size of the particles. To take this effect into account, they introduced the idea of a statically empty annulus around the exit opening. The area through which the material would flow corresponds to an effective exit diameter D' given by

$$D' = D - k_1 \tag{2.6}$$

where k_1 can vary from 1 to 4 particle diameters.

This idea of an effective diameter has been used to reduce experimental data (Williams [111]) even though Bosley et al [4] noted that such an empty space was observed only in a flat bottom hopper and none was found in a mass flow hopper.

The empirical correlations of the mass flow rates vary widely since they depend on the individual experimental conditions. These drawbacks have motivated efforts to derive an expression of the flow

rate from an analytical solution of the flow problem. Such analytical solutions are quite involved since the equations of motion must be solved in conjunction with the constitutive postulates. This will result in a complicated system of non linear partial differential equations which are to be solved with the boundary conditions of the flow field.

A number of investigators have chosen an indirect approach to obtain the mass flow rate from the hopper. Brown [10] studied the problem using an energy approach. He assumed that the material would flow when the total kinetic and potential energies are at a minimum. From this, he derived an expression for the mass flow rate. Johanson [53] considered the balance of the forces at the exit diameter to obtain an expression of the acceleration in that part of the flow. The exit velocity (and hence the flow rate) is obtained by assuming that this acceleration is due to the convergence of the flowing channel. An expression of the mass flow rate is obtained from this analysis. It depends on the material properties through the use of the flow function of the material and the flow factor of the hopper (Jenike [42]).

Other approximate solutions of the flow problem have been obtained by making assumptions concerning the velocity field, the orientation of the body force and the magnitude of the stress components. Davidson and Nedderman [18] obtained analytical expressions of the velocity and stress distribution. Their solution assumed that the shear stress was equal to zero and that the body force was in the radial direction. This solution then gave an upper limit to the flow rate. Sullivan [96] solved the same problem in his unpublished thesis. Williams [111] derived the upper and lower limits of the flow rate by

solving the flow equations on the center line and along the hopper wall respectively. This solution contains some assumptions which are difficult to justify. The approximation used in these solutions limit their validity to some special hopper configurations; for example, the hopper angle θ_w has to be very small (body force in the radial direction only). The solutions usually overpredict the flow rate and should be used only as a guide to the understanding of the qualitative behavior of the flow field.

The complete equations of flow have been solved by a number of investigators using various approximate methods. Savage [82] used a perturbation scheme based on the wall friction angle to solve the problem of flow in a hopper. Up to the order presented, the velocity and stress fields are weak functions of the angular position θ (see Fig. 1). Brennen and Pearce [9] solved the problem for a two-dimensional hopper. They used a perturbation scheme based on the angular position θ, introduced modified boundary conditions at the upper and lower discharge surfaces and found that the free surface at the hopper exit did not coincide precisely with the cylindrical surface at the exit radius. It took the shape of an arch which spanned the outlet. The resulting theoretical mass flow rates were in good agreement with the experiments for hoppers with half-angles up to 40°.

Another quality which is important in the design of hoppers is the stress which the material exerts on the hopper wall. Stress distributions were measured by Walker and Blanchard [106] with a full scale hopper. They found that the initial stress distribution when the hopper is filled is quite different from the distribution when the material is

being discharged from the hopper. They recorded a fluctuating wall stress pattern when the material is moving and observed that the value of the wall stress near the exit is very much reduced if some material is removed from the hopper discharge while it is being filled.

Actual experiments are nearly always performed with a vertical bin on top of the hopper. The stress distribution is then quite different since the two different stress patterns in the hopper and in the vertical bin have to match each other at the bin/hopper transition corner. This will result in a large, concentrated force at the bin/hopper corner and it is an important factor to be considered in the design of hoppers and bins (Perry [73], Jenike and Johanson [45]). The measured wall stress distribution also shows a difference between the value when the bin is full of static material and the value when the material is flowing. When the granular material in the bin is static, the direction of the major principal stress is in the vertical direction and the material is in an active stress state. As soon as the material begins to discharge from the bin, this principal direction is reoriented in a direction normal to the hopper wall; this is known as a passive stress state. The value of the wall stress in a passive stress state is higher than the one in an active stress state and this explains the change in the recorded wall stress. Experimental evidence of this switch in the stress field was recorded by Jenike [47].

Experimental investigations of the stress are either done with a pressure gauge mounted flush with the hopper wall (Van Zanten [103], Deutsch [21]) or by using a "radio pill" (a transducer imbedded in the material which transmits information by radio signals) to record

the internal stress in the material (Perry [73], Lakshman Rao [54]). The results of these different measurements reveal similar qualitative phenomena.

Janssen conducted an analytical study of the static stress in a vertical bin filled with granular materials. Using the free body diagram of a slice of material across the full section of the bin, he obtained an expression of the vertical stress in the material in the form

$$\frac{\sigma_v}{\rho g D} = \frac{1}{4\mu_w K}\left[1 - e^{-4\mu_w K(\frac{x}{D})}\right] \qquad (2.7)$$

where σ_v is the vertical stress in the material

ρ is the material bulk density

D is the bin diameter

μ_w is the coefficient of friction along the wall

K is the ratio of the horizontal stress to the vertical stress (σ_h/σ_v)

x is the distance in the vertical direction measured from the top surface of the material in the bin

At large values of the depth x in the order of a few bin diameters, the vertical stress is independent of the depth of the material in the bin. This is consistent with the experimental observations.

In a recent review of the various studies of the stress in a bin, Cowin [14] addressed the assumptions which were made by Janssen. First, he showed that the stresses σ_v, σ_h and the shear stress along the wall need not be assumed to be constant over the cross section of

the bin but that they should be the average over the cross section and the perimeter of the bin respectively. Secondly, the friction force needs not be fully mobilized along the wall; thus the value μ_w is less than $\tan\delta$ where δ is the wall friction angle. Thirdly, the ratio K should be defined as the horizontal stress averaged over the bin perimeter divided by the vertical stress averaged over the bin cross section. These assumptions are much less severe than those used by Janssen, and Cowin showed that the expression given by Janssen can represent only the lower limit of the possible values of the stress in a vertical bin.

The stress field in a hopper has been studied by many authors using various methods of analysis. The approximate method using a force balance on a differential slice was used by Walker [105], Walters [108, 109] and Enstad [28]. The method can treat both the active and passive stress fields with only slight modifications. Jenike and Johanson [44] considered the "radial stress" field in the hopper. In doing so, they assumed that the mean stress in the material varies linearly with the radial distance from the apex of the hopper. The resulting stress field is only valid near the hopper exit. In a series of papers [45 - 48], Jenike, Johanson and Carson considered the various stress fields which exist in a hopper/bin system. The active and passive stress states are defined and the concentrated peak pressure at the hopper/bin corner is computed. The method of characteristics has also been used extensively by other investigators (Savage [83], Horne and Nedderman [37, 38], Hancock and Nedderman [35], Bransby and Blair-Fish [6]). However, these studies were done for a plane hopper only.

2.4 PRESENT STUDY

2.4.1 Experiments in conical hoppers

In the present experiments, the mass flow rate of various materials are measured and compared to the results from the analytical solution.

Two sets of conical hoppers of different sizes were used and these results will be compared in order to evaluate the effect of the scale of the apparatus on the material behavior.

The first set consisted of four small hoppers of exit diameter 2.03 cm with heights ranging from 6.35 cm to 12.7 cm and half-wall angles from 10° to 40°. The second set consisted of four larger hoppers with heights ranging from 17.78 cm to 33 cm and half-wall angles varying from 10° to 35° ; observations were made with exit diameters of 2.03 cm and 3.3 cm . The small hoppers are made of glass and their inside walls are painted with aluminum paint. The big hoppers are made of aluminum; the walls of both are considered to be of similar smoothness. The flow rate at different exit diameters will be compared to assess any effect of the discrete nature of the materials. Furthermore, a vertical supply bin was provided on top of the small hoppers during the experiments. Any effect that such a vertical bin might have on the flow rate will be assessed by comparing the data from the two sets of hoppers.

Sand (686μm dia.) and glass beads (610μm dia.) were both used to obtain measurements of the mass flow rate. These granular materials are effectively cohesionless and have a size distribution which is fairly uniform. The measured internal friction angles were 31° for sand and 25° for the glass beads; their wall friction angles on an aluminum wall

are 24.5° and 15° respectively (see Table I.). The bulk specific gravity of the flowing material (at critical void ratio) was 1.5 for both materials. The materials used in the present experiments have a fairly small grain size; the interstitial air may therefore have some effect on the flow rate. This effect was studied by Crewdson, Ormond and Nedderman [16] who found that, for particles with diameters below 500μm, the interstitial air will affect the mass flow rate.

The mass flow rate is understood to depend on the hopper half wall angle θ_w and it may be affected by the exit diameter D if this value is not large enough. Individual hoppers of given θ_w were modified in order to obtain results for different exit openings, D. Finally, if the height of the material in the hopper is sufficiently large, the flow rate will be independent of the head.

The experimental procedure consisted of measuring the weight of material which flowed out of each hopper in a time interval of about 7 seconds. Care was taken to ensure that there was sufficient material within the hopper so that the flow rate was constant with time. The resolution of the timing was ±0.1 sec. and that of the weighing about ±0.1 gm. These resolutions will give an expected experimental error of about 15%. The measurements were fairly repeatable with the data points falling around 10% of the average value. Observations of the flow field for the sand and glass beads in a plane channel reveal very different behaviors according to the material used; this will be discussed in greater detail in the next chapter. Glass beads have a very uniform and radial flow field. Sands, on the other hand, flow in the hopper in a quite nonuniform way as previously observed by Lee, Cowin and

Templeton [55], Blair-Fish and Bransby [3] and Drescher, Cousens and Bransby [24].

2.4.2 Analytical Solution

The flow field is assumed to be symmetrical with respect to the axis of the hopper. The geometry of the problem is presented in Fig. 2.1. A spherical coordinate system is used to represent the axisymmetric flow field. The unknowns are the velocity components u and v in the -r and -θ direction respectively, the normal stresses σ_r, σ_θ, σ_α, in the r, θ, α directions and the shear stress $\sigma_{r\theta}$. Compressive stresses were taken to be positive.

The continuity equation is written as

$$\frac{\partial u}{\partial r} + 2\frac{u}{r} + \frac{1}{r}\frac{\partial v}{\partial \theta} + \frac{v}{r}\cot\theta = 0 \quad . \tag{2.8}$$

The equations of motion is spherical coordinates are

$$\frac{\partial \sigma_r}{\partial r} + \frac{1}{r}\frac{\partial \sigma_{r\theta}}{\partial \theta} + \frac{1}{r}[2\sigma_r - \sigma_\theta - \sigma_\alpha + \sigma_{r\theta}\cot\theta] + \rho g\cos\theta = -\rho\left[u\frac{\partial u}{\partial r} + \frac{v}{r}\frac{\partial u}{\partial \theta} - \frac{v^2}{r}\right] \tag{2.9}$$

in the radial direction and

$$\frac{\partial \sigma_{r\theta}}{\partial r} + \frac{1}{r}\frac{\partial \sigma_\theta}{\partial \theta} + \frac{1}{r}[(\sigma_\theta - \sigma_\alpha)\cot\theta + 3\sigma_{r\theta}] - \rho g\sin\theta = -\rho\left[u\frac{\partial v}{\partial r} + \frac{v}{r}\frac{\partial v}{\partial \theta} + \frac{uv}{r}\right] \tag{2.10}$$

in the tangential direction. Since the magnitude of the inertia terms is fairly small except close to the exit, a common practice has been to neglect the inertia terms in the equations of motion. The resulting equilibrium equations will give the stress distribution in the flow field but they cannot give a unique velocity field since the remaining equations are

homogeneous in both velocity and stress. We therefore retain the inertia terms.

In the spherical coordinate system, the Jenike-Shield yield condition and the "isotropy" conditions are written as

$$\left(\frac{\sigma_\theta - \sigma_r}{2}\right)^2 + \sigma_{r\theta}^2 = \left(\frac{\sigma_\theta + \sigma_r}{2}\right)^2 \sin^2\varphi \tag{2.11}$$

and

$$\frac{\sigma_r - \sigma_\theta}{\sigma_{r\theta}} = \frac{\frac{\partial u}{\partial r} - \frac{1}{r}\frac{\partial v}{\partial \theta} - \frac{u}{r}}{\frac{1}{2}\left(\frac{\partial v}{\partial r} - \frac{v}{r} + \frac{\partial u}{r\partial \theta}\right)} \tag{2.12}$$

respectively. The stress components are written in terms of a mean stress σ and a stress angle ψ (Sokolovskii [92]). Thus

$$\begin{aligned} \sigma_r &= \sigma(1 + \sin\varphi \cos 2\psi) \\ \sigma_\theta &= \sigma(1 - \sin\varphi \cos 2\psi) \\ \sigma_{r\theta} &= \sigma \sin\varphi \sin 2\psi \quad . \end{aligned} \tag{2.13}$$

The mean stress σ is defined as $(\sigma_r + \sigma_\theta)/2$ and ψ is the angle between the radial direction r and the major principal stress direction. An interpretation of σ and ψ on the Mohr-Coulomb circle is shown in Fig. 2.2. The use of Eqs. (2.13) guarantees that the Jenike-Shield yield condition will be satisfied identically. Since the flow is axisymmetric the stress in the α direction is a principal stress; for a converging flow field, it is equal to the major principal stress. Thus $\sigma_\alpha = \sigma(1 + \sin\varphi)$.

Using a perturbation technique based on the angular position θ,

the dependent variables σ, ψ, u, v are written as:

$$\sigma = \sigma_0 + \sigma_2\left(\frac{\theta}{\theta_w}\right)^2 + O(\theta^4)$$

$$\psi = \frac{\pi}{2} + \gamma_1\left(\frac{\theta}{\theta_w}\right) + \gamma_3\left(\frac{\theta}{\theta_w}\right)^3 + O(\theta^5)$$

$$u = u_0 + u_2\left(\frac{\theta}{\theta_w}\right)^2 + O(\theta^4) \qquad (2.14)$$

$$v = v_1\left(\frac{\theta}{\theta_w}\right) + v_3\left(\frac{\theta}{\theta_w}\right)^3 + O(\theta^5)$$

Note that when $\theta = 0$, $\psi = \frac{\pi}{2}$ which means that the stress field is in the passive state. The different powers of θ in the expansion are prescribed by the symmetry of the flow field. Substituting these expansions into the equations of flow, the different expansion sequences are obtained. The order θ^0 terms come from the continuity equation and the r-direction equations of motion; they are

$$\frac{du_0}{dr} + 2\frac{u_0}{r} + \frac{2v_1}{r\theta_w} = 0$$

and (2.15)

$$\rho u_0 \frac{du_0}{dr} + (1 - \sin\varphi)\frac{d\sigma_0}{dr} - 4\left(1 + \frac{\gamma_1}{\theta_w}\right)\frac{\sin\varphi}{r}\sigma_0 + \rho g = 0$$

The isotropy condition and the θ-direction equation of motion give the order θ^1 terms

$$2\gamma_1\left[\frac{du_0}{dr} - \frac{u_0}{r} - \frac{v_1}{r\theta_w}\right] = \frac{2u_2}{r\theta_w} - \frac{v_1}{r} + \frac{dv_1}{dr}$$

and

(2.16)

$$\rho\left[\frac{v_1^2}{r\theta_w} + u_0\left(\frac{v_1}{r} + \frac{dv_1}{dr}\right)\right] - \rho g\theta_w - 2\sin\varphi\gamma_1\frac{d\sigma_0}{dr} - \frac{\sigma_0\sin\varphi}{r}\left[\frac{2\gamma_1^2}{\theta_w} + 6\gamma_1\right] .$$

$$+ \frac{2}{r\theta_w}\left[\sigma_2(1+\sin\varphi) - 2\sigma_0\sin\varphi\gamma_1^2\right] = 0$$

The order θ^2 terms in the continuity equation and the r-direction equation of motion give

$$\frac{du_2}{dr} + 2\frac{u_2}{r} + \frac{4v_3}{r\theta_w} - \frac{v_1\theta_w}{3r} = 0$$

$$\rho\left[u_2\frac{du_0}{dr} + \frac{2u_2v_1}{r\theta_w} - \frac{v_1^2}{r} + u_0\frac{du_2}{dr}\right] - \rho g\frac{\theta_w^2}{2} + 2\gamma_1^2\sin\varphi\frac{d\sigma_0}{dr} + \qquad (2.17)$$

$$(1-\sin\varphi)\frac{d\sigma_2}{dr} - \frac{3\sin\varphi}{r\theta_w}\left[2\sigma_2\gamma_1 + \sigma_0\left(2\gamma_3 - \frac{4}{3}\gamma_1^3\right)\right] - \frac{\sigma_2\sin\varphi}{r}\left(4 + \frac{2\gamma_1}{\theta_w}\right) +$$

$$\frac{\sigma_0\sin\varphi}{r}\left(6\gamma_1^2 - \frac{2\gamma_1\theta_w}{3} - \frac{2\gamma_3}{\theta_w} + \frac{4}{3}\frac{\gamma_1^3}{\theta_w}\right) = 0 \quad .$$

These equations are solved subject to the following boundary conditions imposed by the geometry of the problem.

Along the hopper wall, $\theta = \theta_w$, the stresses have to satisfy the yield condition

$$\frac{\sigma_{r\theta}}{\sigma_{\theta}} = -\tan\delta \tag{2.18}$$

where δ is the wall friction angle. Using (2.13), the value of ψ along the wall is then determined by the equation

$$\sin\varphi \sin 2\psi_w = -\tan\delta(1 - \sin\varphi \cos 2\psi_w) \ . \tag{2.19}$$

The normal velocity along the wall should be equal to zero. Thus $v_1 + v_3 + \ldots = 0$. The discussion on the free surface condition will be delayed until later.

If only the terms of the expansion up to order θ^2 are retained the expansions of v and ψ will only have one term. Thus

$$v = v_1 = 0 \quad \text{and} \quad \psi = \psi_w = \frac{\pi}{2} + \gamma_1 \quad \text{on} \quad \theta = \theta_w \ .$$

The equations are solved by simple integration, giving

$$u_0 = U\left(\frac{r_1}{r}\right)^2$$

and

$$\frac{\sigma_0}{\rho g r_1} = \frac{1}{(\omega - 1)(1 - \sin\varphi)}\left(\frac{r}{r_1}\right) - \frac{2F}{(\omega + 4)(1 - \sin\varphi)}\left(\frac{r}{r_1}\right)^{-4} + A\left(\frac{r}{r_1}\right)^{\omega} \tag{2.20}$$

where U and A are the constants of integration, $F = U^2/gr_1$ is a modified Froude number and

$$\omega = \frac{4\sin\varphi}{(1 - \sin\varphi)}\left(1 + \frac{\gamma_w}{\theta_w}\right)$$

Substituting these expressions for u_0 and σ_0 into equations (2.17) will give expressions for u_2 and σ_2 as follows:

$$u_2 = -3\gamma_w\theta_w U\left(\frac{r_1}{r}\right)^2$$

$$\frac{\sigma_2}{\rho g r_1} = \left[\frac{\gamma_w(4\theta_w+3\gamma_w)\sin\varphi}{(\omega-1)(1-\sin^2\varphi)} + \frac{\theta_w^2}{2(1+\sin\varphi)}\right]\left(\frac{r}{r_1}\right) + \frac{2\gamma_w(\theta_w-3\gamma_w)F\sin\varphi}{(\omega+4)(1-\sin^2\varphi)}\left(\frac{r}{r_1}\right)^{-4} + \frac{A\gamma_w(\omega\theta_w+3\theta_w+3\gamma_w)\sin\varphi}{1+\sin\varphi}\left(\frac{r}{r_1}\right)^{\omega} . \tag{2.21}$$

2.4.3 Boundary Conditions on the Free Surface

The analysis in this section is based on the work of Brennen and Pearce [9]. Along the free surfaces, the mean stress is equal to zero. This will give the condition on the expansion terms σ_0 and σ_2. If these free surfaces are taken to be the circumferential surfaces at the upper and lower radius, then

$$\sigma(r_1) = \sigma_0(r_1) + \sigma_2(r_1)\left(\frac{\theta}{\theta_w}\right)^2 = 0$$

and

$$\sigma(r_2) = \sigma_0(r_2) + \sigma_2(r_2)\left(\frac{\theta}{\theta_w}\right)^2 = 0$$

which give

$$\sigma_0(r_1) = \sigma_2(r_1) = 0$$

and

$$\sigma_0(r_2) = \sigma_2(r_2) = 0$$

However, the expressions of σ_0 and σ_2 have only two unknown constants (A and U) which are to be evaluated from the boundary conditions. Therefore, these four conditions on σ_0 and σ_2 along the free surfaces overspecify the problem. This implies that the free surfaces do not coincide with the circumferential surfaces and that their geometries will be determined by the condition of zero stress.

Following Brennen and Pearce [9], we let the free surface Γ and the circumferential lines be separated by a distance $\epsilon(\theta)$. The geometry is then as shown in Fig. 2.3. Assuming $\epsilon(\theta)$ to have a parabolic profile, we have

$$\epsilon(\theta) = \epsilon_1\left[1 - \left(\frac{\theta}{\theta_w}\right)^2\right]$$

The zero stress condition along Γ will be expanded in Taylor series from the stress along the circumferential line. Hence

$$\sigma\Big|_{\text{on }\Gamma} = \sigma\Big|_{r_1} + \epsilon_1\left[1 - \left(\frac{\theta}{\theta_w}\right)^2\right]\frac{d\sigma}{dr}\Big|_{r_1} = 0 \qquad (2.22)$$

Substituting the expansion (2.14) for σ, we have

$$\sigma_0\Big|_{r_1} + \epsilon_1 \frac{d\sigma_0}{dr}\Big|_{r_1} = 0$$

$$\sigma_2\Big|_{r_1} + \epsilon_1 \frac{d\sigma_2}{dr}\Big|_{r_1} - \epsilon_1 \frac{d\sigma_0}{dr}\Big|_{r_1} = 0$$

which are the terms of order θ^o and θ^2 in (2.22). It can be seen then that ϵ_1 is of order θ_w^2 and to this order

$$(\sigma_0+\sigma_2)\Big|_{r_1} = 0$$

$$\epsilon_1 = \frac{\sigma_2\Big|_{r_1}}{d\sigma_0/dr\Big|_{r_1}}$$

This same condition can also be applied along the top surface. Evaluating the constants U and A in (2.20), we have

$$F = \frac{U^2}{gr_1} = \frac{\omega+4}{2(\omega-1)} \left[\frac{1 - \left(\frac{r_2}{r_1}\right)^{1-\omega}}{1 - \left(\frac{r_2}{r_1}\right)^{-4-\omega}} \right] \left[1 + \frac{\theta_w}{2(1+\sin\varphi)} (14\gamma_w \sin\varphi + 5\theta_w \sin\varphi - \theta_w) \right] \qquad (2.23)$$

The exit velocity averaged over the exit area is given by

$$\bar{u} = \frac{\int_0^{\theta_w} u_{r=r_1} \sin\theta \, d\theta}{1 - \cos\theta_w}$$

or, in dimensionless form,

$$\frac{\bar{u}}{\sqrt{gD}} = \sqrt{\frac{F}{2\sin\theta_w}}\left[1 - \frac{3\gamma_w\int_0^{\theta_w}\theta^2\sin\theta\,d\theta}{(1-\cos\theta_w)\theta_w}\right] \tag{2.24}$$

The non dimensional mean stress along the wall can be obtained from Eqs. (2.20) and (2.21). Thus

$$\frac{\sigma}{\rho g r_1} = \left[\frac{(4\theta_w+3\gamma_w)\gamma_w\sin\varphi + 1 + \sin\varphi}{(\omega-1)(1-\sin^2\varphi)} + \frac{\theta_w^2}{2(1+\sin\varphi)}\right]\left(\frac{r}{r_1}\right) +$$

$$F\left[\frac{2\gamma_w(\theta_w - 3\gamma_w)\sin\varphi - 2(1+\sin\varphi)}{(\omega+4)(1-\sin^2\varphi)}\right]\left(\frac{r}{r_1}\right)^{-4} + \tag{2.25}$$

$$A\left[1 + \frac{\gamma_w(\omega\theta_w + 3\theta_w + 3\gamma_w)\sin\varphi}{1+\sin\varphi}\right]\left(\frac{r}{r_1}\right)^{\omega} .$$

Some comments can be made about the solutions (2.24) and (2.25). First the magnitude of the θ^2 terms are smaller than the θ^o terms by factors of $\gamma_w\theta_w$, θ_w^2 or γ_w^2. Thus, the successive terms in the expansion decrease in magnitude and convergence of the regular expansion is expected. Secondly, the value of F (and therefore of $\bar{u}$) is independent of the ratio r_2/r_1 when the head of the material above the exit opening is sufficiently large. This is consistent with the well-known experimental observation of head independent flow.

2.4.4 Solution Using Spencer's Model of Deformation

In this section, we will explore the difference in the analytical solution which would occur if the Spencer model of deformation (Eq. 2.3)

is used instead of St. Venant principle (Eq. 2.2). In a spherical coordinate system with the flow being steady, Eq. (2.3) can be rewritten as

$$\sin 2\psi\left(\frac{\partial u}{\partial r} - \frac{1}{r}\frac{\partial v}{\partial \theta} - \frac{u}{r}\right) - \cos 2\psi\left(\frac{\partial v}{\partial r} - \frac{v}{r} + \frac{1}{r}\frac{\partial u}{\partial \theta}\right)$$

$$+ \sin\varphi\left[\frac{\partial v}{\partial r} + \frac{v}{r} - \frac{1}{r}\frac{\partial u}{\partial \theta} - 2\left(u\frac{\partial \psi}{\partial r} + \frac{v}{r}\frac{\partial \psi}{\partial \theta}\right)\right] = 0 \qquad (2.26)$$

This Eq. (2.26) is identical to Eq. (2.2) only if the last term is equal to zero which is not true in general (Spencer [93]). Substituting the expansions (2.21) of the unknowns (up to order θ^2) and equating the terms of the order θ^1, we have the realtion between u_0 and u_2 as

$$2\gamma_w\left(\frac{du_0}{dr} - \frac{u_0}{r}\right) - (1 + \sin\varphi)\frac{2}{r}\frac{u_2}{\theta_w} = 0 \qquad (2.27)$$

which gives

$$u_2 = \frac{-3\gamma_w\theta_w}{1 - \sin\varphi}U\left(\frac{r_1}{r}\right)^2 \qquad (2.28)$$

This expression of u_2 differs from Eq. (2.21a) by the factor $1/(1 - \sin\varphi)$ which is greater than one. The correction term using the Spencer model is then larger than the correction term using "isotropy" (St. Venant principle) condition. Some computations were carried out and they showed that the flow rate computed using Eq. (2.28) can be as low as half of the value obtained with the isotropy condition.

2.5 PRESENTATION OF RESULTS AND DISCUSSION

2.5.1 Comparison to Experimental Data

In Fig. 2.4 a plot of the dimensionless exit velocity versus the

exit diameters for different hopper angles is presented. It can be seen that the results are fairly independent of the exit opening. This same behavior is also observed when an "empty annulus" is assumed to be present at the exit [11]. Using an effective diameter $D' = D - k$ where k can vary from 1 to 4 grain diameters, the dimensionless exit velocity is still independent of the effective diameter used in the experiments. This is an indication that the ratio D/d of the exit diameter to the particle size is sufficiently large in the present experiments for the "empty annulus" effect to be small.

The dimensionless exit velocities from both sets of hoppers are plotted versus the half wall angle in Fig. 2.5 and 2.6 for sand and glass beads respectively. Experimental data obtained by other authors are also presented. The data of Deming and Mehring [20] for potassium nitrite ($\varphi = 24°$) compare well with the present experiments. However, their values for ammonium phosphate ($\varphi = 36°$) are quite low; this may be due to substantial cohesive effects in this material. The data quoted by Williams [111] for sand ($\varphi = 34°$, $\delta = 25°$) and Nitram ($\varphi = 34°$, $\delta = 19°$) are also plotted on Fig. 2.5. These experiments were conducted in large size hoppers and the results correspond well with the present measurements for smaller hoppers.

In Fig. 2.5 and 2.6, the experimental data for glass beads compare better with the analytical results than the data for sand. A possible explanation is that glass beads have a uniform and spherical particle shape. They are quite free flowing and their surface condition is smooth. This is quite different from the properties of sand which has an angular shape. These differences between the individual particle shapes may

not be completely reflected in the material properties φ, δ used for the continuum model.

The analytical results for the mass flow rate shown in Figs. 2.5 and 2.6 exhibit a dependence on both the hopper wall angle and the frictional properties of the materials. Since the expansion scheme is based on the angular position θ, its validity is limited to small values of the hopper angle θ_w. The deviation between the theory and experiments at large hopper angle is therefore expected. The analytical solution also exhibits a strong dependence on the wall friction angle δ.

The normal stress along the wall ($\sigma_{\theta\theta}$ at $\theta = \theta_w$) is plotted in Fig. 2.7 and compared to the measurements made by Walker [106]. The values obtained from the present solution have the same dependence on the radial position r/r_1 even though they are larger than the experimental values. The peak stresses obtained from the present solution occur at the same value r/r_1 as the value measured by Walker (at $r/r_1 \approx 3.6$). This ability to predict the location of the peak stress could be important in the design of hoppers. The approximate solution derived by Walker is also plotted in Fig. 2.7. It does not compare well with the experimental results; the peak stress occurs at a lower position than that observed experimentally. The other approximate solutions by Walters [109] and Enstad [28] yields results similar to those of Walker.

2.5.2 Comparison to Other Analyses

In the following, the analytical expressions of the mass flow rate derived by Johanson [53], Brown [10], Williams [111] and Savage [82] are compared to the expression obtained in the present solution.

Johanson [53] presented a semi-empirical method for computing

the flow rate of granular materials from hoppers. By considering a balance of forces acting on an arch across the hopper opening, he considered that the material would flow when the flow factor of the hoppers was greater than a critical value. The dimensionless exit velocity is obtained in the form

$$\frac{u}{\sqrt{gD}} = \frac{1}{\sqrt{4\tan\theta_w}}\sqrt{1 - \frac{ff}{ffa}}$$

where ff is the critical flow factor defined by $\frac{\sigma_1}{\rho g D}$

ffa is the actual flow factor defined by $\frac{\sigma_1}{f_c}$; f_c being unconsolidated strength of the material.

This result is fairly general. It is dependent on both the hopper angle θ_w and the material property through the flow factor. The flow factor is determined from the results given by Jenike [42]. The upper limiting curve $u/\sqrt{gD} = (4\tan\theta_w)^{-\frac{1}{2}}$ is presented in Fig. a. 8 since the flow factors for the hoppers used in the present experiments were not available.

Brown [10] used an energy principle to derive the mass flow rate of granular materials through an aperture. He suggested that the material would flow when the total potential and kinetic energies reached a minimum at a certain radius. Taking this radius to be that of the exit opening, he derived an upper limit of the dimensionless exit velocity as

$$\frac{u}{\sqrt{gD}} = \frac{2(1 - \cos^{3/2}\beta)}{3\sin^{5/2}\beta}$$

where β is the angle of the channel formed by the flowing material. For a mass flow hopper, β would be the hopper half-wall angle and is a simple geometric quantity. The results of this expression for the hopper used in the present experiments are included in Fig. 2.8.

Williams [111] derived the upper and lower limiting solutions by solving the equations of the flow along the centerline and the hopper wall respectively. The stresses satisfy the Mohr-Coulomb yield condition and the velocity is assumed to be in the radial direction only. The expression of the centerline velocity is

$$v_o^2 = \left(\frac{k+1}{2k-3}\right) g \frac{r_1^5}{r^4} \quad .$$

Along the wall, the radial velocity is given by

$$v_w^2 = \frac{g}{2}\left(\cos\theta_w - \frac{\sin\varphi \sin 2\psi_w \sin\theta_w}{1 - \sin\varphi \cos 2\psi_w}\right)\left(\frac{B-4}{B+1}\right)\frac{r_o^5}{r^4}$$

where

$$k = \frac{1 + \sin\varphi}{1 - \sin\varphi}$$

and

$$B = \frac{k_2}{k_1}$$

where k_2 and k_1 are defined on page 250 of his paper.

This solution is based on some assumptions which are important. For example, the values of $\partial\psi/\partial\theta$ on the centerline and along the wall are approximations to the actual values. Also, the dependence of the radial velocity on the radial position θ (taken to be $\cos^{-\frac{1}{2}}\theta$) is based on the observation of the frictionless wall solution and may not be representative of the actual velocity profile.

Savage [82] seems to have been the first author to systematically analyze the hopper flow problem by considering the complete equations of motion. His perturbation scheme is based on $\epsilon_1 = (\tan\delta)^{\frac{1}{2}}$ where δ is the wall friction angle and is based upon the limit process $(\tan\delta)/\theta_w \to 0$ as $\theta_w \to 0$. The results are given as

$$\frac{u}{\sqrt{gD}} = \left[\frac{k+1}{2(2k-3)\theta_w}\right]^{\frac{1}{2}} + \frac{\epsilon_1^2 k}{\theta_w}\left[\frac{1}{2}\left\{2(2k-3)(k+1)\theta_w\right\}^{-\frac{1}{2}} - \left\{\frac{k+1}{2(2k-3)^3\theta_w}\right\}^{\frac{1}{2}}\right]$$

where

$$k = (1+\sin\varphi)/(1-\sin\varphi)$$

Because of the above-mentioned limit process it follows that this analysis and flow rate is invalid for wall angles, θ_w, less than about $\tan\delta$. This region of lack of validity is clearly demonstrated in Fig. 8. However provided $\tan\delta/\theta_w$ is small it would appear that Savage's analysis yields results which are closer to the experimental data than the present analysis. In conclusion it would appear that the method presented in the present paper is appropriate for small hopper angles with decrepancies from the experiments occurring at larger θ_w; on the other hand Savage's analysis may be more appropriate for small wall friction values and larger θ_w.

2.6 CONCLUSIONS

The present approximate solution shows that the rigid-perfectly plastic continuum model describes the behavior of granular materials flowing in conical hoppers fairly well. The solution reflects the observed phenomena such as the fact that the discharge rate from the hopper is independent of the head of the material and that the flowing material is in a passive stress state. It also shows that the expressions of the mass flow rate and wall stress depend mainly on the conditions near the hopper exit. The validity of the solution is, however, restricted to the values of θ_w for which mass flow is present in the hopper and to the flow in a hopper without a vertical bin.

A comparison of the results obtained using either the St. Venant principle (Eq. 2.2) or the Spencer's model of deformation (Eq. 2.3) shows that the St. Venant principle gives results which compare more favorably to the experimental measurements. This conclusion is however, restricted to the approximate approach used in the present solution.

Finally, questions on the validity of the approximations used in the analytical solution will be considered in the next chapter where the flow field in a plane hopper is observed experimentally.

TABLE I

Material Properties (*)

Material	Bulk Specific Gravity	Mean Diameter mm	Internal Friction Angle (°)	Wall Friction Angle Lucite Wall (°)	Wall Friction Angle Al Wall (°)
P0170	1.46	0.325	24.6	15.3	17.7
P0280	1.48	0.59	24.3	14.4	15.1
V070	1.71	1.32	26.8	14.2	15.1
Sand No. 1	1.56	0.223	24.1	20.2	-
Sand No. 2	1.30	0.317	30.7	17.9	-
Sand No. 3	1.53	0.68	30.6	14.4	24.5

(*) These measurements were made by Pearce [71]

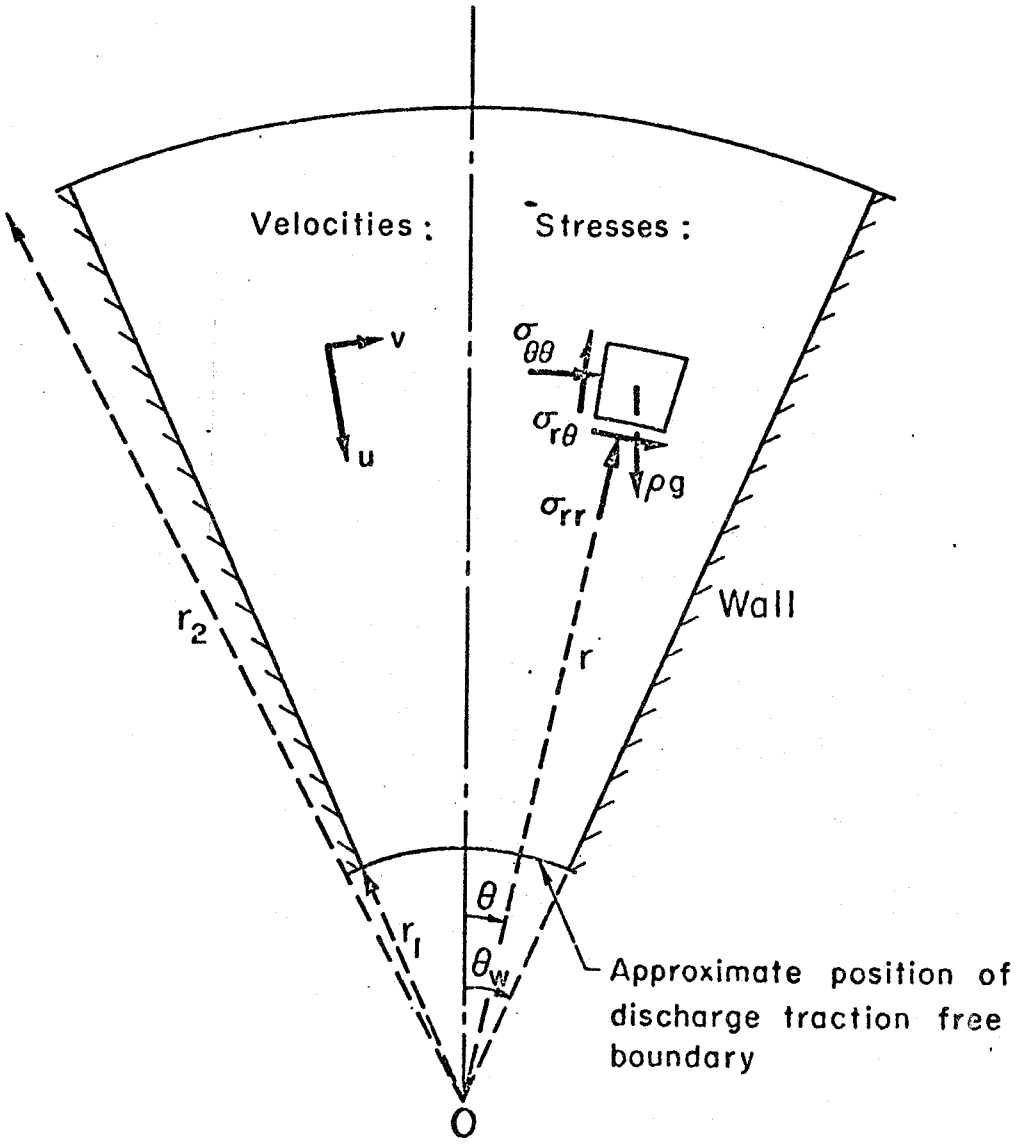

Figure 2.1 Schematic for conical hopper flow.

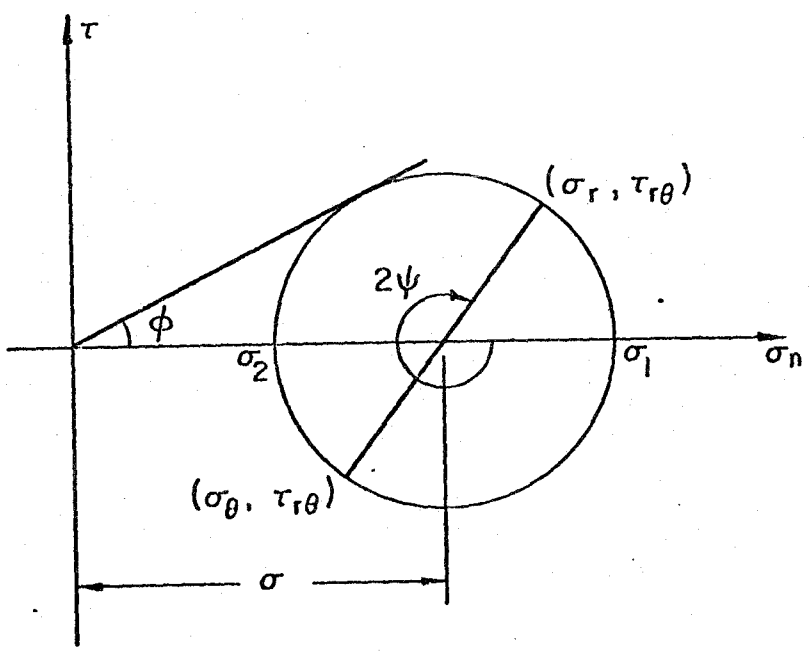

Figure 2.2 Mohr diagram showing the mean stress σ and the stress angle ψ used in the Sokolovskii's expression of the stress components.

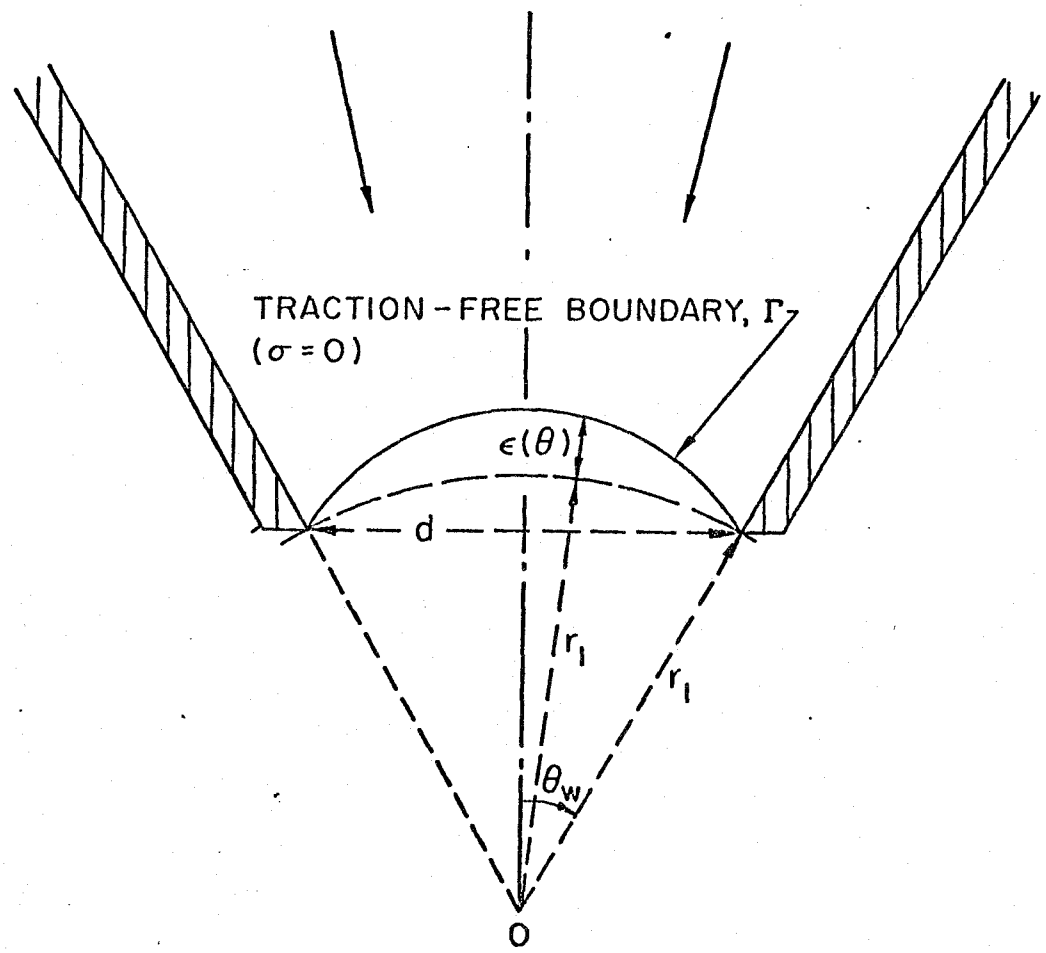

Figure 2.3 Detail of the initially undetermined traction-free boundary, Γ, at discharge from the hopper.

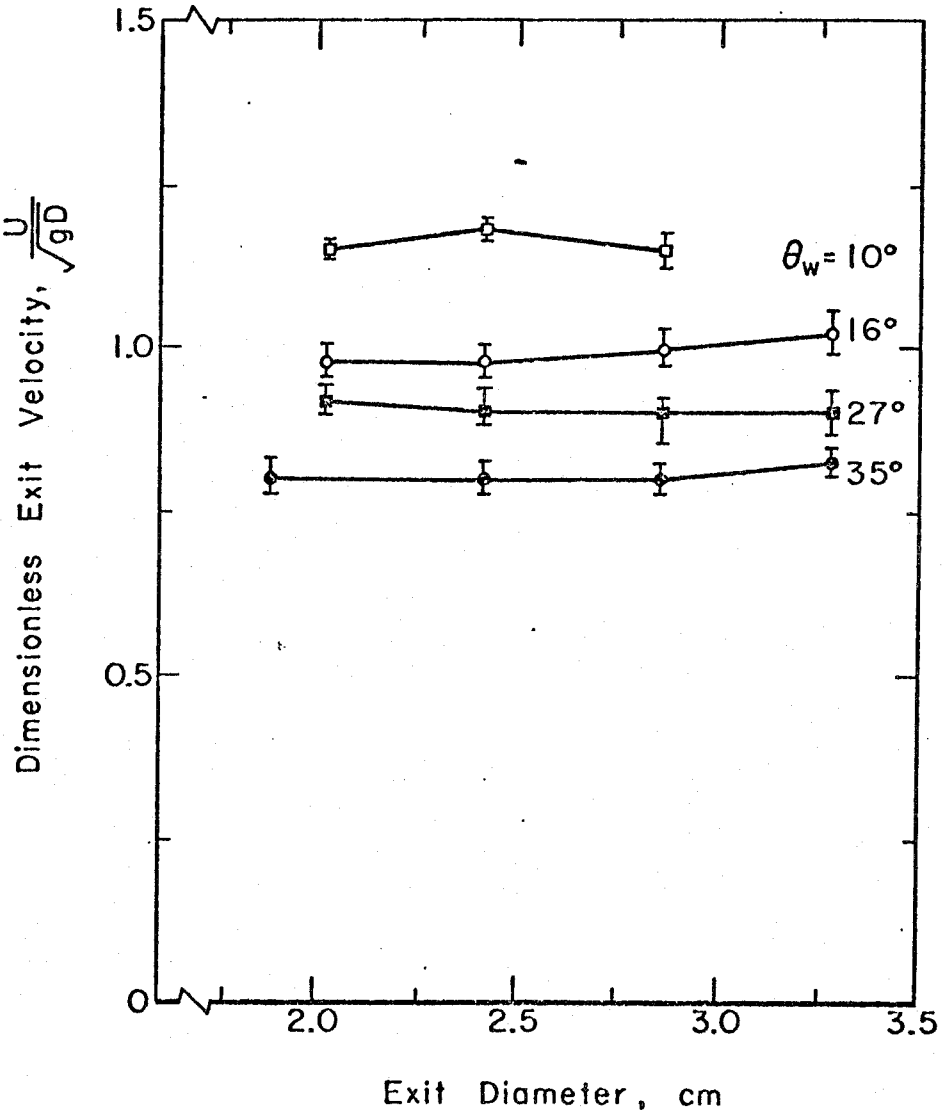

Figure 2.4 Dimensionless exit velocity versus exit diameter for sand flowing in conical hoppers of various half-wall angles.

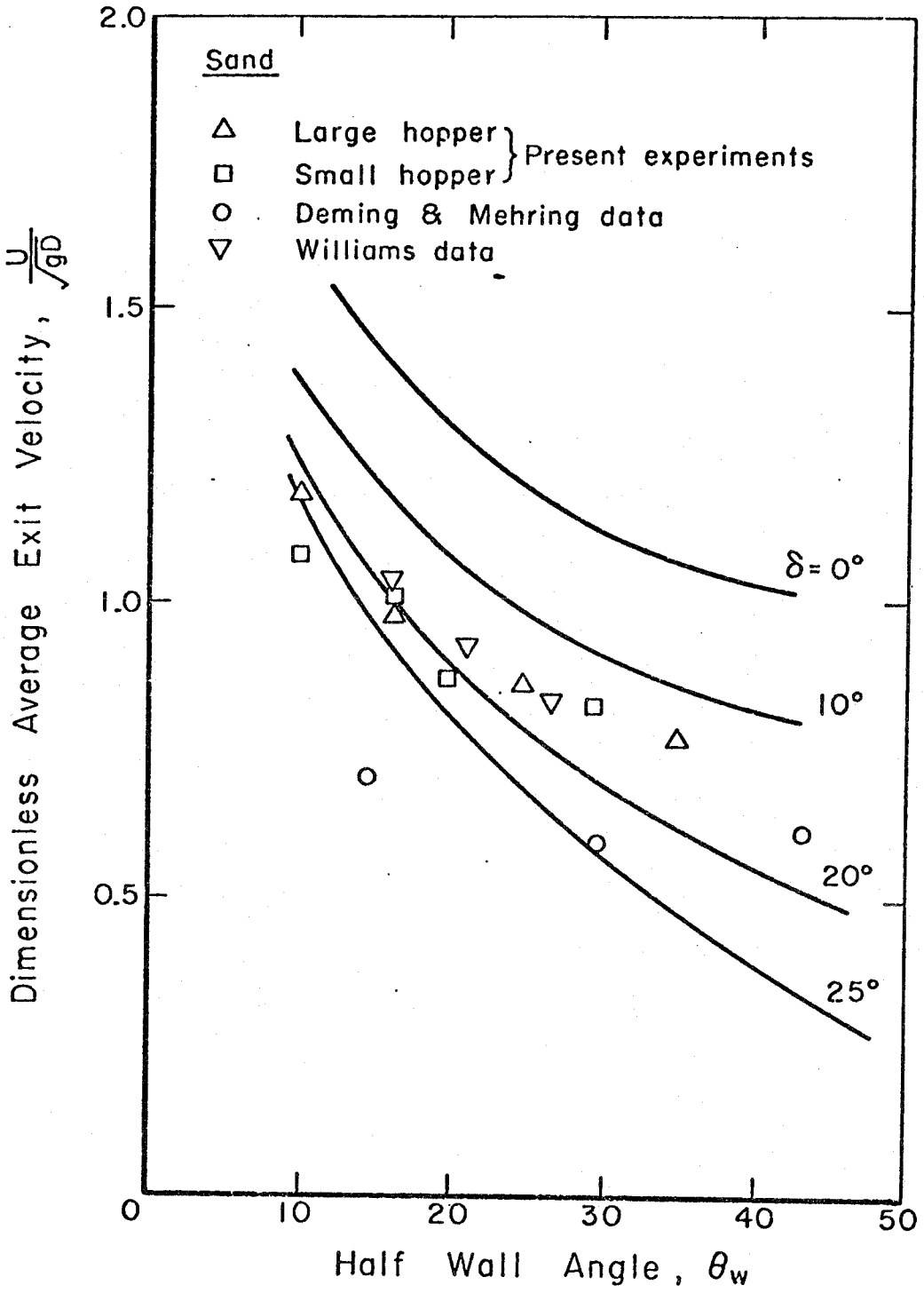

Figure 2.5 The dimensionless average exit velocity for an internal friction angle of $\varphi = 35°$ plotted against the hopper opening angle for various wall friction angles δ. Experimental data are for sand ($\varphi = 31°$) with wall friction angle δ of 24.5°.

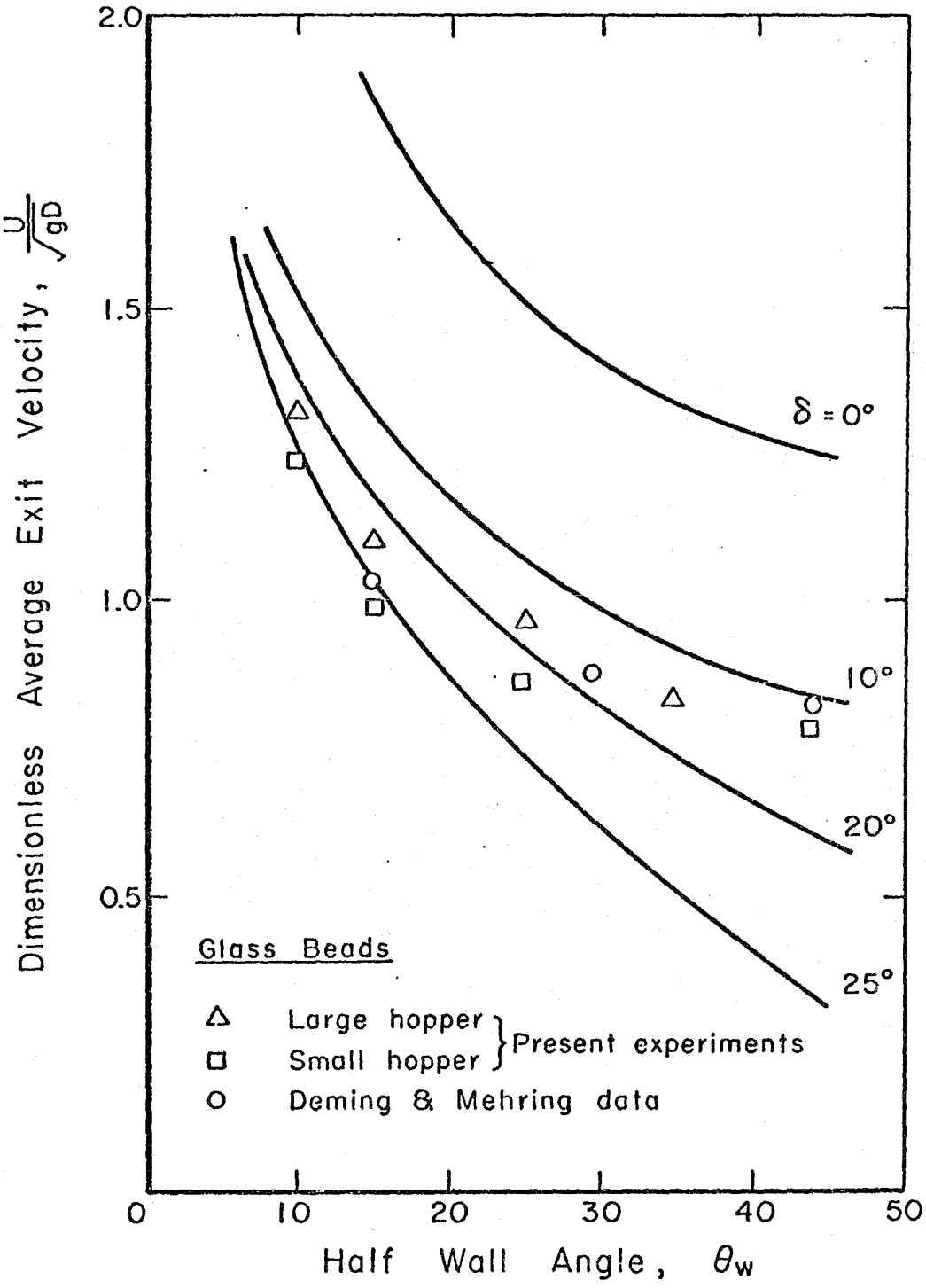

Figure 2.6 Dimensionless average exit velocity for an internal friction angle of $\varphi = 25°$ plotted against the hopper opening angle for various wall friction angles δ. Experimental data are for glass beads ($\varphi = 25°$) with a wall friction angle δ of 15°

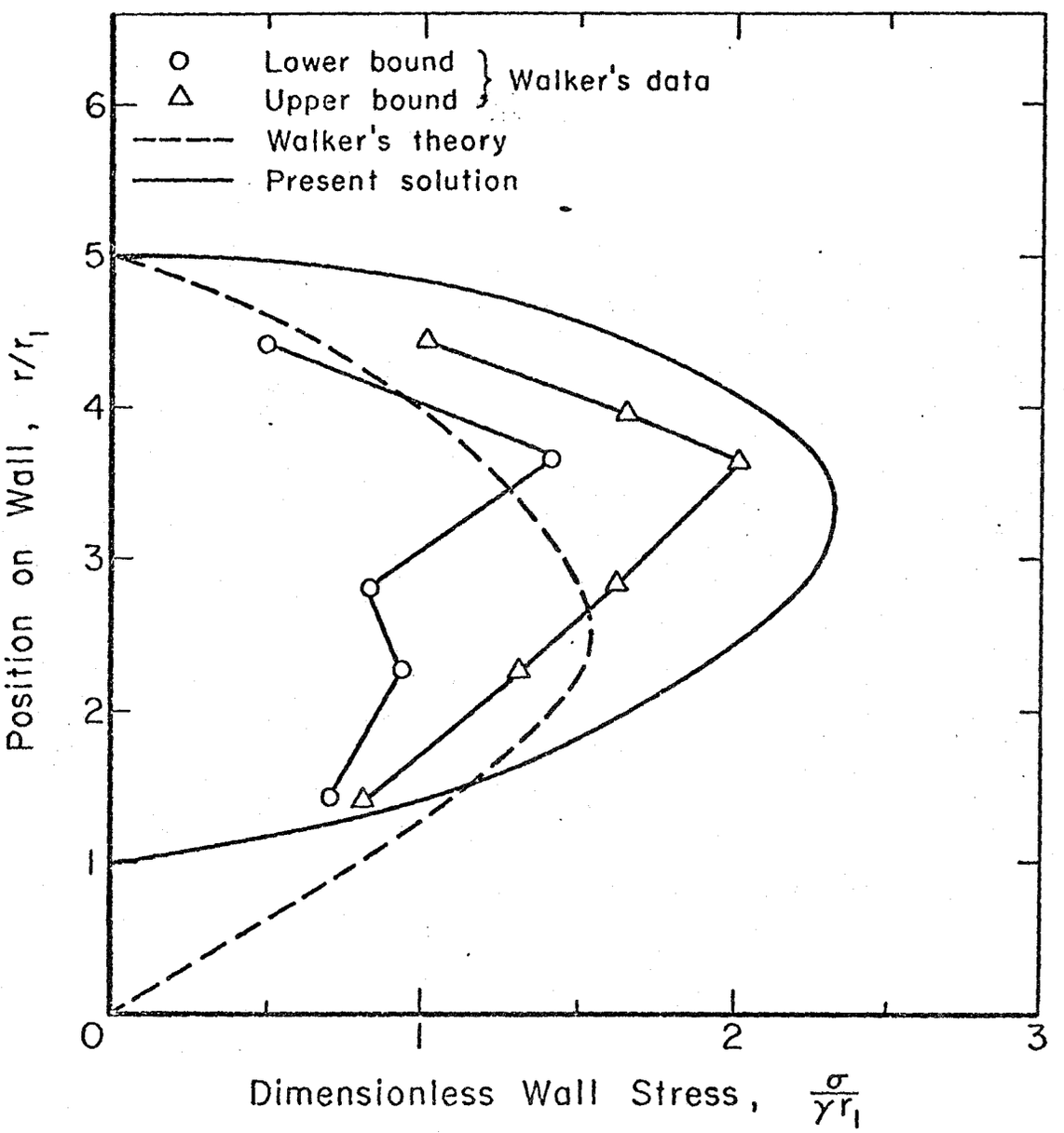

Figure 2.7 Dimensionless wall stress plotted against the position along the wall for a material of internal friction angle $\varphi = 25°$, a wall friction angle $\delta = 15°$ and a hopper opening angle of $\theta_w = 30°$. Also shown are the experimental measurements of Walker [106].

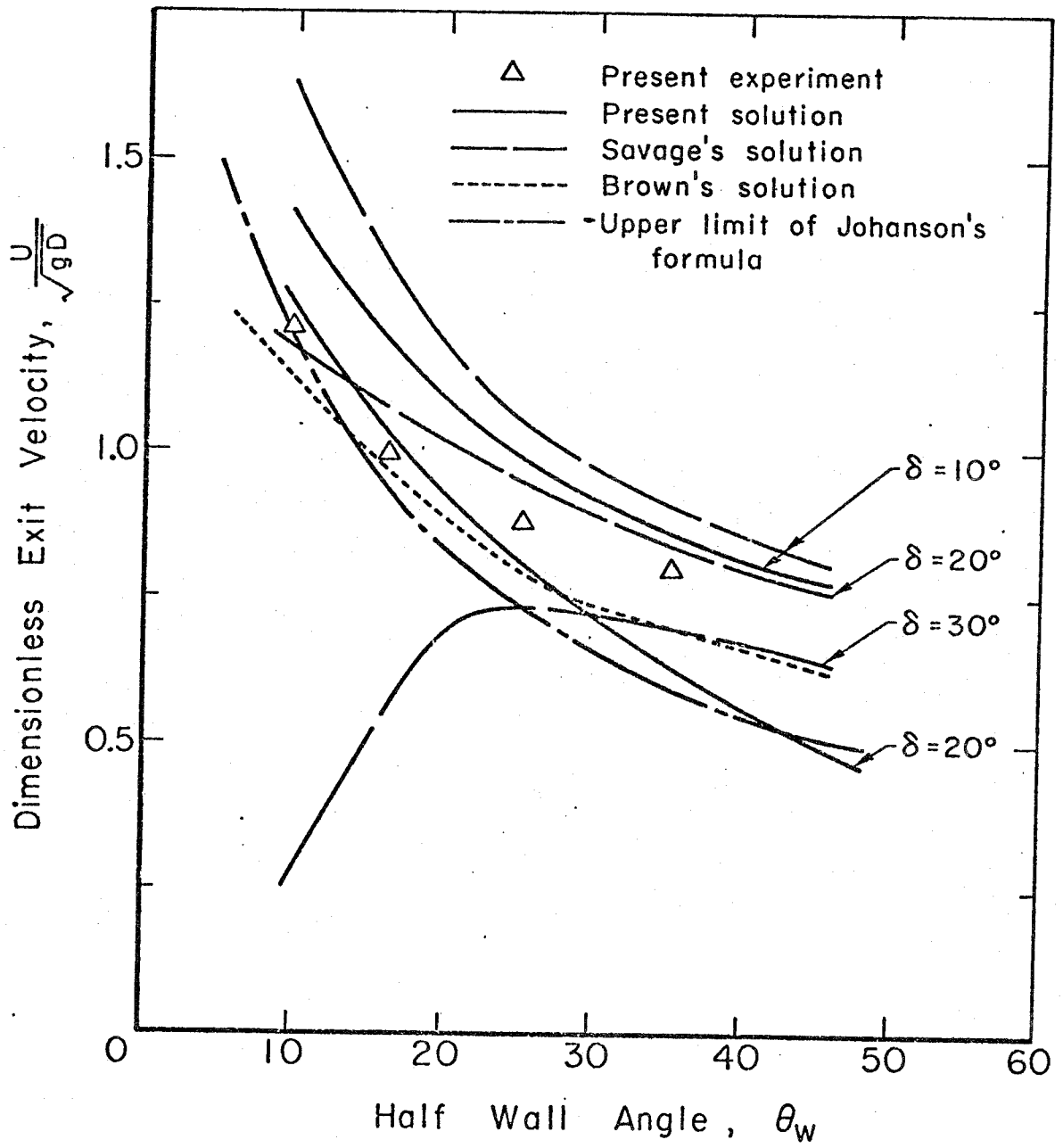

Figure 2.8 Present solution is compared to other analytical results for an internal friction angle of 35° and various wall friction angles.

CHAPTER 3

OBSERVATION OF THE FLOW FIELD IN HOPPERS

3.1 INTRODUCTION

In the analytical studies of the flow of granular materials in hoppers, the flow field has been greatly simplified (Lee et al [55]). The geometry of the problem usually consists of a hopper without a vertical bin and the effect of the presence of such a bin is limited to the fact that it will introduce a pressure distributed over the upper surface of the hopper (Davidson and Nedderman [18]).

Since the hopper walls are usually symmetrical with respect to the vertical axis, the flow field is also assumed to be symmetrical with respect to this axis. Furthermore, the flow is assumed to be steady with time with the understanding that the flow field is developed after flow initiation has taken place. Finally, the material is assumed to deform with a constant void fraction in the flow field.

These assumptions are introduced to simplify the analytical problem and the solutions obtained seem to agree well with the experimental measurements. However, a number of recent experimental studies have raised doubts concerning the validity of the above assumptions. These experiments (Blair-Fish and Bransby [3], Lee et al [55]) show that the kinematics of the deformation of granular materials in a hopper is not smooth and steady; rather, the flow is controlled by zones of large deformation and distortion which are followed by the presence of blocks of materials which slide with little deformation.

This chapter contains experimental observations of the flow field of granular materials in a two dimensional, wedge shape hopper. The deformation pattern of various materials and the recorded wall stresses are compared to the observations made by other investigators.

3.2 REVIEW OF PAST WORK

Two experimental procedures have been used to observe the flow field in hoppers. The first one, called the photographic method, records the motion of the materials which can be seen through the front wall of the hopper. In the second method, the motion of the material within the flow field away from the hopper front wall is observed by X-ray radiography. This is called the radiographic method. It has the advantage that both the velocity and the porosity field can be observed simultaneously.

Photographic observations of the flow field have indicated that the motion of the material in the upper part of the hopper is parallel to the hopper walls with flow in the radial direction occurring at a lower position in the hopper (Brown and Richard [11]). Lines of velocity discontinuity were observed and some asymmetry of the flow field was noted by Pariseau [67]. Bosley et al [4] observed the flow near the hopper exit and found that the flow field was in the radial direction in mass flow hoppers while a non radial velocity component existed in the flow field of funnel flow hoppers. Levinson et al [56] noted the unsteadiness of the velocity field at the time scale of their observations (0.3 sec.) and found that the flow field can be quite asymmetrical, especially near the discharge. A fluctuating wall stress pattern and a symmetrical velocity profile were recorded by Connelly [15] in experiments using glass

pellets (125μm to 177μm grain size).

The use of X-ray radiography to observe the flow field of granular materials in hoppers has revealed important information on the kinematics of the deformation of the materials. The observations made by Cuttress and Pulfer [17], Blair-Fish and Bransby [3] and Lee et al [55] showed that the materials slide as a block along the hopper walls until they reach the rupture zones where they are sheared and deformed. After they leave this rupture zone, the sheared material feeds into the fast moving region near the hopper exit. These rupture zones are bands of low density where the shearing motion and dilatation of the material takes place; they were observed to extend from one hopper wall to the other (see Fig.3.1a). In a hopper with vertical walls, they are formed in an alternating way at the opposing transition corner while only two rupture zones are observed in a hopper without vertical walls (see Fig.3.1a). Drescher et al [24] proposed a model to represent the kinematics of the deformation across these rupture zones in order to compute their shapes. Blair-Fish and Bransby [3] and Templeton [100] measured the wall stresses at the transition corner between the hopper and the vertical walls and found that they fluctuate with time. These fluctuations seem to correspond to the formation of the rupture zones and Templeton [100] recorded the peak wall stresses even before the rupture zones could be observed. These investigations all agree that the flow field in the hopper is not smooth and steady with time; the kinematics of the deformation is a complicated process where deformed materials are followed by rigid materials with a rupture zone being present between them.

3.3 PRESENT WORK

The present experiments were conducted in two parts. In the first part, the wall stress at the transition corner between the hopper and the vertical walls was recorded to detect any fluctuations with time. In the second part, the flow field of various granular materials is compared to the observations made by other investigators and an assessment made of the assumptions used in the analytical solution.

3.3.1 Experimental Apparatus and Procedure

A lucite hopper with a half-wall angle of 30° was used. The width of the exit opening was 0.5 cm (0.2") and the width of the vertical walls was 13.25 cm (6"). The flow field could be observed through the front wall (see Fig.3.1b). The materials used in the experiments were sand and glass beads and their properties are shown in Table I. They are effectively cohesionless; however, the difference between the particle shape and the surface condition of sand and glass beads seems to yield differences in the flow field.

The wall stress was recorded qualitatively by using strain gauges mounted on sensing surfaces along the inclined walls of the hopper (see Fig.3.1b). The location of the vertical walls could be changed so that the location of the strain gauge relative to the corner between the hopper and the bin could be varied. The wall stress patterns on both sides of the hopper were recorded simultaneously.

The flow field was observed by taking movies of the material as it was moving through the hopper. Colored markers were placed in the flow field and their motion recorded. It is assumed that these markers moved with the material and that they did not interfere with the

flow pattern in the hopper (Perry [72]). Film speeds of 32 frames/sec were used and the movies were analyzed frame by frame by recording the coordinates of each colored marker in the flow field. The velocity at each point was obtained by dividing the displacement of the marker in a given time interval by the time elapsed.

3.3.2 Presentation of Results

a) Qualitative Recording of Wall Stress

The recorded wall stress patterns of the various materials are shown in Figs. 3.2 to 3.4. These recordings give the qualitative behavior of the stress exerted on the sensing surface of the strain gauge. Their use is limited to detecting whether this stress is fluctuating with time. The sensing area is very large compared to the individual particle size. The recording therefore gives an indication of the stress averaged over an area contacted by many particles.

The main difference between the recordings in Figs.3.2 to 3.4 is due to the fact that the fluctuating stress only occurred for some materials. The stress recorded for sand (Figs.3.2, 3.3a) always showed some fluctuation having periods of the order of a few seconds. The fluctuations cannot therefore be due to the effect of the individual particles colliding with the sensing surface. The magnitude of these fluctuations increases with the particle diameter and with the angularity of the shape of the particles. The recordings on the two sides of the hopper show that they are out of phase with each other. This seems consistent with the observation that the fluctuations correspond to the formation of the rupture zones at the transition corners and that these rupture zones are formed in an alternating way.

The stress recordings for glass beads are quite different from those of sand. At large grain size (greater than 500μm), they show only random fluctuations at high frequency. These are considered to be the effect of individual particles striking the sensing surface. The recordings for glass beads of small grain size (300μm)(see Fig.3.3b) show a definite fluctuating pattern with a period high enough to be considered as the phenomena associated with the deformation of the material. Such a fluctuating pattern was also recorded by Connelly [15] with glass pellets at small grain size (125μm to 177μm).

The observations of the wall stress fluctuation for the six granular materials used in the present experiments seem consistent with the results obtained by other investigators. However, the present results obtained with glass beads show that this phenomenon also depends on the grain size of the material and may disappear for larger particles.

b) Observation of the deformation of a layer of colored materials

Figures 3.5 and 3.6 show the deformation pattern of a layer of colored material as it proceeds through the hopper. The differences between sand and glass beads are strikingly clear.

As the layer of sand proceeds through the hopper, it is stretched and sheared. Most of the shearing takes place in a narrow central core with the material near the wall being displaced at a much smaller rate. The presence of a definite jump in the deformation pattern of the flow field agress with the observations made by Pariseau [67] and Perry et al [72]. The difference in the deformation between the central core and the material near the wall is so obvious that it must be concluded that two different flow regimes must be occuring. The material in the

central core is shearing while the material outside of the central core seems to slide along the hopper walls until it is fed into the central core. Similar observations were made by Blair-Fish and Bransby [3] and Lee et al [55].

The behavior of a layer of colored glass beads is shown in Fig. 3.6 and reveals a completely different behavior. As it moves through the hopper, the layer is being stretched and sheared. However, the amount of shearing is uniformly distributed over the cross section of the hopper. The deformed layer of material has a smooth bell shape and there is no obvious jump in the deformation of the material in the flow field.

These observations of the deformation of a layer of material have revealed quite different flow patterns for sand and glass beads. The flow field for sand contains a discontinuity which divides the fast flowing central core from the slower moving material near the hopper walls. The flow field of glass beads shows continuous and smooth deformation across the hopper.

c) Observation of the motion of individual particles in hoppers

The observations made in the last section give an overall picture of the deformation pattern across the section of the hopper. To characterize the motion of the material at each point in the flow field, the displacements of the individual colored particles were examined.

Figure 3.7 presents the pathlines of various points in the flow field for sand. The markers start to flow from the same horizontal position level with the corner between the hopper and the vertical walls. The resulting pathlines indicate that the motion of the particles is indeed

composed of two parts. The material first moves in a direction parallel to the hopper walls. Then at some point in the flow field, the material orients its motion in a radial direction. This occurs when the particles enter the fast flowing center core discussed in the last section. These observations provide further evidence of the discontinuity lines in the flow field for sand.

The pathlines of the particles which pass through the same point in the flow field at different times can be superimposed on each other to give an idea of the repeatability and steadiness of the flow field. Such a plot for sand is shown in Fig. 3.8. The resulting picture of the flow field is not very well organized. Pathlines are seen to cross each other with little synchronization from one part of the flow field to the other.

Similar plots of the pathlines for glass beads are shown in Fig. 3.9 and 3.10. The observations differ greatly from those for sand. In glass beads, the material seems to move in a radial direction throughout the flow field and there is no discontinuity in the orientation of the pathlines. The superposition of pathlines at various times is shown in Fig. 3.10 for glass beads. The flow field is well organized and uniform. The pathlines which start from the same point at the top of the hopper are parallel to each other and no pathline crossings occur.

The velocity of the particles at various points along the pathlines can be computed and are shown in Figs. 3.11 and 3.12 for sand and glass beads respectively. Particles are observed to accelerate and their velocity exhibits a dependence on the position of the particle in the horizontal plane.

3.4 CONCLUDING REMARKS

The experimental observation of the flow field in a hopper with a vertical bin reveals a fairly complicated mechanism of the deformation of the material. As the material is being discharged, it changes from a plug flow with little deformation in the vertical bin into a converging flow with large deformation in the hopper. The flow field near the bin/hopper transition corner is therefore a complicated one with zones of large deformation being followed by zones of small deformation. This is observed in the present experiments from the direction of motion of individual particles. Their motion changes from one parallel to the hopper walls into one which is in the radial direction.

The observations revealed quite different behaviors for sand and glass beads. The flow field of sand is not uniform and has lines of velocity (or displacement) discontinuity. Glass beads, on the other hand, have a smooth and well defined flow field. The qualitative recordings of the wall stress for sand fluctuate with time. This is in contrast with the ones for glass beads which are fairly uniform except for very small particle sizes.

The flow field in a hopper without a vertical bin would presumably be different from the one observed in the present experiments. It has been observed by Drescher et al [24] that the complicated deformation pattern exists only near the free surface of the material in the hopper (see Fig. 3.1a). Near the hopper exit, the motion is in the radial direction with the material having a more or less uniform void fraction. The geometry of the analytical solution is usually a hopper without a vertical bin. The flow field is therefore similar to that observed by Drescher et al [24]

and the assumptions being made may be valid near the hopper exit.

The analytical expression of the mass flow rate is independent of the head of the material in the hopper when it is of the order of a few times the value of the exit diameter. This implies that the conditions near the hopper exit are more important than those near the top of the hopper in determining the mass flow rate. Since the actual flow field near the exit is more or less similar to the one assumed in the analytical solution; the agreement between the computed and measured values of the flow rate is justified. In summary, even though the assumed flow field is not valid near the bin/hopper corner, it may be reasonable at points near the hopper exit. For this reason, the computed flow rates are in relatively good agreement with the measured ones.

TABLE I

Material Properties (*)

Material	Bulk Specific Gravity	Mean Diameter mm	Internal Friction Angle (°)	Wall Friction Angle Lucite Wall (°)	Wall Friction Angle Al Wall (°)
P0170	1.46	0.325	24.6	15.3	17.7
P0280	1.48	0.59	24.3	14.4	15.1
V070	1.71	1.32	26.8	14.2	15.1
Sand No. 1	1.56	0.223	24.1	20.2	-
Sand No. 2	1.30	0.317	30.7	17.9	-
Sand No. 3	1.53	0.68	30.6	14.4	24.5

(*) These measurements were made by Pearce [71]

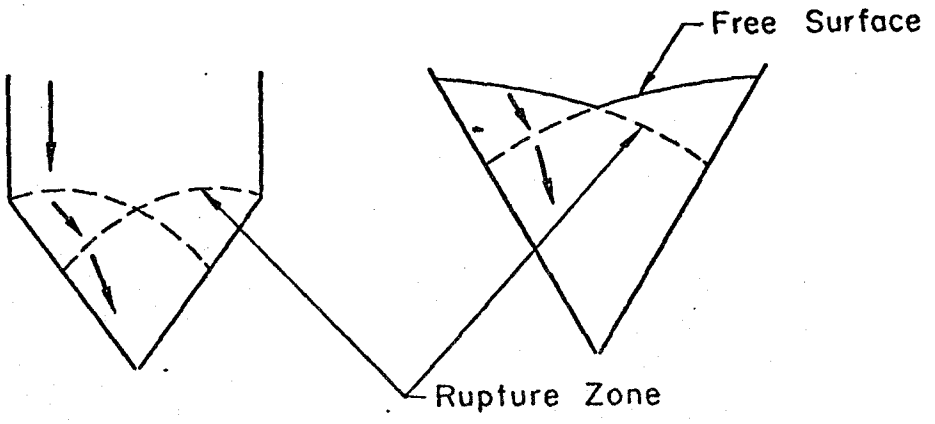

(a)

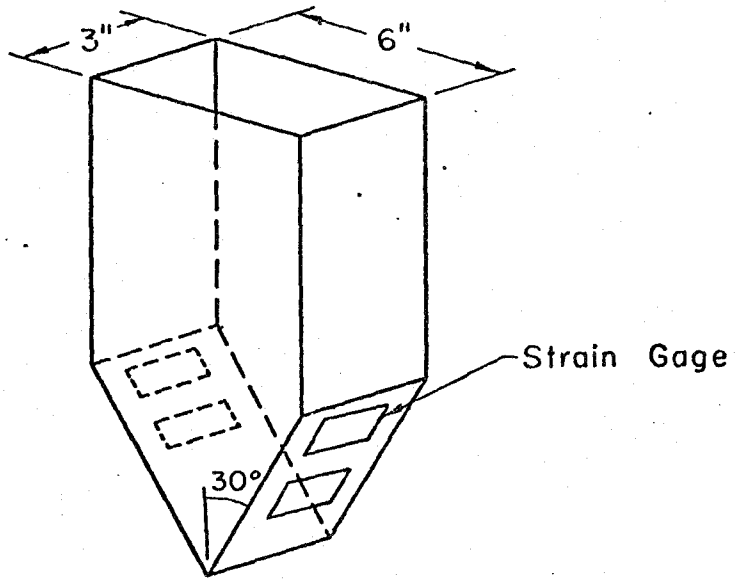

(b)

Figure 3.1 Experimental observation of the flow field in hoppers. (a) geometry of the rupture zones in hoppers with and without a vertical bin, (b) the apparatus used in the present experiments showing the location of the strain gauges.

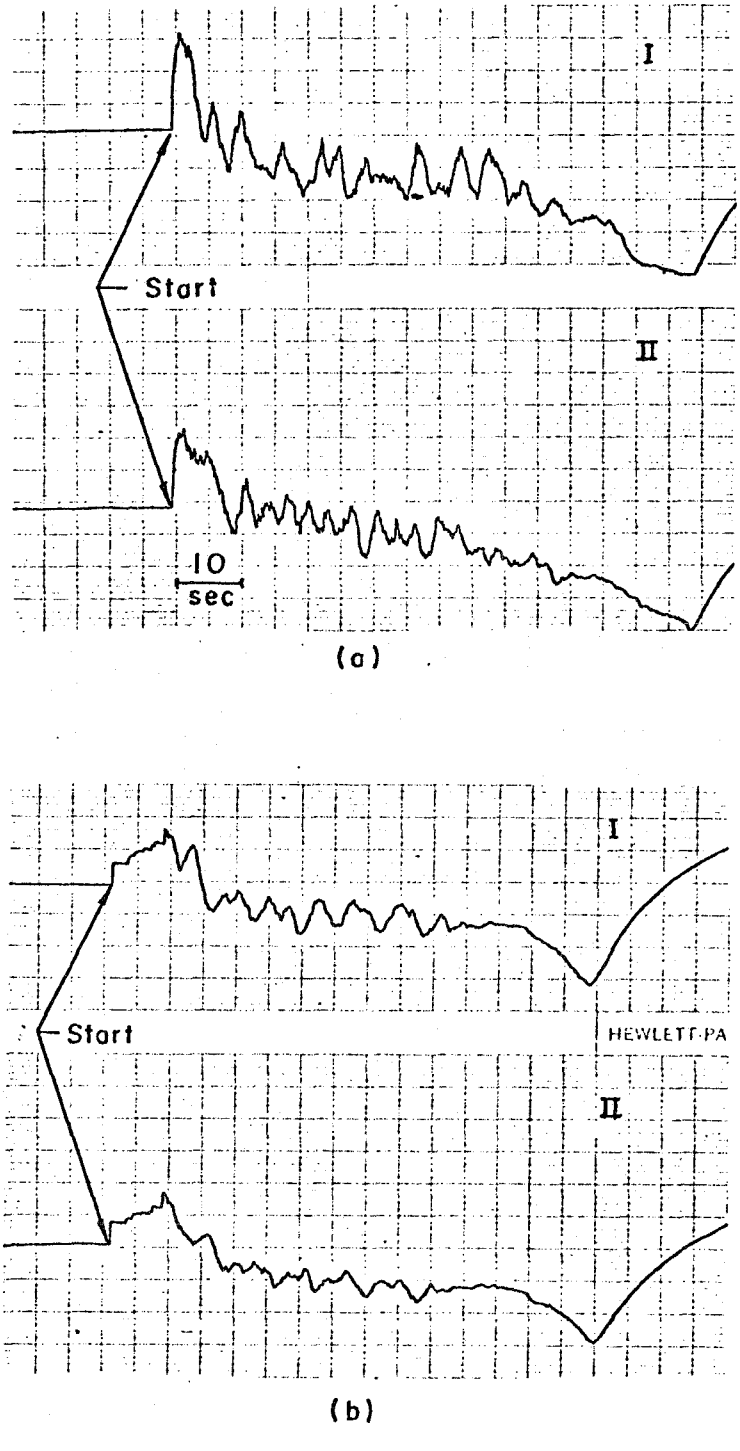

Figure 3.2 Qualitative recording of the wall stress at the bin/hopper transition corner. The materials are sand No.4 (a) and sand No.3 (b).

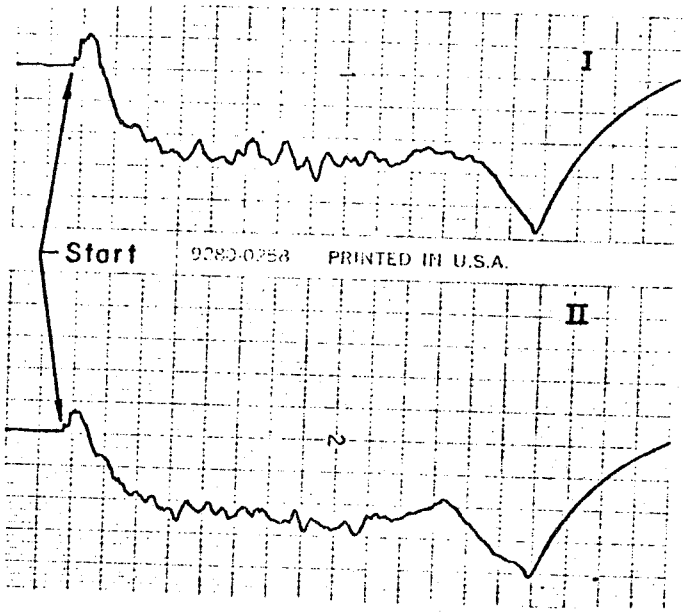

(a)

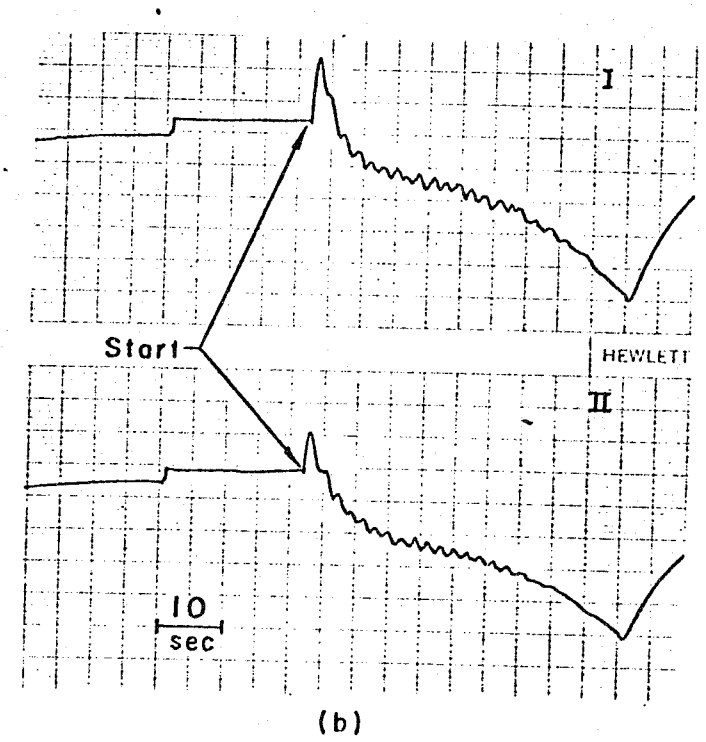

(b)

Figure 3.3. Qualitative recording of the wall stress at the bin/hopper transition corner. The materials are sand No. 2 (a) and glass beads P0170 (b).

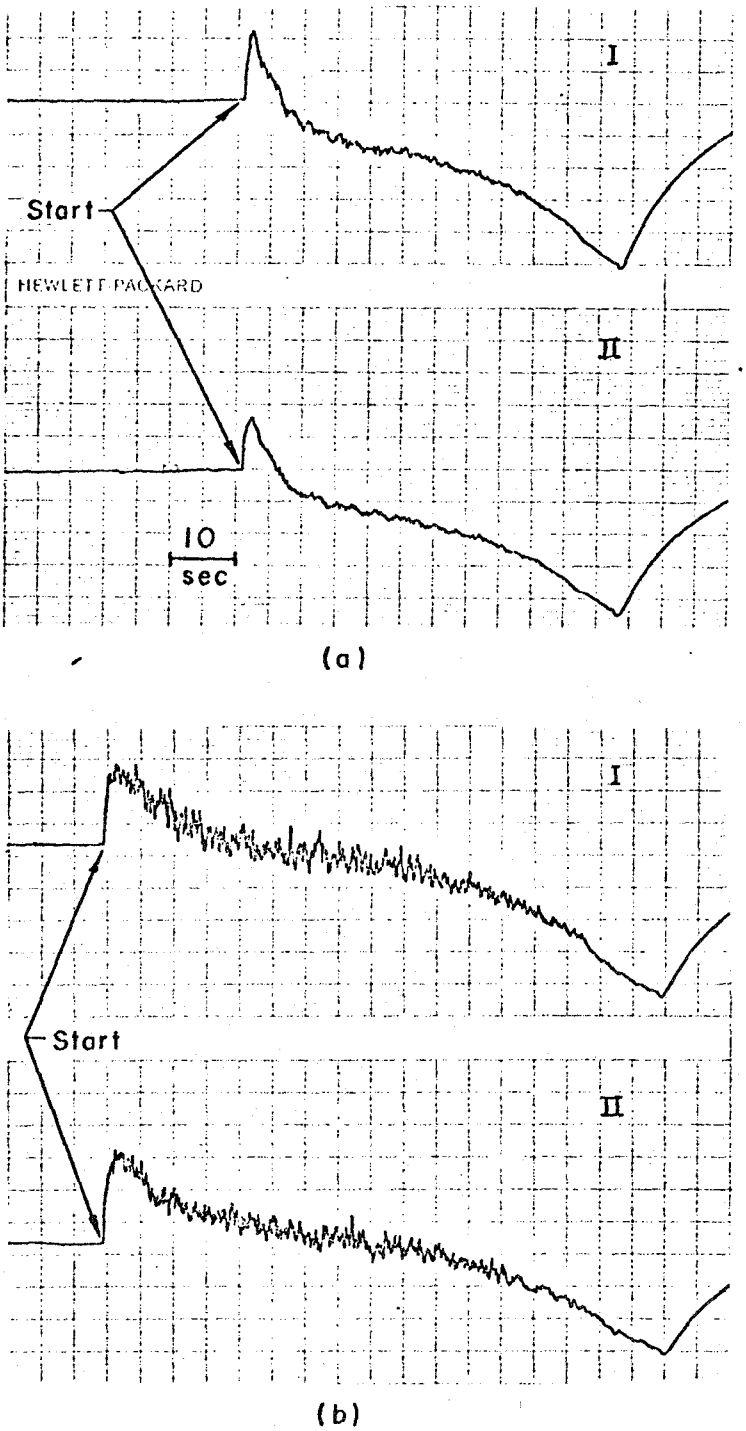

Figure 3.4 Qualitative recording of the wall stress at the bin/hopper transition corner. The materials are glass beads P0280 (a) and V070 (b).

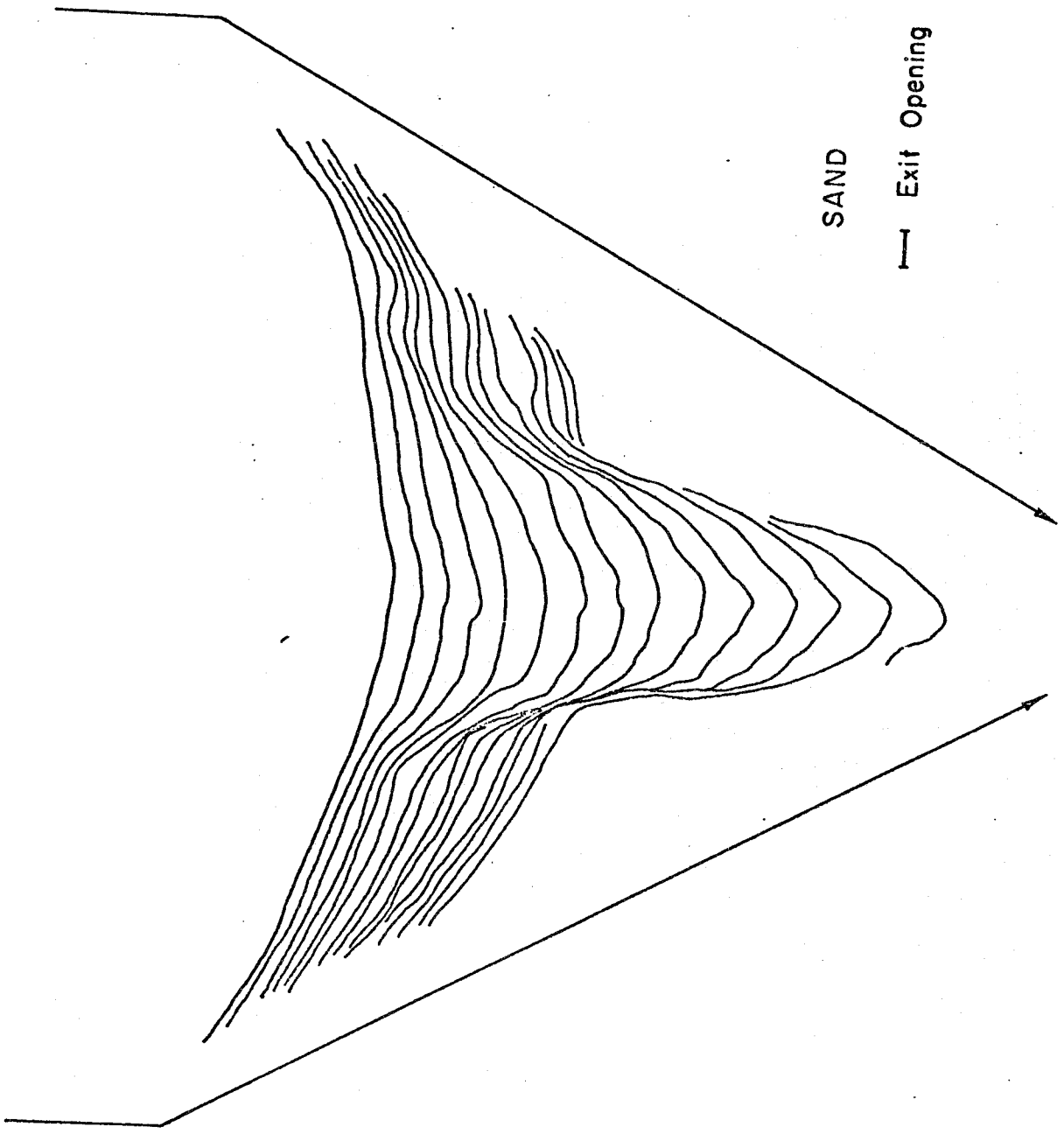

Figure 3.5 Deformation pattern of a layer of colored sand No.3 as it is moving through the hopper. The time interval between each line is 0.3 sec.

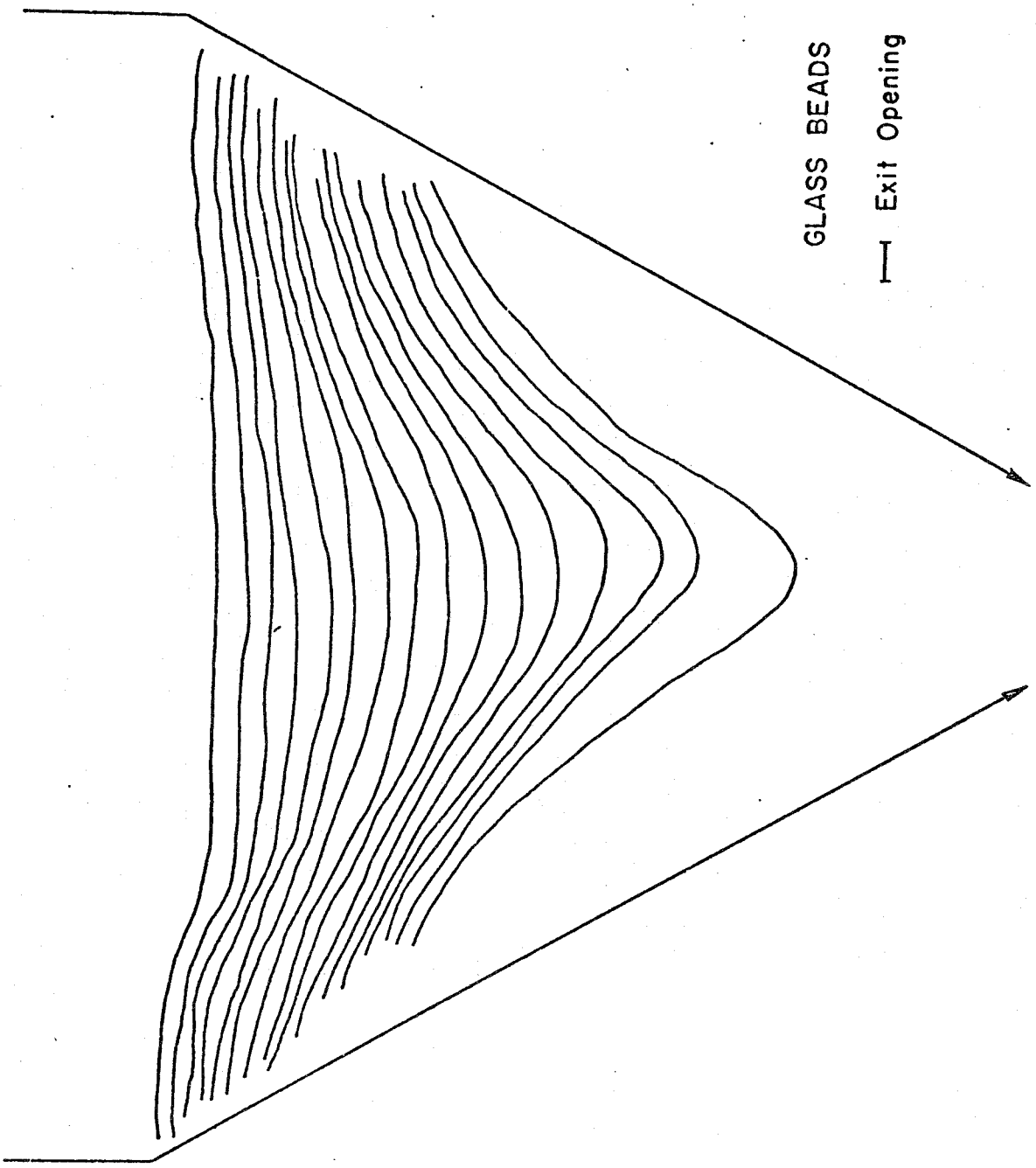

Figure 3.6 Deformation pattern of a layer of colored glass beads (P0280) as it is moving through the hopper. The time interval between each line is 0.3 sec.

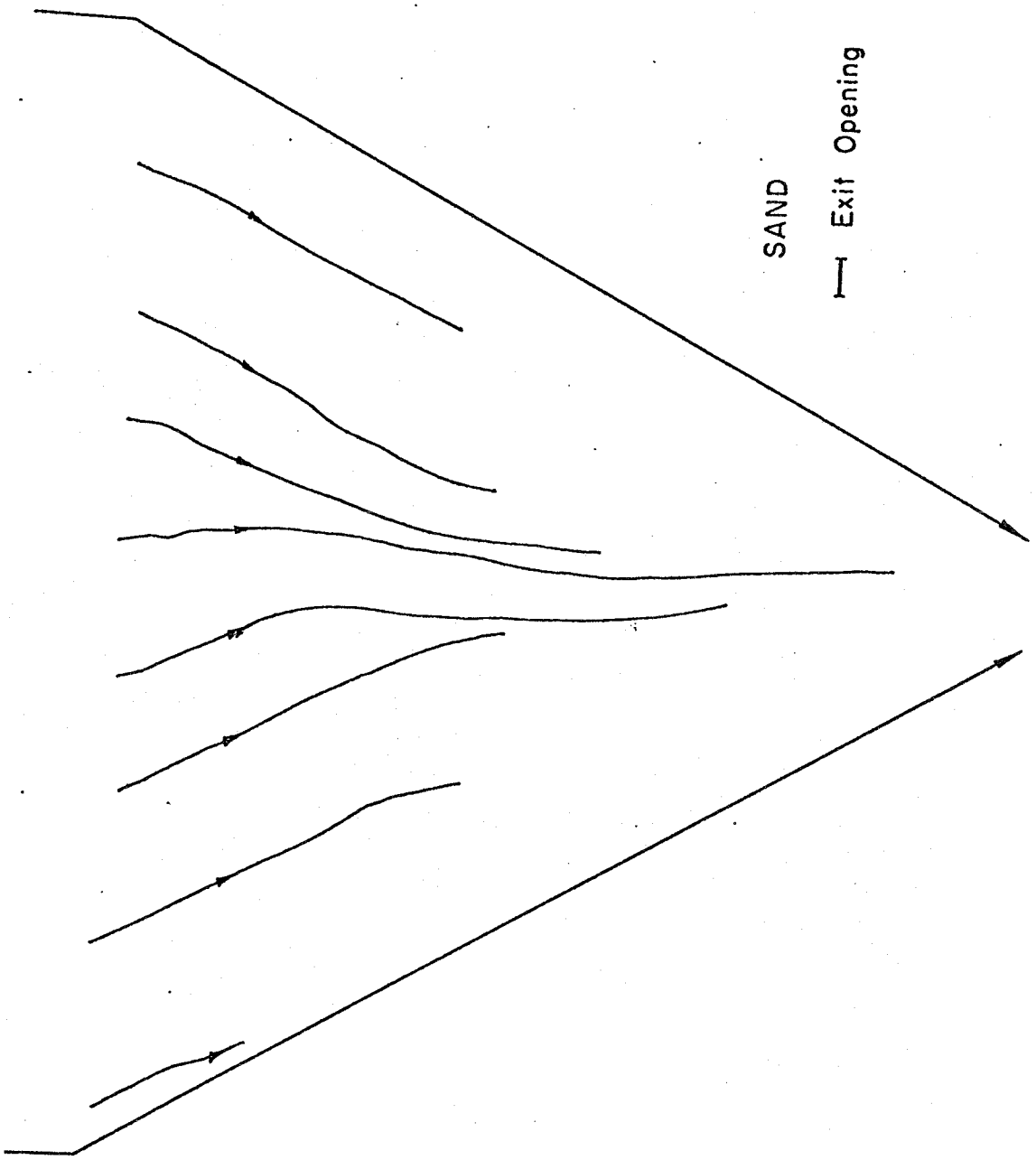

Figure 3.7 Pathlines of individual particles of sand No. 3 which start to flow at the same time from different positions in the hopper.

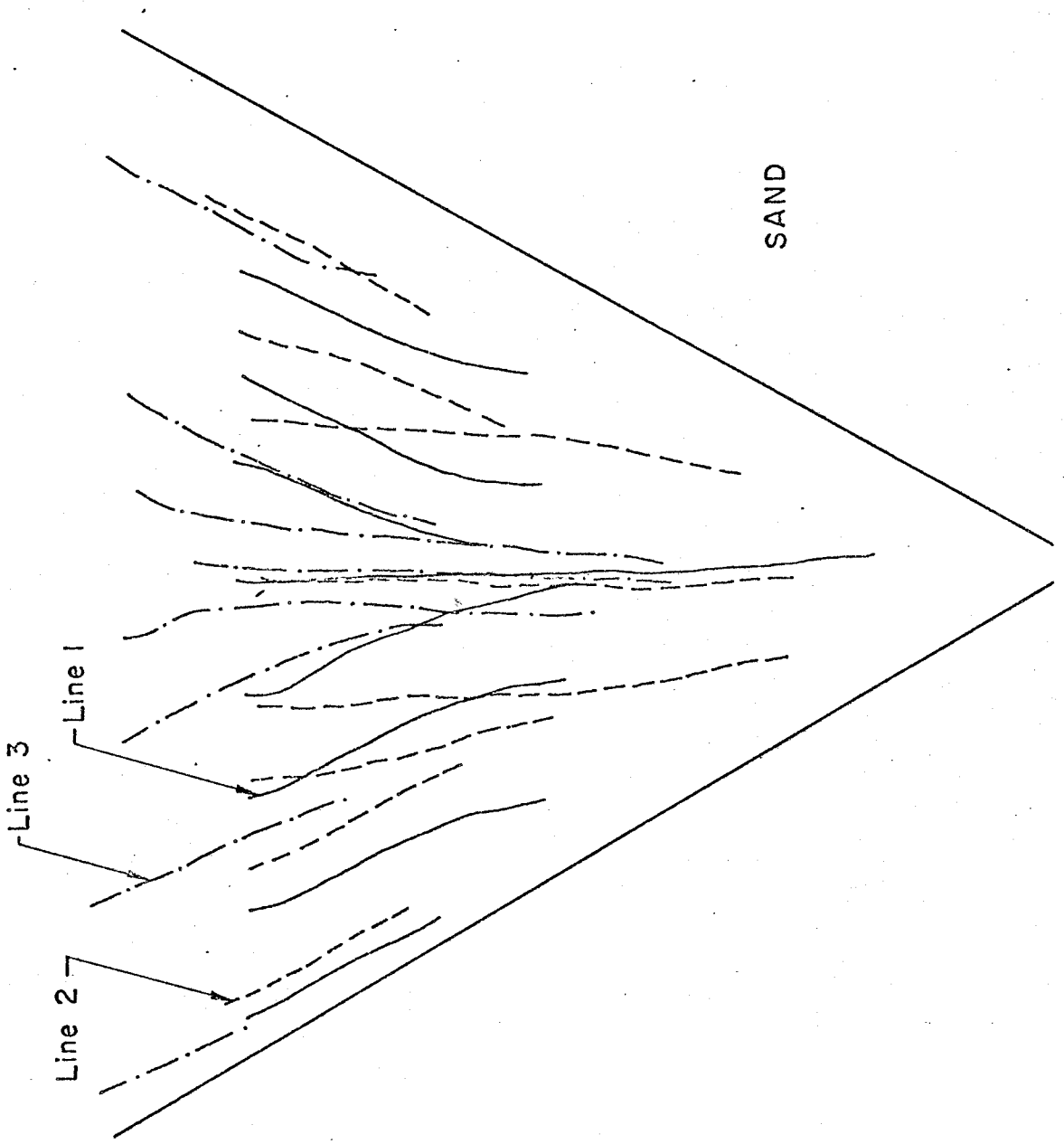

Figure 3.8 Superposition of the pathlines of individual particles of sand No.3 which flow at different times in the hopper.

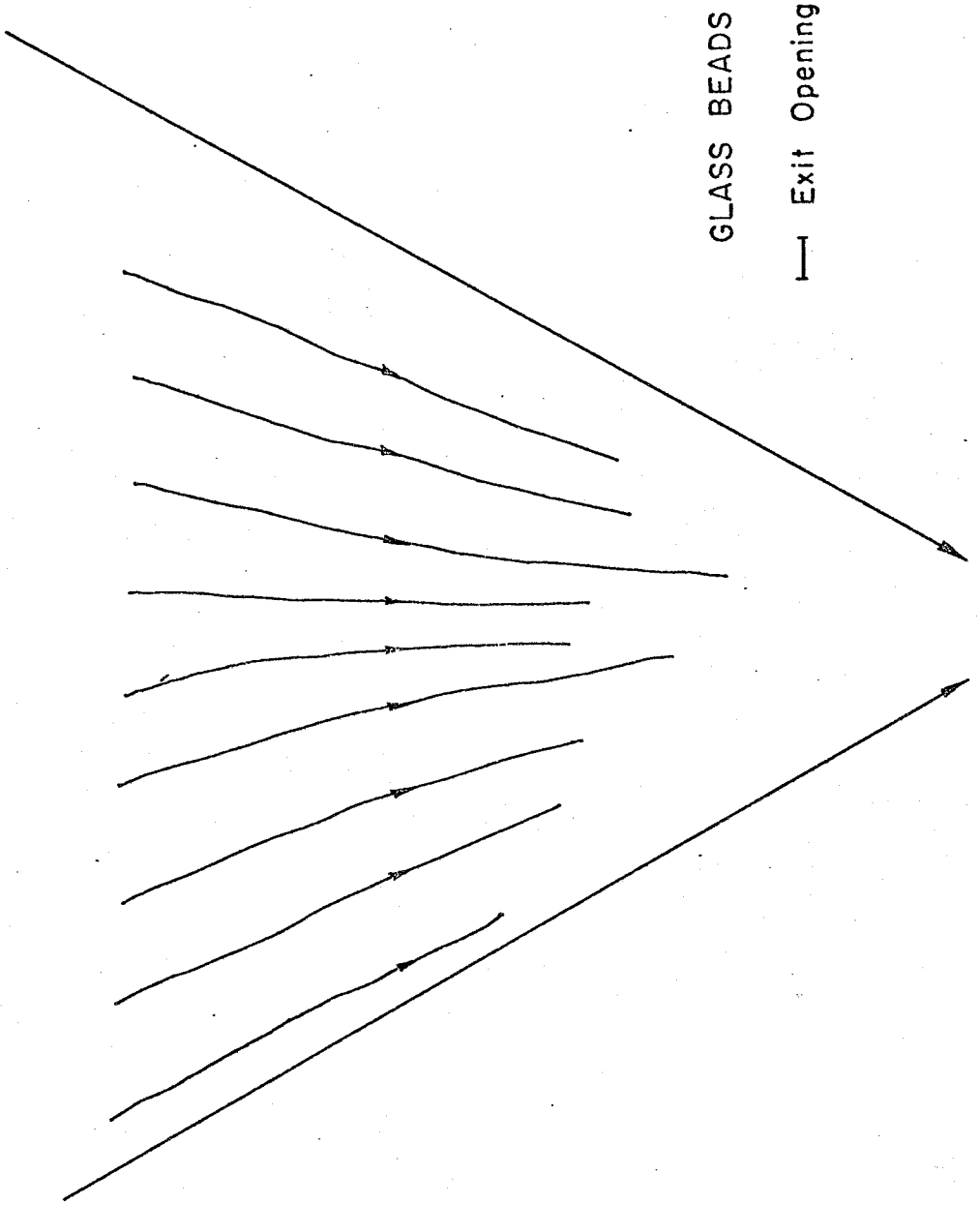

Figure 3.9 Pathlines of individual particles of glass beads (P0280) which start to flow at the same time from different positions in the hoppers.

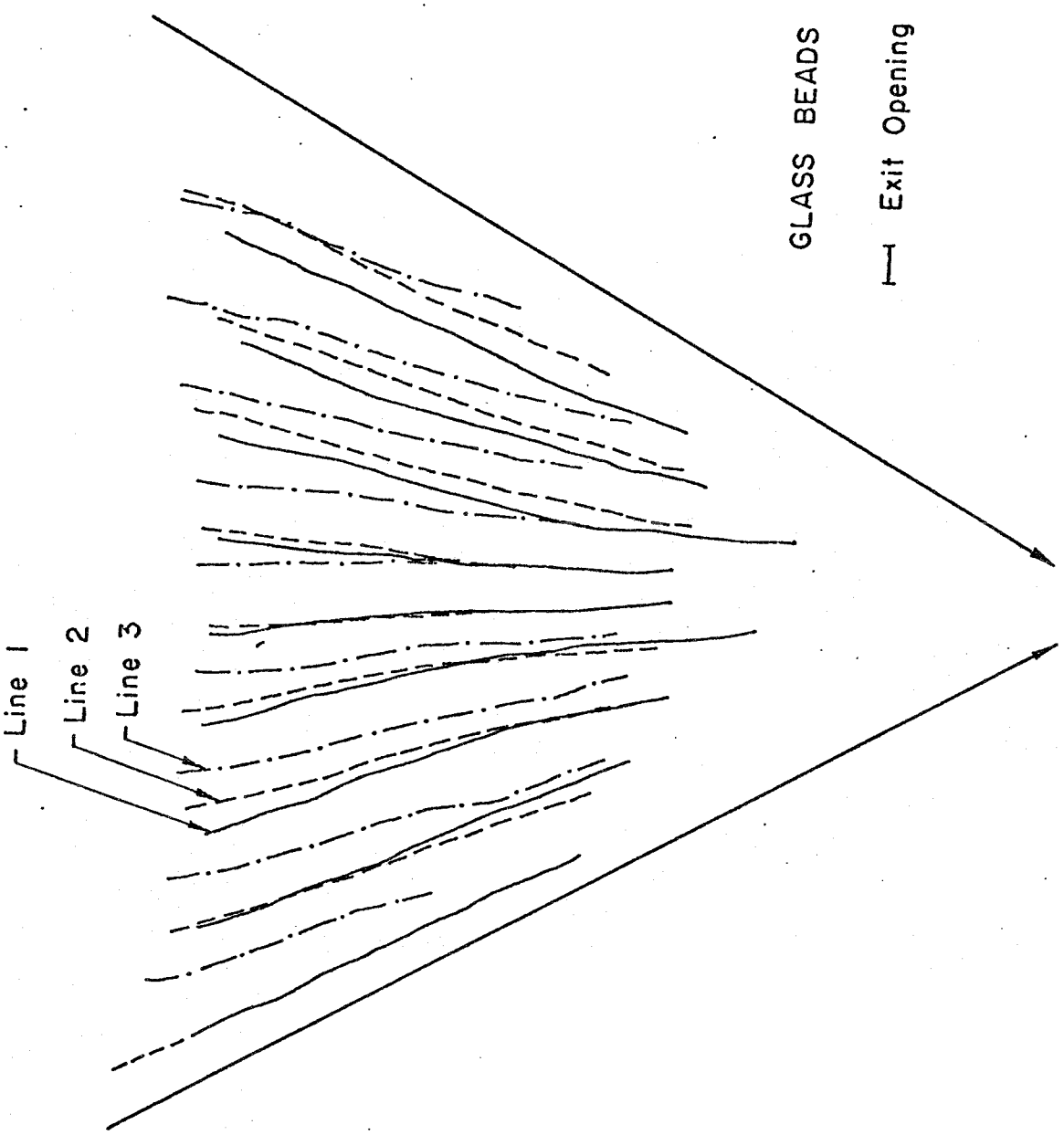

Figure 3.10 Superposition of the pathlines of individual particles of glass beads (P0280) which flow at different times in the hopper.

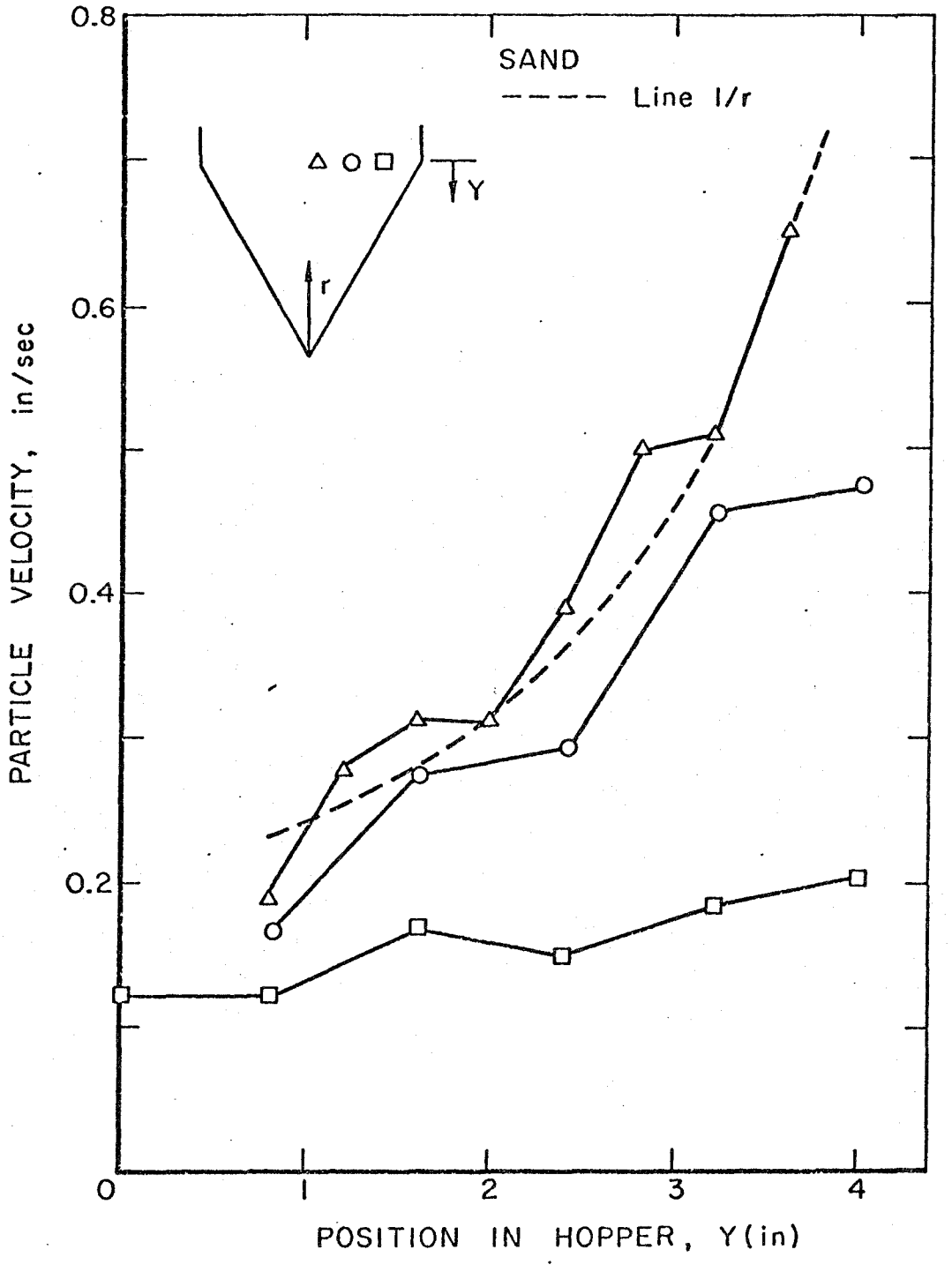

Figure 3.11 Velocity of sand No. 3 at different positions in the flow field.

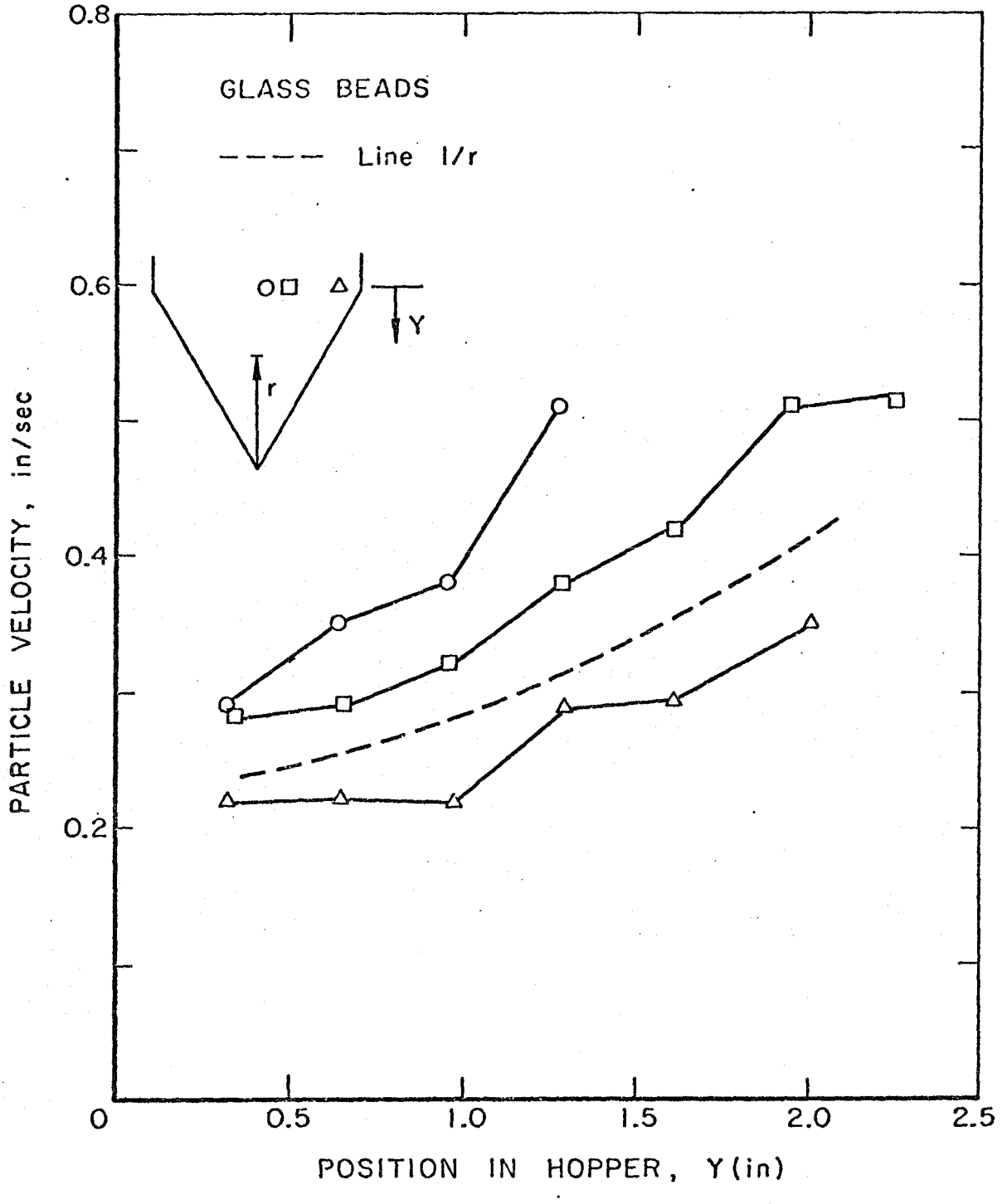

Figure 3.12 Velocity of glass beads P0280 at different positions in the flow field.

CHAPTER 4

FUNNEL FLOW IN HOPPERS

4.1 INTRODUCTION

In the previous chapters, the flow in hoppers was considered under conditions for which all of the material in the hopper was flowing. This type of flow has been called "mass flow". There also exists a flow condition for which a part of the material remains stagnant. The moving material creates a channel which often has a shape similar to that of a funnel and flow with stagnant regions is, therefore, termed funnel flow. Funnel flow is generally undesirable particularly when the materials are subject to deterioration or spoilage.

For the design of hoppers it is, therefore, essential to know just what the parameters are which determine the type of flow in a hopper and what the magnitude of these parameters has to be to assure mass flow. In the design of hoppers, the ability to guarantee mass flow may be even more important than the ability to predict the flow rate, and this problem is addressed in the present chapter.

In this chapter, the flow field in a two-dimensional wedge shape hopper is observed experimentally. The different types of flow which exist in the hopper are defined and the transitions from one type of flow to another are investigated. The shape of the boundary between the moving and stagnant material is recorded and its dependence on the hopper geometry is described.

4.2 BACKGROUND

Funnel flow hoppers have received very little attention in the past. Most of the efforts were understandably directed toward determining the limits of the hopper geometry for which stagnant material begins to appear in the flow field.

O'Callaghan [65] observed two types of funnel flow in flat-bottom bins. In one type of flow, called the "deep bin flow", the stagnant material is present only near the bottom of the bin. In the other type of flow, "shallow bin flow", there is a stagnant layer of material next to the bin walls which extends to the free surface of the material in the bin. The existence of these types of flow depends on the head H of the material in the bin. O'Callaghan described the boundary of the flowing central core as a logarithmic spiral. Gardner [31] measured the boundary of the funnel in a plane hopper. Since his apparatus was built with rough walls, he observed a stagnant layer near the corner between the hopper and the vertical walls even at low wall angles. The funnel shape was observed to be independent of the hopper angle. Brown and Richards [11] studied the kinematics of the discharge of granular materials from flat-bottom bins. They defined the angle of approach β which the funnel makes with the vertical at the exit and observed that the value of β in a plane hopper is greater than that in an axisymmetrical one. Wieghardt [110] claimed that the angle of approach β must be the same in both plane and axisymmetrical flows. He distinguished two cases depending on whether the stress at the hopper bottom is independent of the height of the material in the bin or not. In the first case, β is equal to $90° - \alpha$ where α is the angle of repose of the material and in the second

case, β is equal to $45° - \alpha/2$. The experimental data of Brown and Richards [11] lie between these limits. Other authors (Toyama [102], Levinson et al [56]) have mentioned the existence of stagnant material in the flow field without studying the details of funnel flow regime.

Experimental observations of the flow field in axisymmetric hoppers and bins have been conducted by a number of investigators. The main difficulty here is to observe the flow field without disturbing it. A number of investigators used markers placed at different locations in the hoppers and noted the order in which these markers were discharged from the hopper to obtain an approximate picture of the flow field. Van Zanten [104] used the markers method in conical hoppers and observed the two types of funnel flow defined by O'Callaghan [65]. Observations of axisymmetric flow fields using the marker method were also conducted by McCabe [57]. A second method of studying the flow field is to follow the path of radioactive tracers imbedded in the granular material. The signal emitted by the tracers will give information on the displacement of the material in the hopper. This method was used by McCabe [57]. Another method used by Giunta [34] and Johanson [51] consists of looking at the flow pattern by stopping the flow during discharge. As the bin is tilted into a horizontal position, the material on the top half of the bin is removed and observation is made on the mid-plane of the bin. Giunta [34] observed the funnel boundary in the bin by this method and found that it is independent of the flow rate of the material from the bin.

Jenike [42] studied the conditions on the hopper geometry for which mass flow would occur. By balancing the stress at the exit against the strength of the material, he derived an upper limit of the hopper

angle θ_w which would give mass flow in the hopper. A minimum size of the exit opening D is required to avoid arching of the material. The design criteria are then given in terms of the hopper angle θ_w and the exit opening D. Despite a number of studies which have questioned the validity of these limits, (Walker [107], Eckhoff [27], Wright [114]), the results have been used extensively in the past twenty years for the design of hoppers and bins.

The main objective of the present investigation was to study the dependence of the flow field in the hopper as a function of its geometry. The hopper geometry is therefore varied extensively and the flow fields related to the effect of each individual dimension of the hopper. The effects of different material properties are also studied.

4.3 THE EXPERIMENTS

The experiments were conducted in a plane, wedge shape hopper and the results are presented in two parts:

a) In the first part, the different flow regimes which exist are noted as a function of the hopper geometry. The apparatus has a vertical bin on top of the hopper and it will be shown that other parameters in addition to the hopper angle θ_w and the exit opening D are needed to completely define the flow field in a hopper.

b) In the second part, the shape of the funnel which exists in the hopper is recorded as a function of the hopper geometry.

4.3.1 Experimental Apparatus

The experimental set up as shown in Fig. 4.1 consists of a plane hopper and a supply bin. The hopper is made of lucite and the flow field is observed through the front wall. It was built such that all the dimensions could be varied independently. The walls are set into position by clamping them together; they can be moved to any desired position.

In the experiments, the hopper walls were set at angles θ_w from 15° to 90°; the width W of the vertical walls was varied from 17.8 cm (7") to 33 cm (13") and the width D of the exit opening was set at values up to 3.8 cm (1.5 cm). In tests where the height H of the material in the bin has to be kept at a fixed value, a supply bin is provided on top of the hopper. Most of the observations were done in hoppers having a thickness of 15.25 cm (6"). However, some of the tests were also conducted in hoppers with thickness of 7.6 cm (3") and 22.9 cm (9") in order to assess the effect of the front and back vertical walls. Finally, a series of experiments were conducted in hoppers with rough inclined walls and smooth vertical walls to observe the effect of inclined wall roughness on the flow field.

4.3.2 Granular Materials Used

The four materials used in the experiments are sand, glass beads, polystyrene pellets and rice; their shape ranges from spherical (glass beads) to elongated (rice). They are practically cohesionless and their grain size distributions are fairly uniform. Their physical properties, measured according to the procedures described by Pearce [71], are shown in Table I. In Table I, the internal friction angle of polystyrene is highest ($\varphi = 39°$) while the value of glass beads is the lowest ($\varphi = 25°$).

The high value of the internal friction angle of polystyrene is surprising because its wall friction angle is quite low. A possible explanation is that its particle size is large and it has the shape of a pellet; this may have impeded the shearing along the plane of the shear cell. In this respect one would expect that the friction angle of rice should reflect the effect of its elongated shape.

4.3.3 Experimental Procedures

1. Flow Regimes Observations.

During each test, the hopper is set at a fixed value of θ_w, W and D (see Fig. 4.2) while the height H of the material in the bin is changing. As the material is discharged, the flow regime which is present is observed; any transition from one type of flow to the other is noted and the value of H at the transition is recorded.

At each value of θ_w, two values of D and three values of W are used and the tests are repeated for eight values of the hopper walls angle θ_w. The tests with sand are done in hoppers with thickness of 7.62 cm (3") and 15.2 cm (6").

2. Funnel Boundary Observation

When stagnant material is present in the flow field, the boundary between the flowing and stagnant material is well defined and long time-exposure photographs of the flow field are taken to record its shape.

The tests were done with various values of W, D, H and θ_w taken in various combinations in order to study their individual effect on the funnel shape. The tests with sand were also done with two hopper thicknesses (7.62 cm and 15.2 cm). In these experiments, the material in the hopper was loosely packed. A tighter packing could be obtained

by tapping the hopper walls after loading. Some limited observations with tighter packing indicated results similar to those for loose packing.

4.4 RESULTS AND DISCUSSION

The main conclusions of the present study are that the flow field in the hopper can be classified into three different types and that the occurrence of each type of flow depends strongly on the hopper geometry. The results also show that a transition from one type of flow into another always occurs at some critical condition of the hopper geometry. These observations could be useful in the design of hoppers and bins since they clearly defined the necessary conditions on the hopper geometry in order to obtain a given type of flow field.

4.4.1 Flow Regimes in Hoppers

The observed flow regimes are classified as type A, B or C flows. They are shown in Fig. 4.2 and in Appendix A.

Type A flow is known as the mass flow regime. It is usually observed in hoppers at high values of H/W and/or low values of the wall angle θ_w. The flow field of a mass flow hopper has the whole mass of granular material moving without any stagnant material. Mass flow hoppers have many desirable properties in the handling and storage of bulk solids and they have been the subject of many investigations (Jenike [42]).

The flows which are designated as type B and C flows are part of what is known as the funnel flow regime. In this type of flow, stagnant material is present in the flow field with the moving material forming a flowing central core.

In type B flow, the stagnant material appears only near the

hopper/bin transition corner (see Fig.4.2). It is called the "stagnant corner" flow and it usually occurs at large hopper angles θ_w and high values of H/W. Finally, type C flow has a stagnant layer of material next to the hopper walls which extends to the free surface of the material in the bin. Type C flow occurs at large values of the wall angle θ_w and low values of H/W. At intermediate values of θ_w, type C flow also occurs for a range of values of H/W.

In the lower part of the hopper near the exit, the stagnant material may end at a merge point S which is some distance from the edge of the exit opening. The material will slide along the wall below this merge point S. Consequently, mass flow is present in a localized region near the exit of the hopper. In this respect, two subtypes of flows B and C are defined (see Fig.4.2). The subtypes B2 and C2 have a merge point S on the hopper wall while in the subtypes B1 and C1 the merge point coincides with the edge of the discharge.

4.4.2 Transition of the Flow Field in Hoppers

In this section, the transition between the different types of flow and the dependence of the flow patterns on the hopper geometry will be discussed.

At each value of the hopper angle θ_w, the type of flow which is present depends on the ratio H/W of the height of the material in the vertical bin and the width W of the vertical walls. As the ratio H/W decreased to some critical value, the flow field will undergo a transition from one type of flow into another one. The nature of the transition (from type A to type C or type B to type C) depends on the value of θ_w.

Figure 4.3 is a plot of the critical ratio H/W against the ratio

W/D at given values of θ_w for sand. The experimental data fall around two critical values of H/W depending on the hopper angle θ_w. At large values of θ_w (greater than 70°), the transition occurs at a ratio H/W around 1.5 and the transition is from type B flow into type C flow. At hopper angles lower than about 60° the transition is from type A flow into type C flow. The same plot for glass beads, shown in Fig. 4.4, exhibits a similar behavior. The main observation which can be made from Figs. 4.3 and 4.4 is that the critical ratio H/W at the transition is more or less independent of the ratio W/D. The characteristics of the flow field can therefore be better illustrated by plotting this critical ratio H/W against the hopper angle θ_w. Such a plot will map the different types of flow present in the hopper as a function of its geometry (θ_w and H/W).

Figure 4.5 shows the flow map of sand in a hopper with smooth walls. The critical values H/W fall close to the lines in this figure. For example, a hopper with a hopper wall angle θ_w equal to 60° yields mass flow (type A) at large values of H/W. If H/W is decreased to a value of about 1 there is a transition into funnel flow of type C. As the ratio H/W is further reduced to about 0.5, a second transition from type C flow into type A flow will occur. Similar interpretations can be made at other hopper angles θ_w. Figures 4.6 to 4.8 are the flow maps for the other three materials.

The flow map of each material can be better understood if the possible values of θ_w from 0° to 90° are divided into three intervals from 0° to θ_{w_1}, from θ_{w_1} to θ_{w_2} and from θ_{w_2} to 90°. The values of θ_{w_1} and θ_{w_2} are functions of the frictional properties of the materials.

They are shown on Table I for the four materials used in the experiments. When θ_w is between $0°$ and θ_{w_1} mass flow (type A) occurs in the flow field independently of the ratio H/W. For values of θ_w between θ_{w_1} and θ_{w_2}, a dual transition behavior is observed. There is first a transition from type A flow into type C flow at some critical ratio $(H/W)_1$. This is followed by a second transition from type C flow into type A flow at a lower critical ratio $(H/W)_2$. Finally, for values of the hopper angles θ_w greater than θ_{w_2}, the transition in the flow field is from type B flow into type C flow with stagnant material being always present in the flow field. It should however be mentioned that some non-uniqueness can occur when the wall angles are close to the angles θ_{w_1} and θ_{w_2}; different flow regimes histories can result for nominally identical tests.

The flow map indicates that the complete geometry of the hopper/bin system is important in determining the flow regimes which are present in a given hopper. The common practice of using only values of θ_w and D as the only relevant dimensions would give a very incomplete picture of the flow field. This can be seen clearly in the flow maps in Figs. 4.5 to 4.8. The broken lines on these figures represent the ratio H/W in a hopper without vertical side walls for large values of W/D. This line is observed to lie in the mass flow (type A) region even at intermediate values of the hopper angles (between θ_{w_1} and θ_{w_2}) where funnel flow is known to occur. The flow field in a hopper without vertical side walls would therefore exhibit mass flow regime until a large wall angle is reached.

In addition to the hopper geometry, the material properties will certainly play a role in determining the flow pattern. Particles with an

elongated shape seem to align themselves in the direction of the flow and this may affect the flowability of the material. Such a dependence on the material properties is reflected in the values of θ_{w_1} and θ_{w_2} for the different granular materials used. The higher the friction angle of the material, the lower the values of θ_{w_1} and θ_{w_2} will be. Except for glass beads, the values on Table I substantiate this. The flow map of glass beads indicates that funnel flow tends to appear at lower values of θ_w and this is inconsistent with their low frictional properties. This behavior could be due to the small grain size of this material which is about 300μm. In this range of grain size, the interstitial air may affect the discharge of the material from the hopper. This has been shown by Crewdson and Nedderman [16] who observed that the interstitial air is important when the particle diameter is less than 500μm.

The transition of the flow field probably results from the change in the stress pattern in the bin. As the material is being discharged, the stress in the bin changes from a depth independent distribution into a depth dependent one. At the critical value of the height H of the material in the bin, the condition on the matching of the stresses at the hopper/bin corner may have caused the transition of the flow field.

4.4.3 Comparison to Other Studies

Funnel flow has been observed by a number of investigators (Toyama [102], Levinson et al [56], Van Zanten [104]). However, the conditions under which either type of funnel flow would occur have not been determined. The experiments conducted by O'Callaghan [65] resemble the present experiments most closely. Since his experimental apparatus is a flat-bottom bin, the transiton of the flow field is from

type B flow into type C flow. O'Callaghan measured critical values of H/W equal to 1.47, 1.49 and 1.77 for wheat ($\varphi = 32°$), barley ($\varphi = 38°$) and fertilizer ($\varphi = 42°$) respectively. These values are shown in Figs. 4.5 and 4.6. The values of H/W and W/D in which the experiments of Gardner [31] and Levinson [56] were conducted are indicated in Fig. 4.3. These points do not refer to critical values but to regimes of operations. Gardner's photographs provide clear confirmation that his flows were of type B. Levinson's values of H/W are marginal and this is reflected in the fact that the flow of clover seeds tended toward type B whereas the flow with sand, having a larger internal friction angle, is closer to type C. Though Brown and Richard [11] did not give the dimensions of their apparatus, their value of H/W appears to be about 1.5 and flows of type C were observed for a large number of granular materials. In Toyama's [102] experiments flows of type B were encountered with large values of H/W of 10 and 6.5. Jenike [42] proposed two limiting values of the hopper angle θ_w. The first one, defined as the smaller of $(90° - \delta)$ or $60°$ where δ is the wall friction angle, is the maximum theoretical value of θ_w for which mass flow would occur in the hopper. The second limit is a lower value of θ_w which is recommended to be used in the design of hoppers "in order to prevent the development of excessive non-flowing regions on the sides and at the top of a bin"(Jenike [42]). The first is a theoretical limit obtained for the flow in hoppers without a vertical bin. The second limit is obtained from the experimental observation of the flow field in a hopper with vertical side walls. These limits correspond to the angles θ_{w_1} and θ_{w_2} observed in the present study. Johanson and Colijin [52] introduced the minimum value of the height H of the material in the bin which would

yield mass flow in a hopper at a given wall angle θ_w. These conditions are obviously introduced to avoid the funnel flow of type C which exists in the flow field at intermediate values of the hopper angles (i.e. for values of θ_w between θ_{w_1} and θ_{w_2}).

Finally, it is also worth mentioning that trends similar to those reported above for plane hoppers also appear to occur in axisymmetrical hoppers. Van Zanten [104] and Giunta [34] observed flows of type C in conical systems with values of H/W of 2.57 and 1.33 respectively. On the other hand, Novosad and Surapati [64] obtained flows of type B for H/W ranging from 4 to 8. McCabe [57] observed a change in the flow field for values of H/W of about 2. Thus, it would appear that conical hoppers exhibit results qualitatively similar to those reported here for wedge-shaped hoppers and that the critical value of H/W is between 2 and 3 depending on the properties of the material.

4.4.4 Variation of Funnel Shape

When the hopper is operating in the funnel flow regime, the boundary between the flowing and stagnant material is no longer a simply determined quantity. The study of the flow field will then depend on the understanding of the behavior of this boundary as a function of the material properties and hopper geometry.

Funnel shapes for types B and C flows will be plotted in a non-dimensional coordinate system. The lengths are divided by the bin half-width, W/2, and the origin of the coordinate system is at the edge of the exit opening (see Fig. 4.1). Thus, the funnel shapes of types B1 and C1 flow pass through the origin while the funnel shapes of types B2 and C2 flow end at a merge point S in the figures. The location of this merge point S on the hopper walls depends on both the hopper

geometry and material properties. Figure 4.9 shows the plot of S/W versus θ_w for various materials used. The non-dimensionalized distance S/W is more or less independent of the dimensions D and H of the hopper and appears to be a function mainly of θ_w.

1. Funnel Shape of Type B Flow in Hoppers with Smooth Walls

The funnel shape of type B flow is understood to be independent of the height H of the material in the bin provided that H is sufficiently large. The hopper dimensions which may affect the shape of the funnel boundary are the wall angle θ_w, the width W of the vertical walls and the exit opening D.

Figure 4.10 shows the funnel shape at various values of the exit opening D at a hopper angle equal to 80°. It can be seen that the dimensionless boundary of the funnel is independent of D. In a dimensional coordinate system, the funnel boundary is displaced by the same distance in the direction that the exit opening is changed. The width W of the vertical walls is also changed in Fig. 4.10 which shows that the non-dimensionalized shape also seems to be independent of the bin width W. Finally, the plot of the funnel shape as a function of the hopper wall angle as shown in Fig. 4.11 does not indicate a strong dependence on θ_w.

The observation of the funnel shape of the type B flow indicates that, as far as we can tell, the funnel shape is independent of the hopper geometry. Figure 4.12 shows the funnel shapes of the four materials used in the experiments flowing in hoppers with similar dimensions. The dependence of the funnel boundary on the material properties is not very strong.

2. Funnel Shape of Type C Flow in Hoppers with Smooth Walls

The four materials used exhibit similar behavior in type C flow.

In the following, the discussion will be illustrated with the results using sand; however, it should be stressed that the results for other materials are very similar.

The occurrence of funnel flow of type C at each value of θ_w depends on the value of H/W. As H/W is decreased, the flow in the hopper will change from type A or type B flow (depending on the hopper angle θ_w) into type C flow. The funnel shape might therefore be expected to exhibit a dependence on the ratio H/W. In Fig. 4.13, the funnel shapes at values of H/W ranging from 0.7 to 1.47 are plotted. They fall along two distinct curves depending on whether H/W is greater than 1 or less than 1. At values of H/W greater than 1, the funnel shape is wider and is approaching the shape of type B flow. The value of H/W equal to 1 can be considered to be the limit with regard to the variation of the funnel shape. For values of H/W less than 1, the funnel shape is truly of type C flow and it is more or less independent of the values of H/W. Figure 4.14 shows the funnel shape for various hopper angles, θ_w. The only noticeable difference between the various funnel boundaries is in the location of the merge point S. As the wall angle θ_w is reduced, the merge point is moved away from the edge of the exit opening and the funnel shape is shifted outward closer to the vertical walls. The behavior of the funnel shape at various values of the exit opening D is similar to the observations made with the type B flow. The funnel boundary is essentially independent of D as shown in Fig. 4.15. This is valid as long as the ratio D/d of the exit opening to the particle diameter is sufficiently large. In Fig. 4.16, the funnel boundary of polystyrene when D is equal to 1.3 cm (0.5") deviates

considerably from the boundaries at larger values of D; this difference comes mainly from the effect of the particle size on the flow field. Finally, Fig. 4.17 presents the funnel shapes when W and D are varied for the same values of H and θ_w. The results seem to confirm that the funnel boundary is independent of W/D. The greatest discrepancy occurs with the boundary when H/W = 1.17 and this may represent the beginning of the transition to type B flow.

Since flow of type C is observed to occur after a transition from type A or type B flow, it is interesting to see whether the funnel shape depends on the nature of the transition of the flow field or not. The funnel shapes in Fig. 4.14 for wall angles less than 60° have arisen after a transition from type A flow while the other shapes have followed a transition from type B flow. The only difference between these funnel shapes is in the location of the merge point S. Otherwise, they seem to be independent of the past history of the flow field.

The funnel shape also depends on the frictional properties of the material. Since the material next to the hopper walls is stagnant in funnel flow of type C, the wall friction angle is important only in determining the location of the merge point S and the funnel shape depends mainly on its internal friction angle. The curvature of the boundary, especially near the exit, is presumably a function of the internal friction angle. Figure 4.18 shows the funnel shape of the four materials flowing in hoppers with similar dimensions. There is a difference between the funnel boundary of polystyrene and the other three materials. This may represent the effect of the material properties.

3. Comparison to Other Studies

The funnel shape of the flow corresponding to our type B was studied by Gardner [31]. Since his apparatus has rough walls, the funnel shape is narrower than the one observed in the present experiments as shown in Fig. 4.19. The funnel boundaries of type B flow recorded by O'Callaghan [65] are compared to the shapes observed in the present experiments in Fig. 4.20. The funnel boundaries correspond well to each other with the only difference being manifest in the location of the merge point S.

4.4.5 Effects of the Front and Back Walls

While the flow field in a two-dimensional plane hopper can be observed most easily through transparent front or back walls, an appropriate question which is often raised is whether the flow field is truly in a plane strain condition. A true plane flow condition cannot exist due to the presence of the front and back walls of the hopper. However, as the thickness of the hopper is increased, the flow field is expected to approach a limiting behavior where the effects of the front and back walls are much reduced. Bosley et al [4] and Brown and Richard [11] studied the effect of the front and back walls and found that they will not change the qualitative behavior of the material flow even though their velocity near the walls is substantially less than that in the center.

The effect of the front and back walls was studied in the present experiments by comparing the observations made in hoppers with different thicknesses. Hoppers with thickness of 7.6 cm (3") and 22.9 cm (9") were used in addition to the 15.2 cm (6") thick hopper whose results were presented above.

Figure 4.21 shows the flow map of sand in a 7.6 cm thick hopper. It is very similar to the flow map shown in Fig. 4.5 for sand flowing in a 15.2 cm thick hopper. The three types of flow are present and the transition from one type of flow into another one is well defined. However, the flow field in the 7.6 cm thick hopper has a greater tendency to exhibit stagnant regions. The funnel shapes for sand flowing in hoppers with three thicknesses are compared in Fig. 4.22. The funnel shapes for the two large thicknesses (15.2 cm and 22.9 cm) are close to each other. The funnel shape of the hopper with the smallest thickness (7.62 cm) seems significantly narrower throughout its length.

It may therefore be tentatively concluded that the friction of the vertical front and back walls begins to alter the flow regime and the funnel shape when the ratio b/W of the hopper thickness b to the width W of the vertical walls is less than 0.5.

4.4.6 Effects of Wall Roughness

It was envisaged that the wall roughness would affect the value of the wall friction angle and therefore the flow in the hopper. As the wall becomes rough, the motion of the particles next to the wall is impeded until a stagnant layer of material is formed next to the wall. The wall friction angle is then equal to the internal friction angle and the wall is called fully rough. This is an advantage of using rough walls in experiments since they eliminate the uncertainty in the value of the wall friction angle.

A number of investigators have conducted experiments in hoppers with rough walls to compare the results with those obtained in tests done in hoppers with smooth walls. In the present study, the

experiments with sand were repeated in a hopper with rough inclined walls and smooth vertical walls. Experiments in which the vertical walls are also rough are discussed later. The roughness of the walls is obtained by depositing a layer of sand on the wall covered by a double-stick tape (Savage [86]).

When the wall is rough, there is a thin layer of material near the wall which is stagnant. A new type of flow then occurs at small values of the hopper angle θ_w. In this type A′ flow, the stagnant material forms a thin and uniform layer along the hopper walls as shown in Fig. 4.26. The effect of the wall roughness is then to increase the friction angle along the hopper walls. Funnel flows of type B and C are also observed with the same characteristics as defined in Section 4.4.1.

Figure 4.23 shows that the flow map in a hopper with rough walls is quite different from that in a hopper with smooth walls (see Fig. 4.5). At small values of θ_w, the flow field is of type A′ flow with a transition to type C flow occurring at some critical value of the ratio H/W. At wall angles larger than 40°, the transition is from type B into type C flow. This limit is about 20° less than the value observed in a hopper with smooth walls.

Funnel shapes of types B and C flows in hoppers with rough inclined walls are shown in Figs. 4.24 and 4.25. The funnel boundaries are almost independent of the hopper geometry and the behavior is quite similar to that in hoppers with smooth walls. The comparison of the funnel shape in hoppers with smooth and rough walls, shown in Figs. 4.24 and 4.18, indicates that the main difference between the two flows is in the location of the merge point S.

When the vertical walls are also rough, the stagnant layer of material is observed to extend from the free surface of the material in the bin to the edge of the discharge opening. The funnel is narrower than that observed when the vertical walls are smooth and type A′ flow is not observed even at low values of the wall angle θ_w. This observation differs from that made by Gardner [31]. In his experiments, the thickness of the stagnant layer along the vertical walls is very thin.

The effect of the wall roughness on the flow field is to increase the tendency of stagnant material to appear in the flow field and to reduce the range of mass flow operation of the hopper.

4.4.7 Mass Flow Rate in Hoppers With Smooth and Rough Walls

The effect of the wall roughness on the flow field of granular materials in hoppers has an effect upon the mass flow rate. A number of investigators (Bosley et al [4], Savage and Sayed [86]) have found that the discharge rate out of a hopper with rough walls is greater than that out of a hopper with smooth walls when the wall angle θ_w is greater than some critical value. This is contradictory to one's expectation since wall roughness virtually always increases the wall friction angle and reduces the discharge rate.

This same behavior was also recorded in the present experiments as shown in Fig. 4.27. However, it can be partially understood by observing the flow field in hoppers with smooth and rough walls as shown in Fig. 4.26. The flow field in a hopper with rough walls varies as a function of the hopper angle θ_w in the following fashion. At low hopper angles (when θ_w is less than about 37°) the flow field is of the type A′. The effect of the wall roughness is to increase the wall friction angle

and to reduce the mass flow rate below that for a hopper with smooth walls. As the wall angle θ_w is increased, stagnant material begins to appear in the flow field and extends to the edge of the exit opening (see Fig. 4.26). The material is then flowing in an effective hopper whose geometry is more or less independent of the angle at which the hopper walls are set. The discharge rate depends only weakly on the hopper wall angle. In a hopper with smooth walls, the flow field changes from type A into type C2 and type C1 as the wall angle θ_w is increased. For hopper angles up to 85°, the material near the exit is sliding along the hopper wall and the discharge rate depends on the hopper wall angle θ_w (see Fig. 4.26). At intermediate hopper angles ($37° \leq \theta_w \leq 85°$), the discharge rate from a hopper with smooth walls is less than that from a hopper with rough walls because the effective hopper angle is less for the rough walled hopper than for the smooth walled hopper. At large hopper angles, the merge point S for the smooth walled hopper is moved to the edge of the exit opening and the flow is of type C1 (see Fig. 4.26). The measured flow rate from a hopper with smooth walls should then approach that for a hopper with rough walls as shown in Fig. 4.27.

The effect of the wall roughness on the flow rate is therefore a consequence of its effects on the flow field. It may also be concluded that the rate of discharge from hoppers depends mainly on the condition near the exit and the location of the merge point S is a characteristic of the condition of the hopper wall.

4.5. Analytical Studies of Funnel Flow Regime

4.5.1. Background

In the analytical study of funnel flow in hoppers, the number of

unknowns are increased since the geometry of the flow field is not defined. The validity of such analyses depends on their ability to describe the observed phenomena such as the transition of the flow field and the shape of the funnel. A number of attempts have been made to study these phenomena; however, the presence of the new unknowns necessitate the introduction of assumptions about the flow field.

O'Callaghan [65] studied the transition phenomena using the stress distribution in the bin. He wrote the equilibrium equation in a cartesian coordinate system as

$$\frac{\partial \sigma_y}{\partial y} + \frac{\partial \sigma_{xy}}{\partial x} = \rho g$$

$$\frac{\partial \sigma_x}{\partial x} + \frac{\partial \sigma_{xy}}{\partial y} = 0 \qquad (4.1)$$

Where y is in the vertically downward direction and x is in the horizontal direction. By assuming a form of the shear stress $\sigma_{xy} = axy$ and using the symmetry of the stress field, he derived the expressions of σ_y and σ_x as

$$\sigma_y = \rho g y - \frac{a}{2} y^2$$

$$\sigma_x = f(y) - \frac{a}{2} x^2 \qquad (4.2)$$

The function $f(y)$ is defined with the use of the ratio $K = \sigma_x / \sigma_y$. O'Callaghan postulated that the transition from type B flow into type C flow would occur when the coefficient of friction $\mu_w = \sigma_{xy} / \sigma_x$ reaches a maximum. The depth y_0 at the transition is therefore obtained

from the relation $d\mu_w/dy\big|_{y_0} = 0$. This solution yields some predictions which compare well with his experimental results, however, it involves assumptions which are hard to appreciate. For example, by taking the stress σ_y to vary quadratically with the depth y, the validity of the solution is restricted to very small values of y since σ_y is known to vary exponentially with y in a shallow bin. The main assumption that the transition would occur at the point where the coefficient of friction is at a maximum is not based on any physical model. While it is true that the stress field is changed from a depth-independent into a depth-dependent distribution at the transition, there is no explanation as to why the coefficient of friction should go through a maximum at that location.

Jenike [44] considered the balance of the force in the vertical direction across the plane of the transition corner between the hopper and the vertical bin. In Ref. 44, a condition is given for the determination of whether flow of type A or C will prevail. Implementation of this condition requires the comparison of a quantity q_H for the hopper with a value q_B for the bin. The appropriate choice of q_B depends on whether the material is in a passive or active state. Hence it probably depends implicitly though not explicitly on the geometry H/W, W/D etc.

When the hopper is being operated in the funnel flow regime, the boundary between the stagnant and flowing material must be determined as a part of the solution of the flow problem. The presence of a new unknown in the problem necessitates the introduction of new conditions on the boundary between the stagnant and flowing material in order to complete the mathematical problem.

O'Callaghan [65] empirically correlated the funnel shape as a logarithmic spiral. This is an extension of the results obtained in soil mechanics where failure lines have a curved shape which is approximated by a logarithmic spiral (Sokolovskii [92]). The funnel boundary is therefore represented by $r = r_0 \exp(\theta \tan\varphi)$ where the constant r_0 and the origin of the spiral are specified by the geometry of the bin. This logarithmic spiral describes the funnel shape in a shallow bin (type C1 flow) very well. However, the shape of the funnel boundary in a deep bin (type B1 flow) is not as well represented. A possible explanation is that the geometry and mechanism in a shallow bin approaches more closely the phenomena which are occuring in the earth pressure problem in soil mechanics. This similarity was mentioned by Brown and Richard [11] who referred to the work of Airy in which he computed the angle θ_m of the plane along which a wedge of material near a vertical wall would slide (see Fig. 4.28a). The value of θ_m is obtained by maximizing the value of the horizontal force P which the wall exerts on the material and it is given by

$$\tan\theta_m = \tan\varphi \sqrt{\frac{\tan\varphi \sec^2\varphi}{\tan\varphi + \tan\delta}} \qquad (4.3)$$

It is interesting to observe that Eq. (4.3) which is for a plane flow condition gives values of θ_m which are actually closer to the experimental measurements of the angle of approach of an axisymmetrical flow field than to those for a planar flow field.

Gardner [31] divided the stress field of type B flow into three parts (see Fig. 4.28b). In the upper part above line OB, the material

is in a plastic state and the stress distribution is independent of the depth of the material in the bin. The equilibrium equation would then give the values of the mean stress σ and the stress angle ψ along OB (which is a stress characteristic). In the lower part of the hopper near the exit, represented by the region OCDO in Fig. 4.28b, the material is assumed to be in a radial stress state as proposed by Jenike [42] and Sokolovskii [92]. The mean stress σ and the stress angle ψ along the stress characteristics OC is therefore defined. Finally, the stress field in the region OBCO in Fig. 4.28b is computed numerically from the data along the characteristics OB and OC and the boundary BC of the flow is taken to be a stress characteristic of the same family as OC. A comment which can be made about this solution is that the funnel boundary BC depends on the wall angle θ_w; on the other hand, the experimental observations of BC are more or less independent of θ_w (see Fig. 4.29). A possible explanation is that the stress characteristic OC may not be well defined at large hopper angles. As the hopper angle is increased, point O is moved farther away from the hopper exit and the validity of the assumption of a radial stress field in OCDO is questionable. Jenike [43] and Johanson [51] have shown that the convergence of a radial stress state occurs only at points very close to the hopper exit. Finally, Gardner experimented with a hopper with rough inclined and vertical walls because he believed that under these conditions the wall friction angle is defined and equal to the internal friction angle. However, as discussed in Section 4.4.6, the presence of roughness on the hopper wall will not only change its frictional properties but it may also change the behavior of the layer of stagnant

material. It is thus unjustified to believe that one can describe funnel flow in a hopper with smooth walls simply by specifying a value of the wall friction angle different from the internal friction angle. More specifically, while no stagnant material would be present in the flow field of a hopper with smooth walls at small values of $\theta_w (\theta_w \approx 10°)$, Gardner's solution still gives a boundary BC of the flow field. His solution may therefore be valid only for hoppers with rough walls.

Giunta computed the boundary of the funnel of type C flow in an axisymmetric flat-bottommed bin. His solution is based on two major assumptions proposed by Jenike [42] and Johanson [51]. The first assumption claims that a radial stress state exists in the flowing channel near the discharge and the second assumption claims that the boundary of the funnel coincides with a velocity characteristic (see Fig. 4.28). The value of the funnel angle β is obtained from the radial stress solution such that the stress angle ψ_w along the boundary is equal to $3\pi/4$. Some empirical conditions are introduced in order to obtain a unique value of β. The solution gives values of β ranging from 12.5° to 1.5° for values of the internal friction angle ranging from 30° to 60°. This solution uses some assumptions which are difficult to justify. The funnel shape, which is divided into a conical part with a vertical bin, is at best an approximation of the actual boundary. Secondly, it is hard to appreciate the conditions used to obtain the value of β apart from the fact that they guarantee a unique value of β. This approach was used to solve for the funnel shape in a plane hopper during the present study. However, it was found that it does not give a possible value of β for all values of φ.

4.5.2. Present Study

In the present study, two attempts have been made to analyze funnel flows.

The first is an attempt to describe the transition of the flow field (A-C and B-C transitions). The solution relies mainly on the suggestion made by Jenike [44] concerning the balancing of the forces in the vertical direction at the transition between the hopper and the vertical bin. Jenike [44] claimed that the peak stress at the bin/hopper corner comes from the difference between the vertical force Q_H in the hopper and the one in the vertical bin, Q_B. When the hopper is in the funnel flow regime, this peak stress is damped out. The difference $Q_B - Q_H$ changes from a positive value into an unknown one as the flow field changes from mass flow into funnel flow. At the transition between the types of flow, he assumed that $Q_B = Q_H$.

The force Q_H is computed from the radial stress solution by integrating the vertical stress across the width of the hopper. It is given by the formula

$$Q_H = q\rho g W^{2+m} b^{1-m} \tag{4.4}$$

where q is a constant

ρg is the bulk gravity force

W is the bin diameter for a cylindrical bin or the width of the bin for a plane hopper

b is the thickness of a plane hopper

m is equal to 0 for a plane flow and 1 for an axisymmetric flow.

The force Q_B is obtained from the stress distribution in the vertical bin. Using the Janssen expression of the wall stress and the ratio k of the stresses in the vertical and horizontal directions, an expression of Q_B is obtained as

$$Q_B = (\frac{\pi}{4})^m \rho g W^{2+m_b} 1-m \left(\frac{1 - e^{-\lambda h/W}}{\lambda}\right) \tag{4.5}$$

where

$\lambda = 2(1+m)K \tan \delta$

$K = \sigma_v/\sigma_h$

h is the height of the material in the vertical bin.

For plane flow, the condition $Q_B = Q_H$ gives an expression of the critical ratio h/W as

$$(\frac{h}{W})_{cr} = - \frac{1}{\lambda} \ell n(1 - \lambda q) \tag{4.6}$$

The total head of the material above the hopper exit is then equal to

$$(\frac{H}{W})_{cr} = (\frac{h}{W})_{cr} + \frac{1}{2} \cot \theta_w \tag{4.7}$$

A number of comments can be made about this solution. First, the stress distribution in the vertical bin is obtained from the Janssen expression and gives only the lower limit of the stresses. Secondly, the ratio $K = \sigma_v/\sigma_h$ is not very well defined as discussed by Sundaram and Cowin [97]. The following results are computed using Eq. 4.7 and a value of K equal to 0.4.

Material	φ (°)	δ (°)	θ_w (°)	Transition Type	H/W from (4.7)	H/W from expt.
Sand	30	15	50	A-C	1.14	1
Sand	30	30	>70	B-C	1.58	1.5
Polystyrene	39	12	50	A-C	0.87	1.1
Polystyrene	39	39	>60	B-C	2.1	1.3

The computed results show some agreement with the experimental measurements. However, it cannot constitute proof of the correctness of the approach due to the uncertainties in the somewhat heuristic model used.

The second solution consists of an attempt to compute the angle of approach β of the funnel boundary. It considers the flow field near the merge point S at which the funnel ends along the hopper wall. A polar coordinate system with its origin at the merge point S is then introduced and the region in the immediate vicinity of S is considered. The resulting geometry of the problem as shown in Fig. 4.30 consists of two regions. In region I, the material is flowing while it is in an undeformed state in region II. The line $\theta = \theta_1$ is the boundary between the flowing and the stagnant material.

For given values of θ_1 and the friction angles δ_0 and δ_1 along $\theta = 0$ and θ_1, the solution in region II is obtained by solving the elastic equilibrium equations. The solution in region I is obtained by solving the equilibrium equations with the stress components satisfying the Mohr-Coulomb yield condition. Since θ_1 is a line of discontinuity in the flow field, the normal and shear stresses on both sides of the line must

balance (Schofield and Wroth [87]). The stress components in region I along θ_1 are then known and the equations can be integrated from θ_1 to $\theta = \pi$.

The wall friction angle δ_2 along $\theta = \pi$ is obtained from Coulomb friction as

$$\delta_2 = \arctan\left(\frac{\sigma_{r\theta}}{\sigma_{\theta\theta}}\right)_{\theta=\pi}$$

The value of δ_2 is a function of θ_1 for given values of δ_0 and δ_1.

Although it seems to be straightforward, the solution has some inherent computational difficulties and a solution has not yet been obtained.

4.6. CONCLUDING REMARKS

In the present study, the various types of flow which exist in a hopper with a vertical bin have been identified and classified. The experimental observations show that the presence of the vertical bin will cause funnel flow to occur at lower values of the hopper wall angle θ_w. The ratio of the height of the material in the bin to its width (H/W) is important in determining the type of flow which is present and the transition from one type of flow into another.

The non-dimensionalized funnel boundary is found to be independent of the hopper angle θ_w, the width of the exit opening D and the width of the vertical bin W. It is mainly a function of the material properties. Some changes in the flow field due to the proximity of the front and back walls are observed when the hopper thickness falls below a certain limit. Finally, the presence of the wall roughness affects the flow field of the

hopper by causing stagnant material to appear at lower values of θ_w. This change in the flow field is responsible for the fact that the rate of discharge from a hopper with rough walls is actually slightly higher than that from a hopper with smooth walls when the hopper wall angle θ_w is greater than a certain limit.

An attempt to study the funnel flow phenomena analytically has been made. However, the solution has some inherent difficulties which remain to be studied.

TABLE I

Material Properties

Material	Bulk Specific Gravity	Mean Diameter mm	Internal Friction Angle (°)	Wall Friction Angle Lucite Wall (°)	Wall Friction Angle Al Wall (°)	θ_{w_1} (*) (°)	θ_{w_2} (*) (°)
Sand	1.5	0.5 -1	31	15	18	40	70
Polystyrene	0.56	0.25-0.39	39	12	17	35	60
Glass Beads	1.46	0.325	25	15.3	17.7	30	50
Rice	0.8	-	30	-	-	55	70

(*) Values of θ_{w_1} and θ_{w_2} are for a smooth walled hopper with a thickness equal to 15.2 cm.

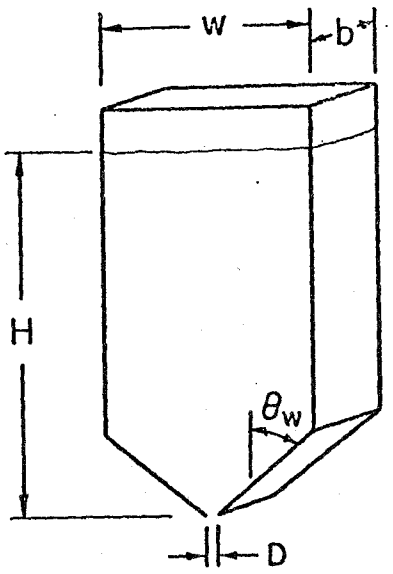

$$0.25 < \frac{b}{w} < 0.75$$

$$0.82 < \frac{H}{w} < 1.5$$

$$8 < \frac{w}{D} < 16$$

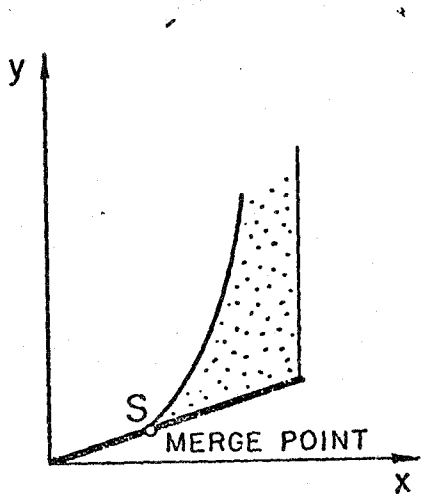

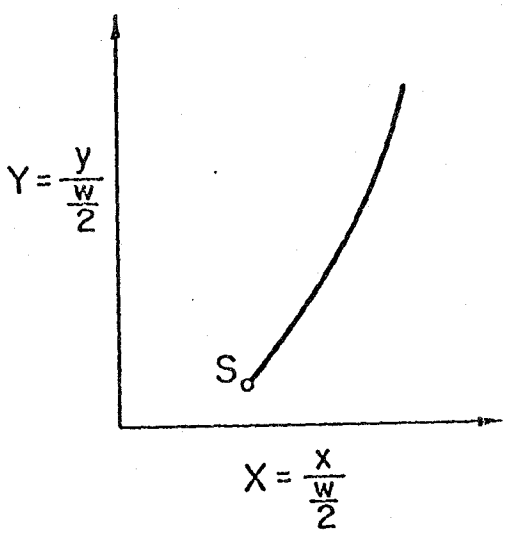

Figure 4.1 Geometry of the experimental apparatus (a), the observed funnel boundary and its representation in a non-dimensionalized coordinate system (b).

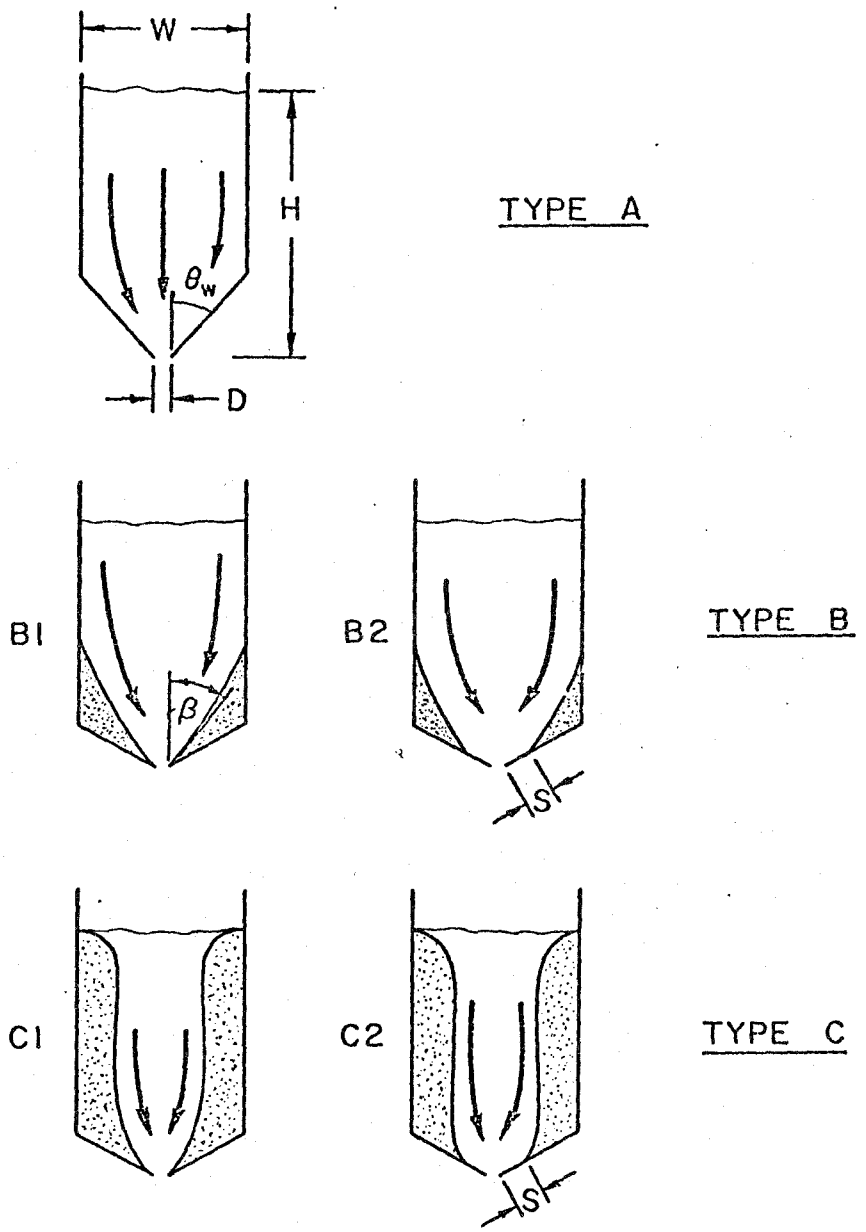

Figure 4.2 Schematic indicating the different flow patterns observed. Type A is mass flow. Type B has a stagnant corner and Type C has stagnant side walls.

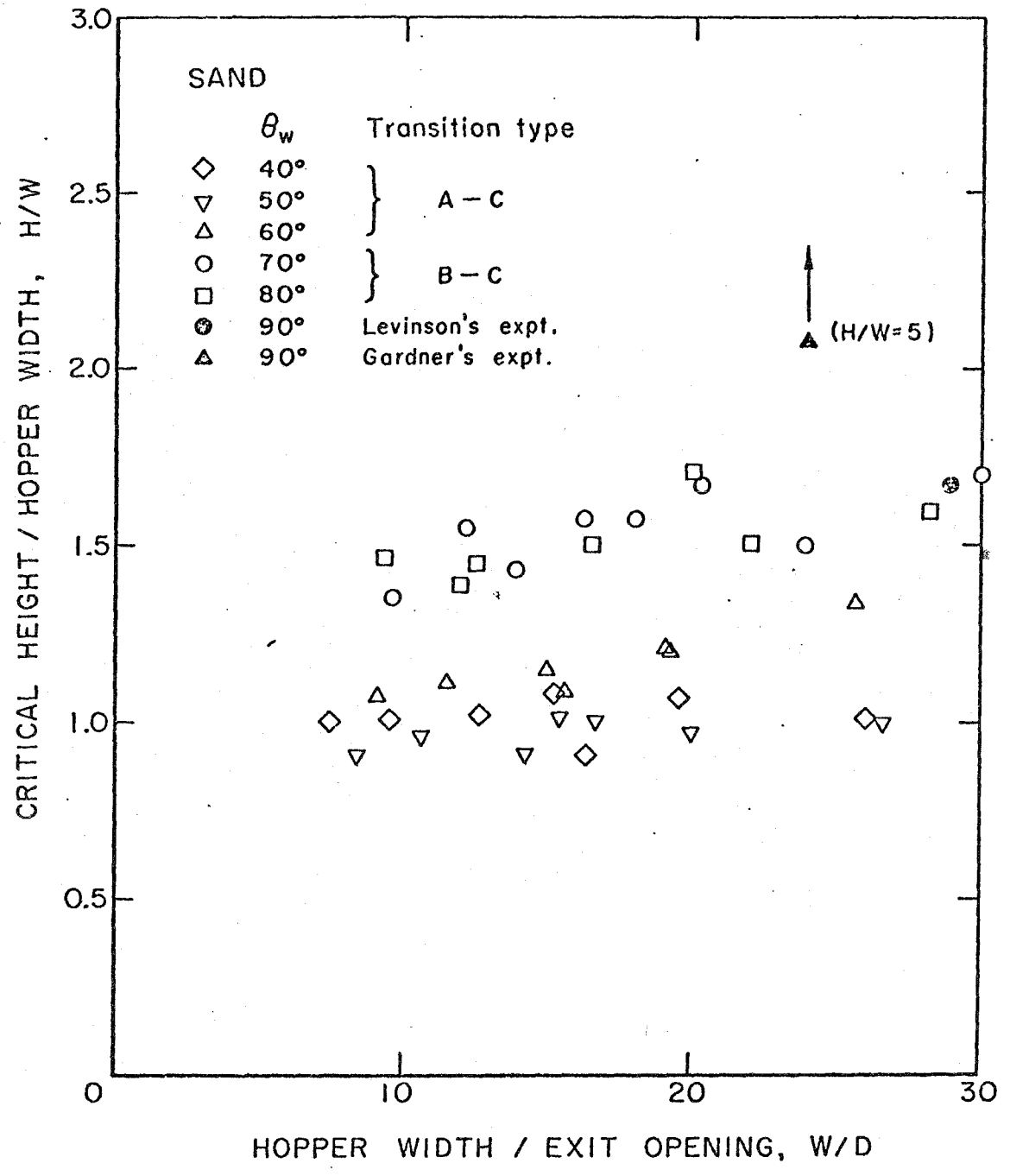

Figure 4.3 Critical values of H/W plotted against W/D for various hopper angles. The material is sand ($\varphi = 31°$, d = 0.5-1 mm).

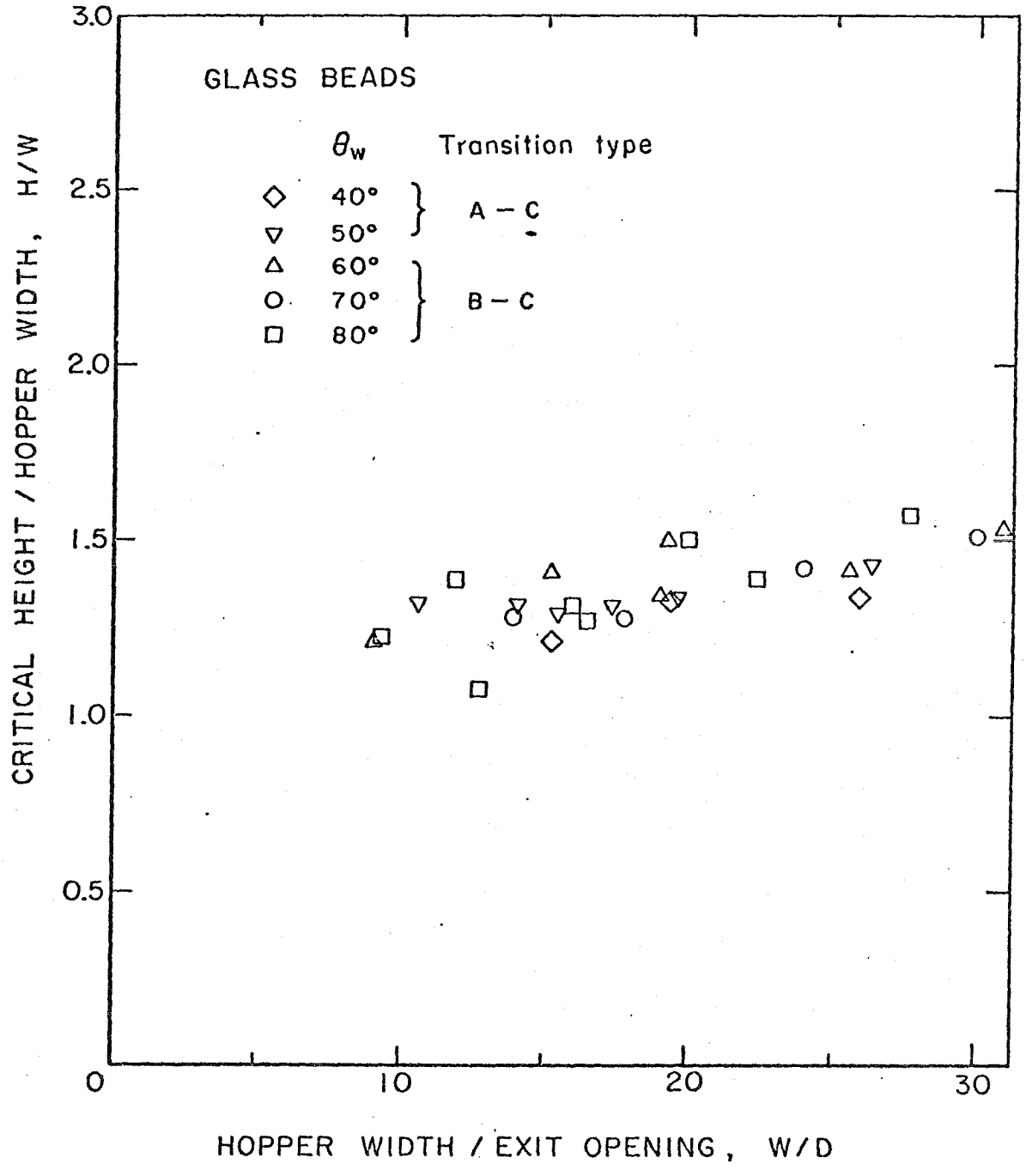

Figure 4.4 Critical values of H/W plotted against W/D for various hopper angles. The material is glass beads ($\varphi = 24.6$, $d = .32$mm).

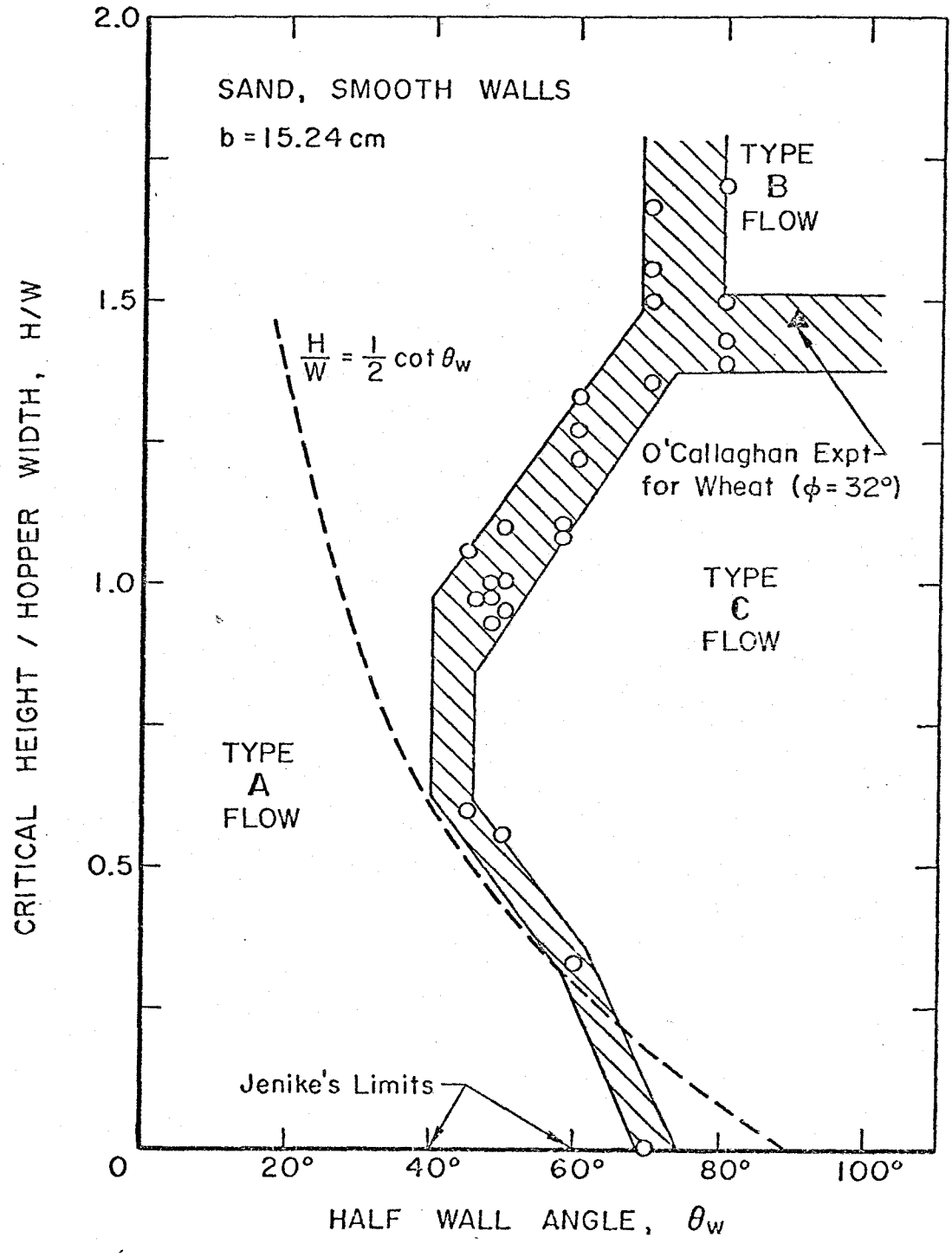

Figure 4.5 Map of the different types of flow which exist as a function of the hopper geometry. The material is sand flowing in a smooth walled hopper with a thickness b of 15.24 cm.

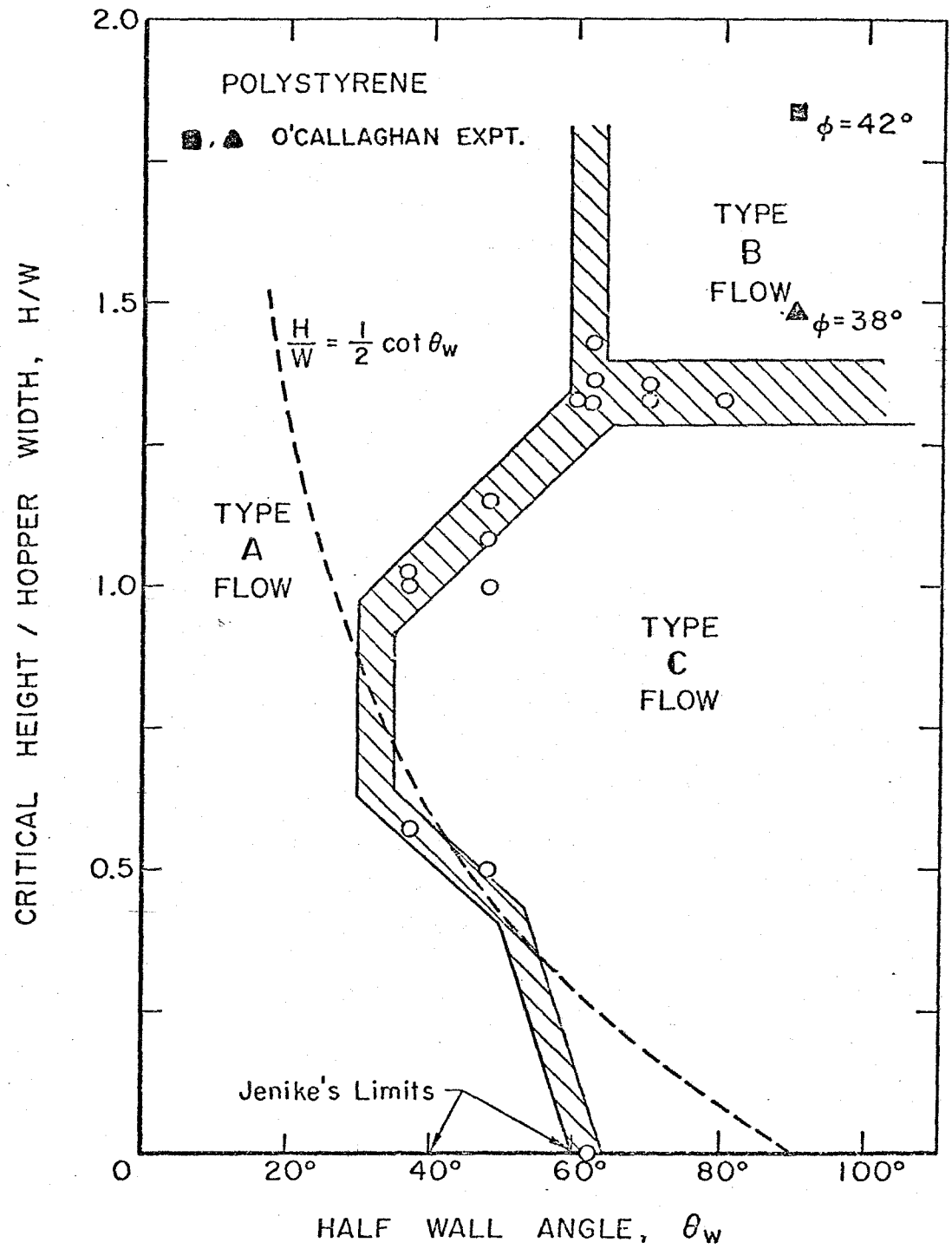

Figure 4.6 Map of the different types of flow which exist as a function of the hopper geometry. The material is polystyrene flowing in a smooth walled hopper with a thickness b of 15.2 cm.

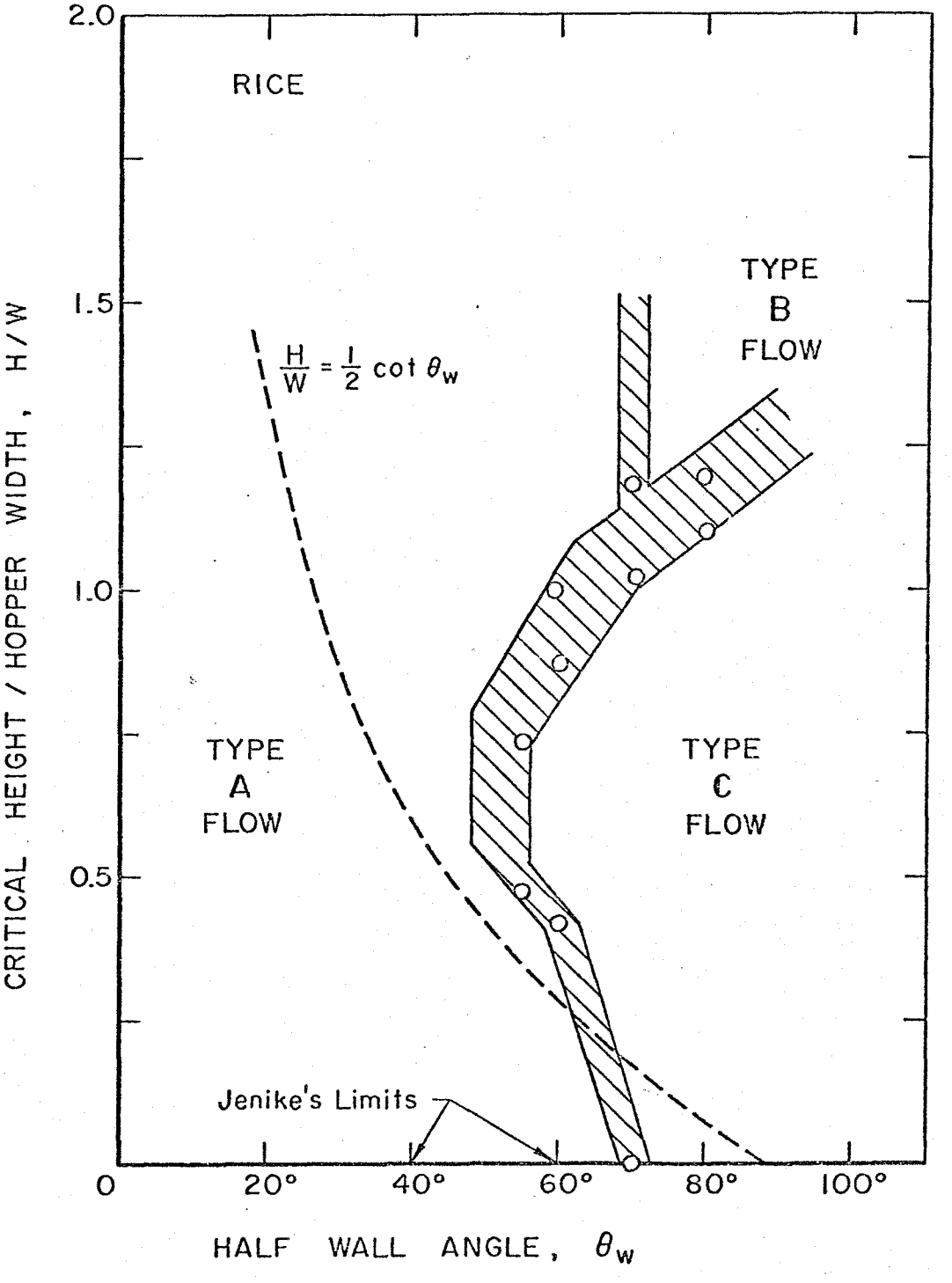

Figure 4.7 Map of the different types of flow which exist as a function of the hopper geometry. The material is rice flowing in a smooth walled hopper with a thickness b of 15.2 cm.

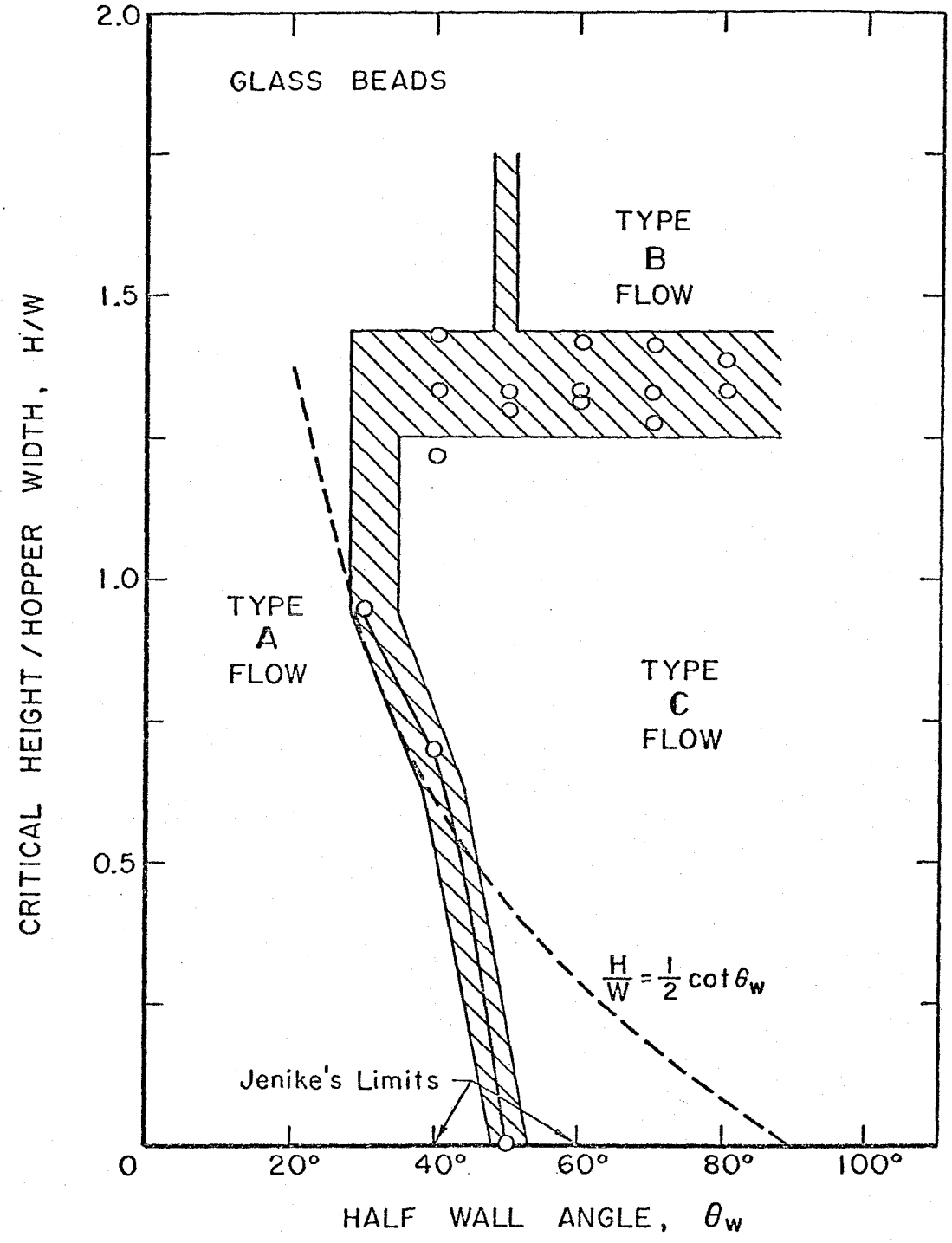

Figure 4.8 Map of the different types of flow which exist as a function of the hopper geometry. The material is glass beads flowing in a hopper with a thickness b of 15.2 cm.

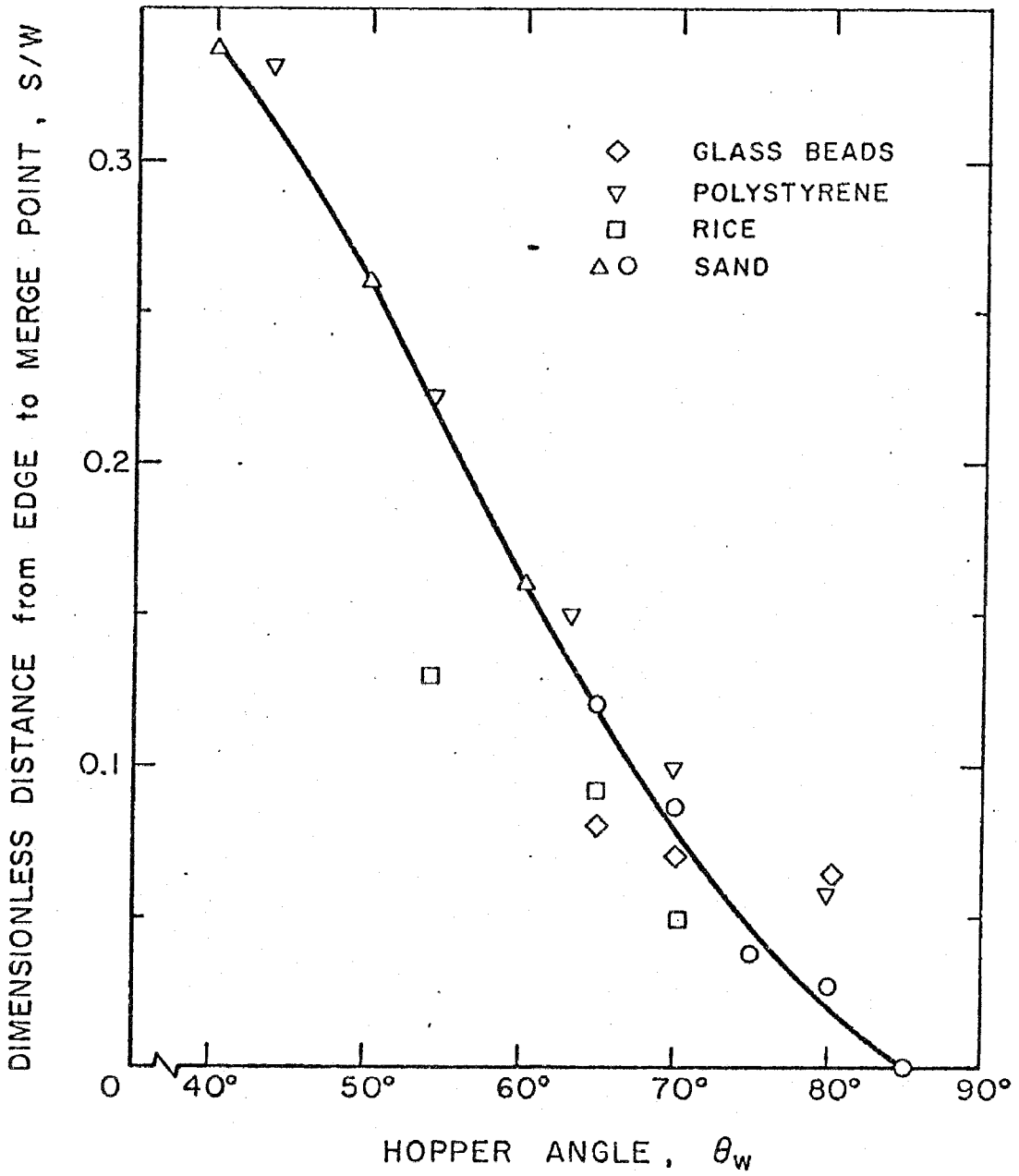

Figure 4.9 Dimensionless hopper slip length S/W plotted against the hopper angle θ_w for the four materials used in the experiments.

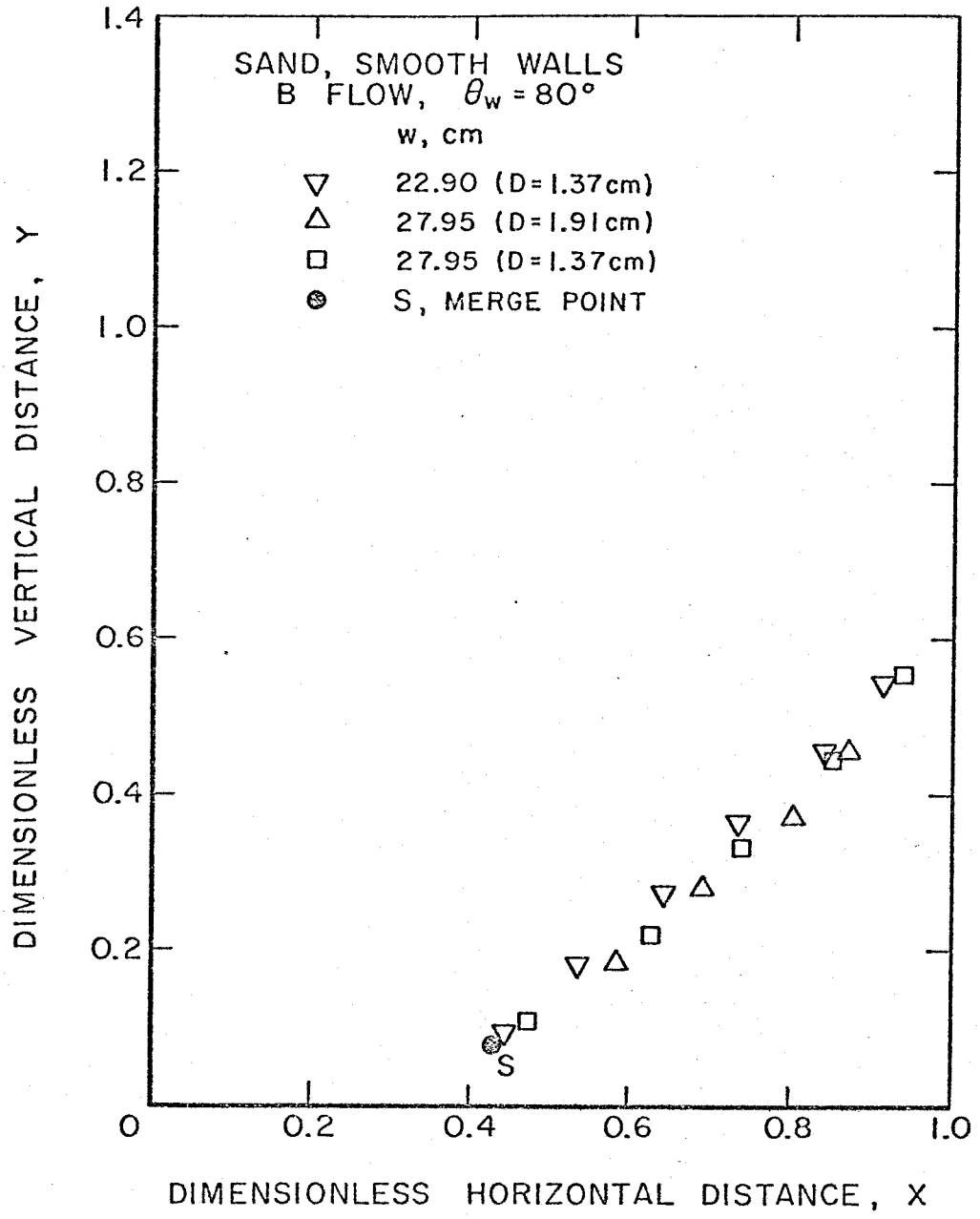

Figure 4.10 Funnel shapes of type B flow for different values of the bin width W and exit opening D. The material is sand ($\varphi = 31°$, d = 0.5-1 mm).

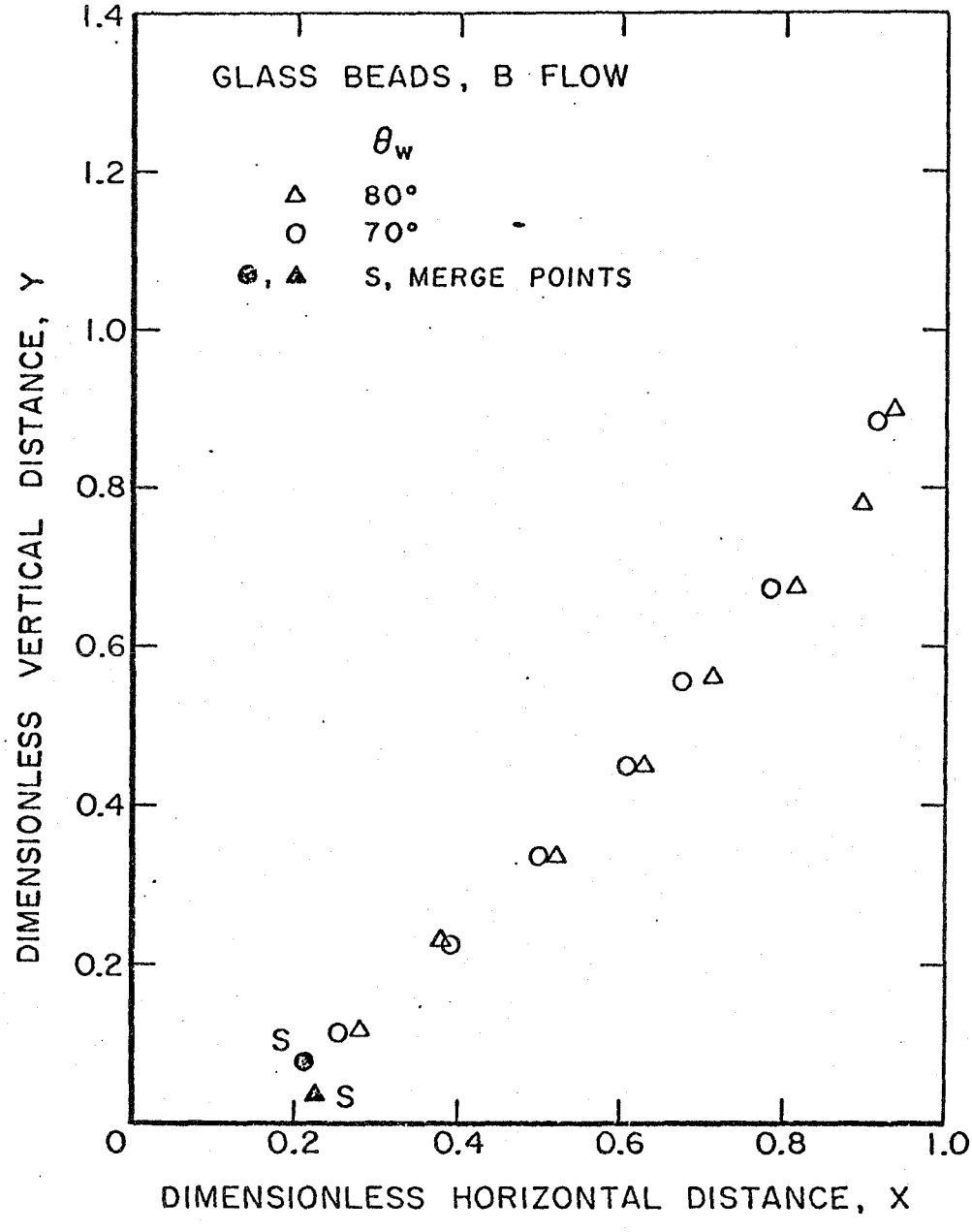

Figure 4.11 Funnel shape of type B flow for different values of the hopper angle θ_w. The material is glass beads ($\varphi = 25°$, $d = 0.32$ mm).

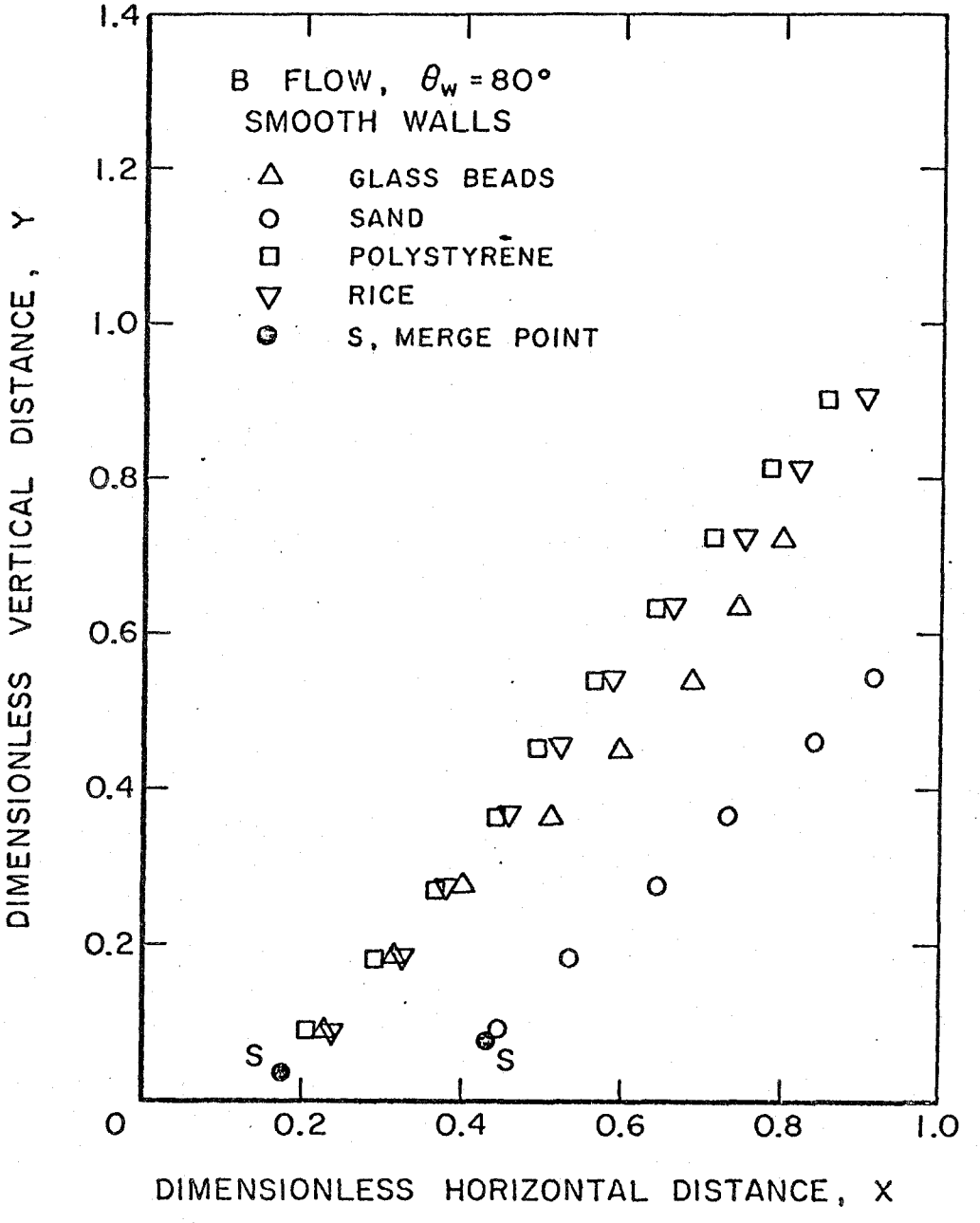

Figure 4.12 Funnel shape of type B flow of the four materials used ($\theta_w = 80°$, $W/D = 15$, $H/W \gg 1$).

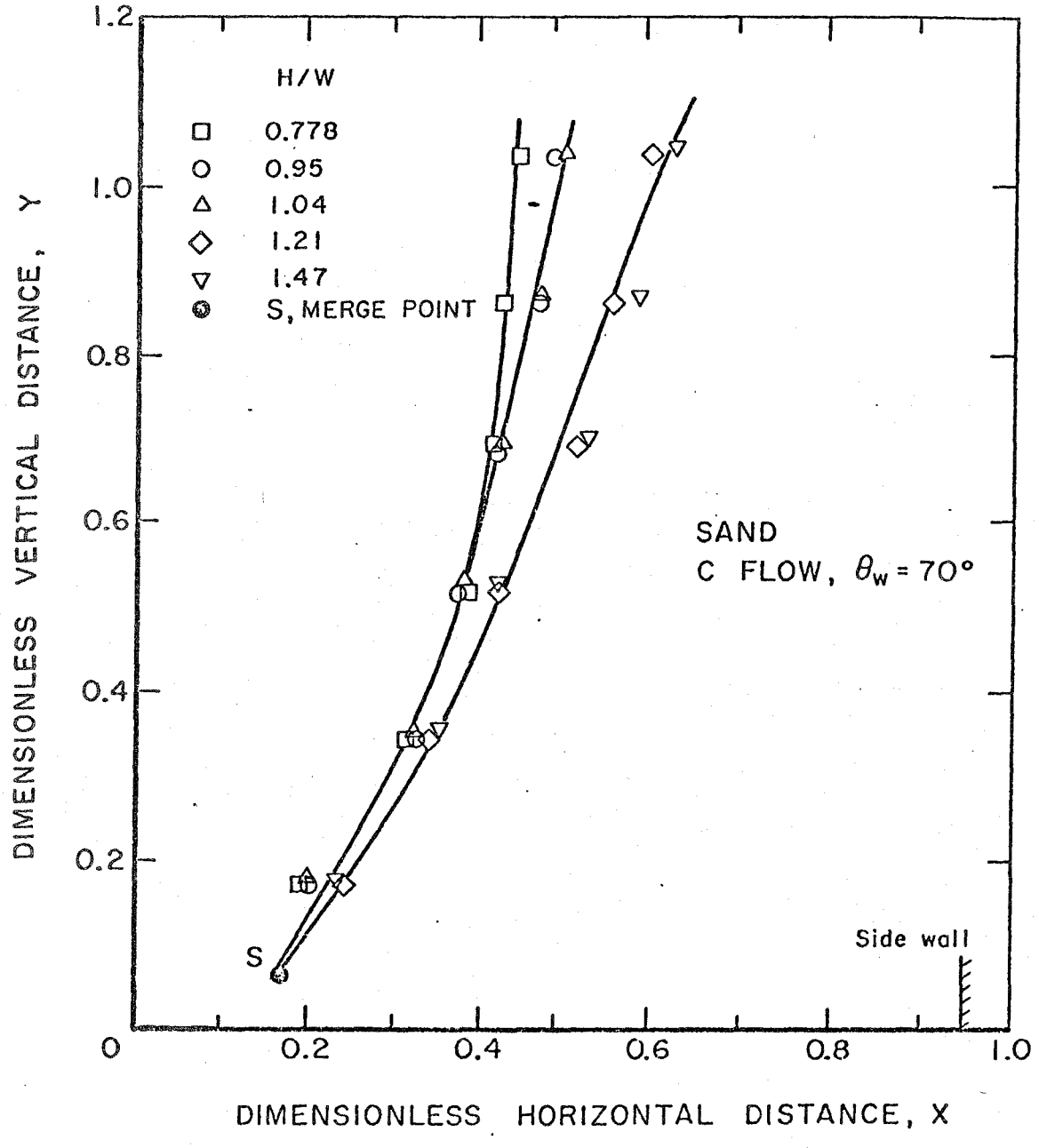

Figure 4.13 Funnel shape of type C flow for various values of the head H of material in the vertical bin for fixed values of W, D and θ_w. The material is sand ($\varphi = 31°$, d = 0.5-1 mm).

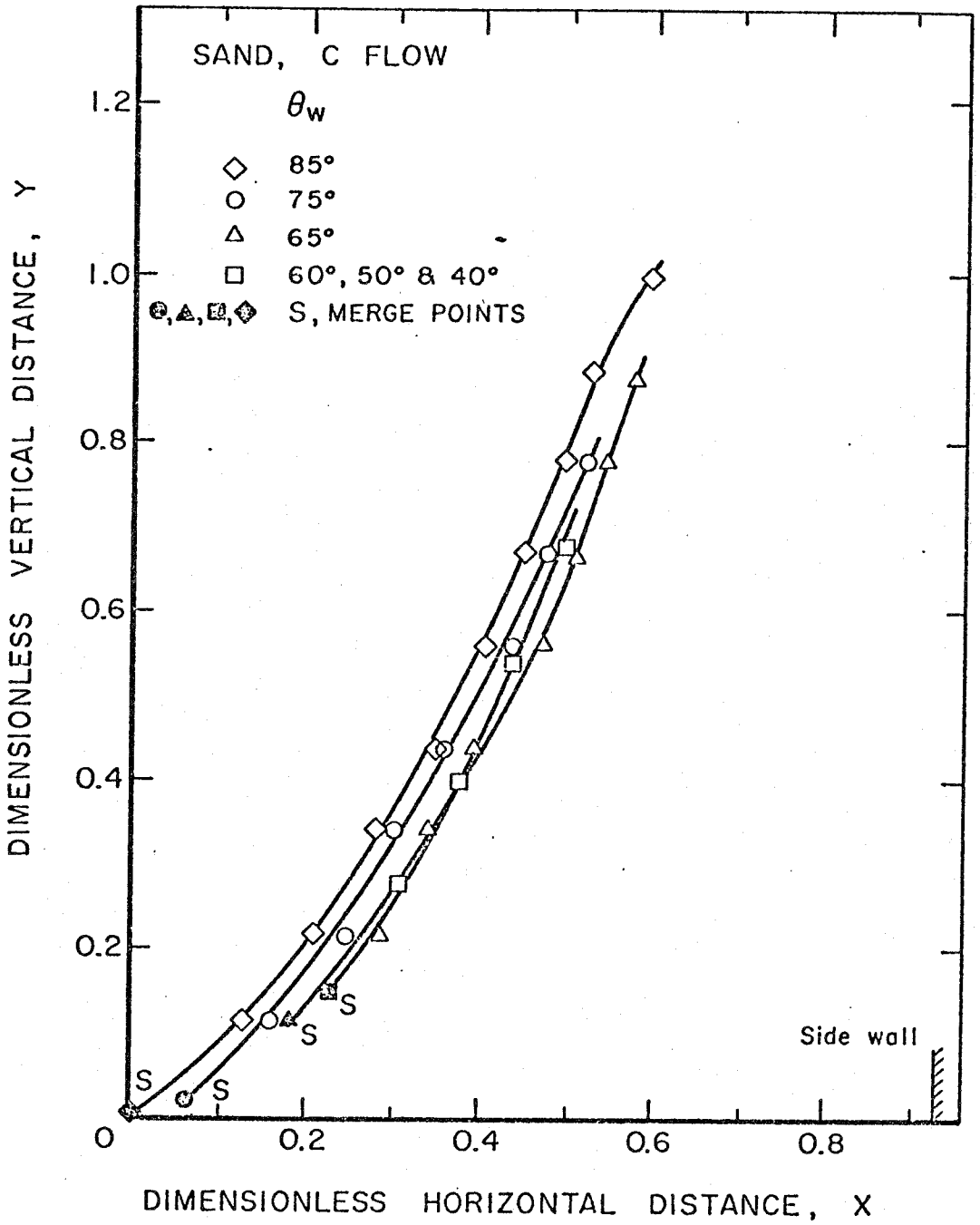

Figure 4.14 Funnel shape of type C flow for various hopper angles θ_w at fixed values of H, W and D. The material is sand ($\varphi = 31°$, d = 0.5-1 mm).

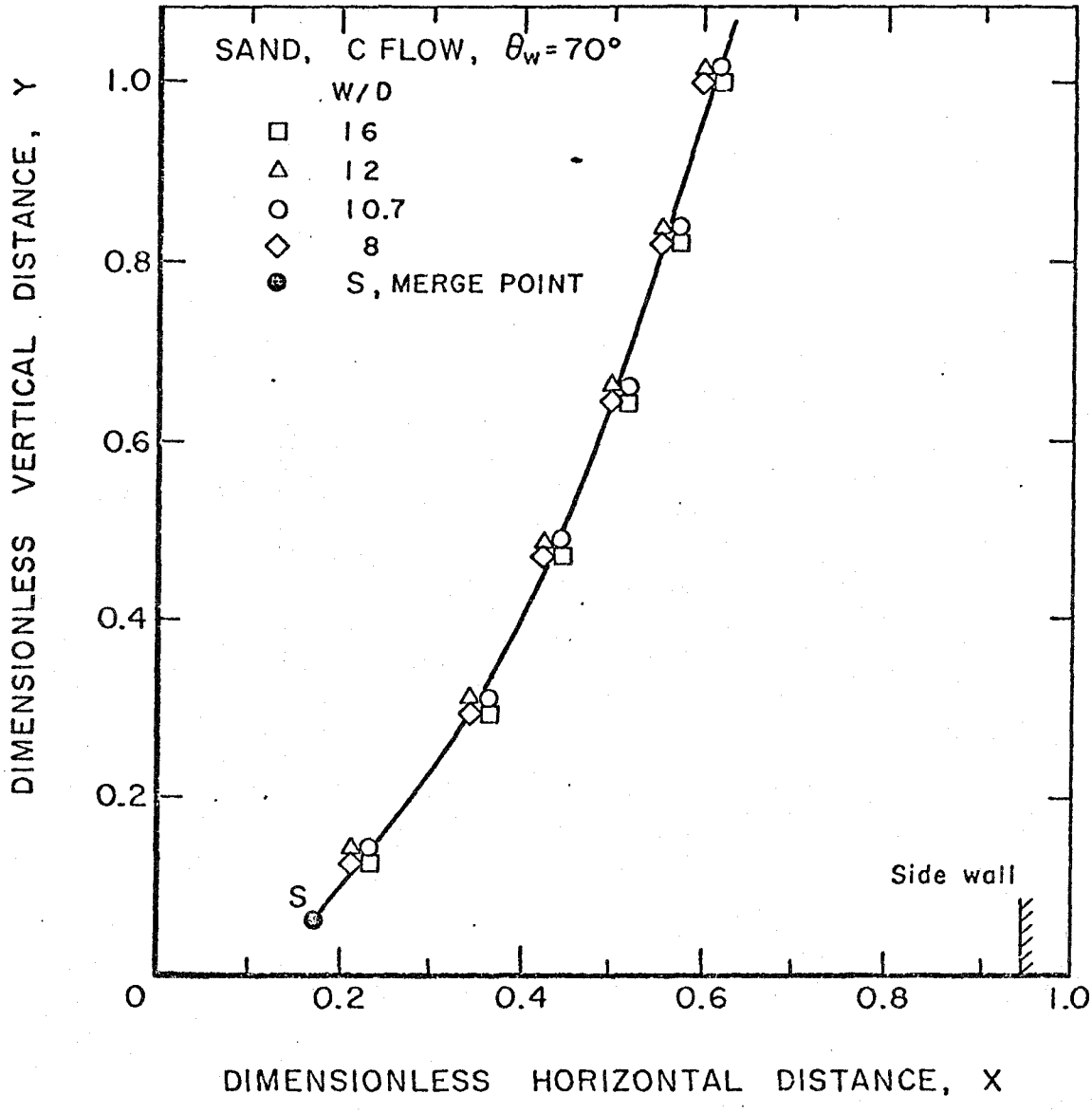

Figure 4.15 Funnel shape of type C flow for various values of the exit width D and fixed values of θ_w, H, W. The material is sand ($\varphi = 31°$, d = 0.5-1 mm).

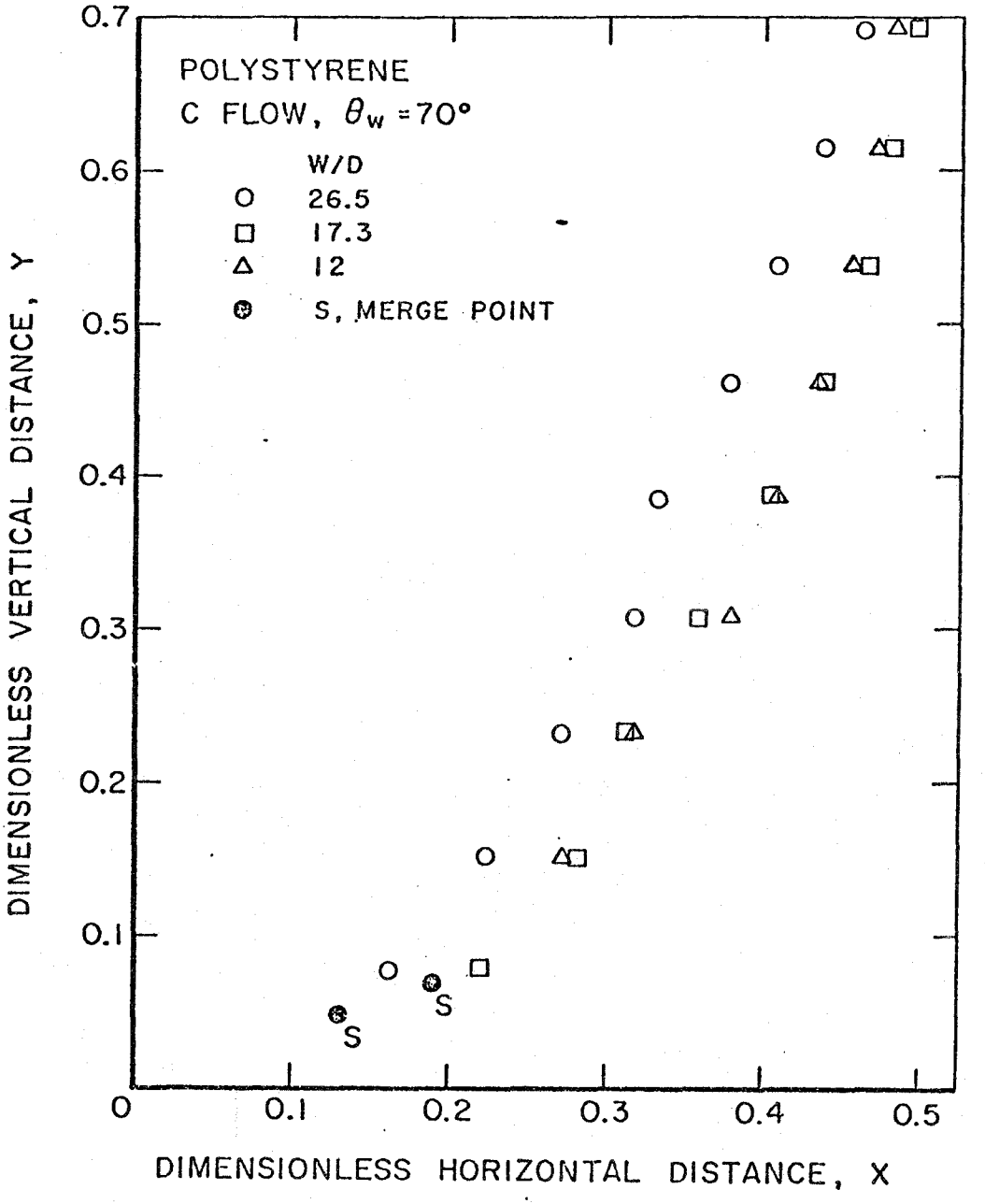

Figure 4.16 Funnel shape of type C flow for various values of the exit width D showing the effect of the particle size. The material is polystyrene ($\varphi = 39°$, d = 0.25-0.39 mm).

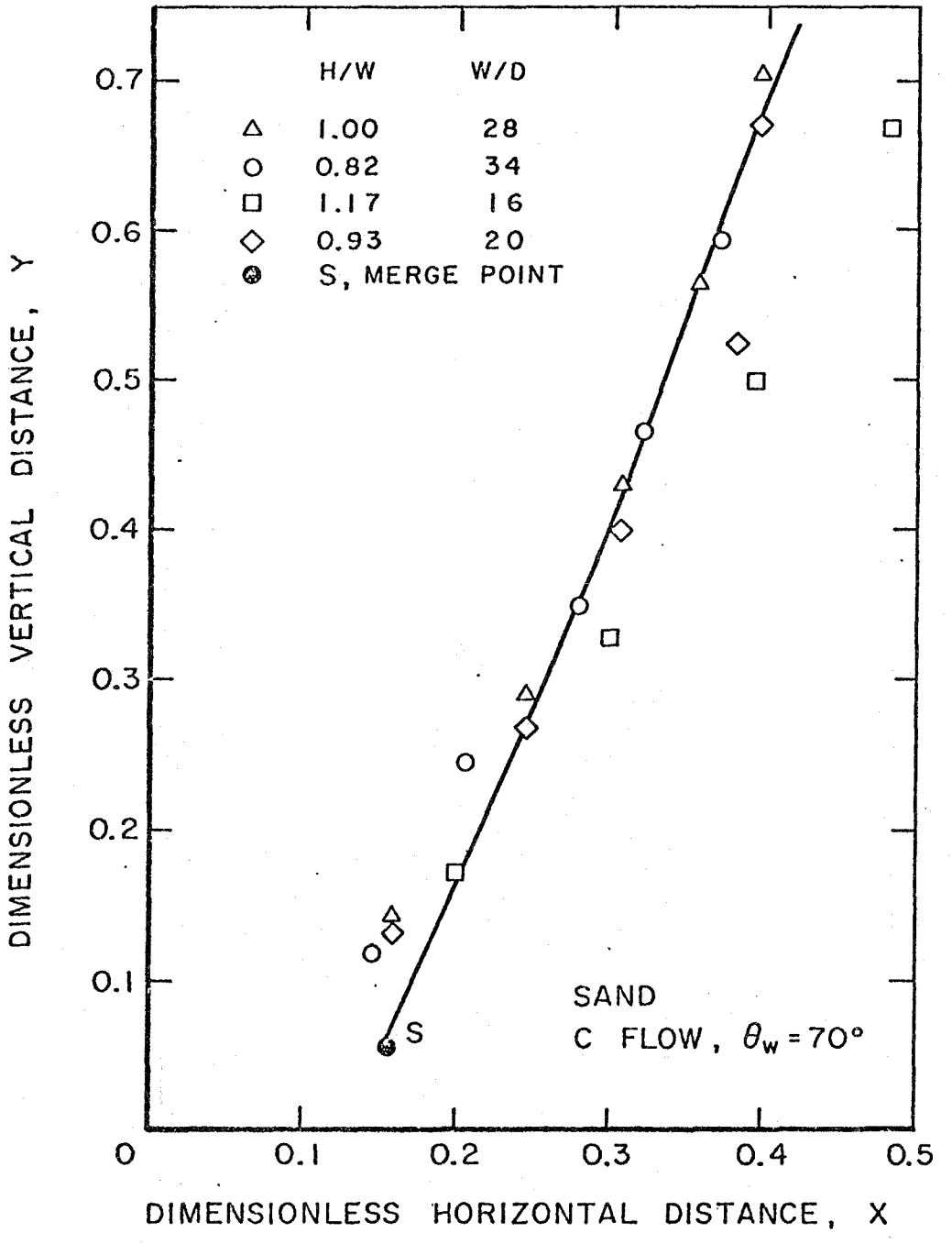

Figure 4.17 Funnel shape of type C flow for various values of the bin width W for fixed values of θ_w, H. Two values of the exit opening D were used. The material is sand ($\varphi = 31°$, d = 0.5-1 mm).

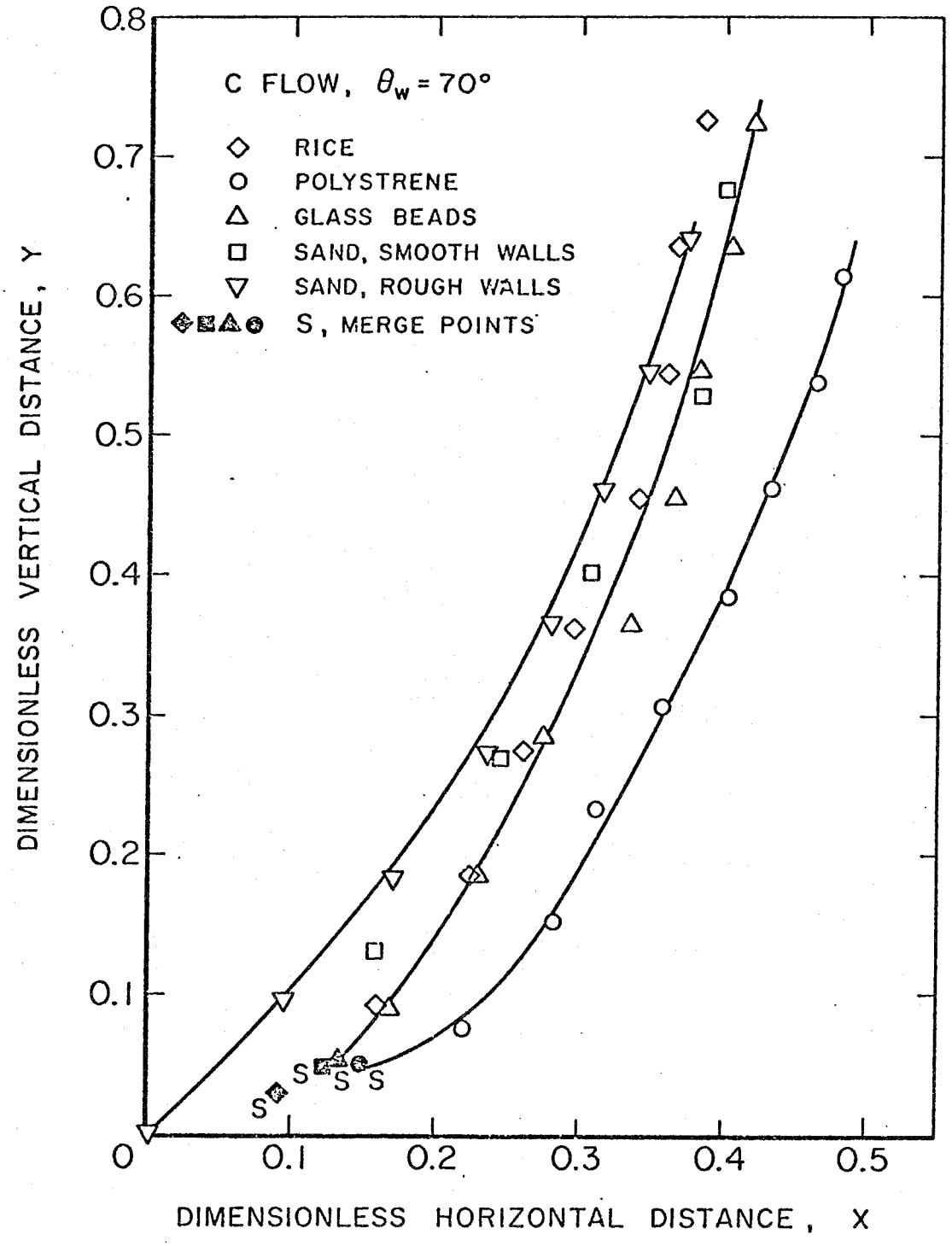

Figure 4.18 Funnel shape of type C flow for the four materials used in the experiments.

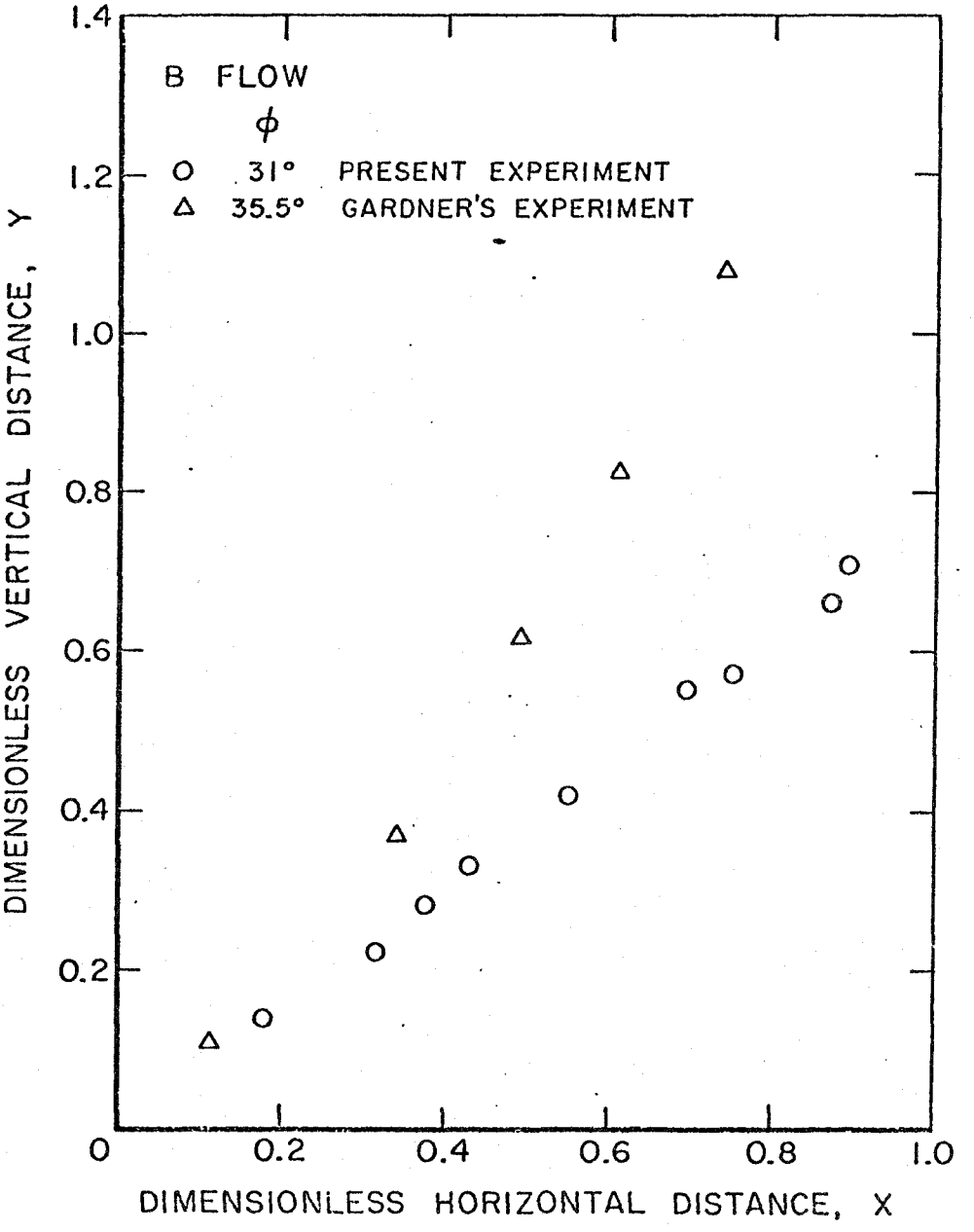

Figure 4.19 Comparison of the funnel shape of type B flow between Gardner's experiments ($\varphi = 35.5°$) and the present experiments ($\varphi = 31°$).

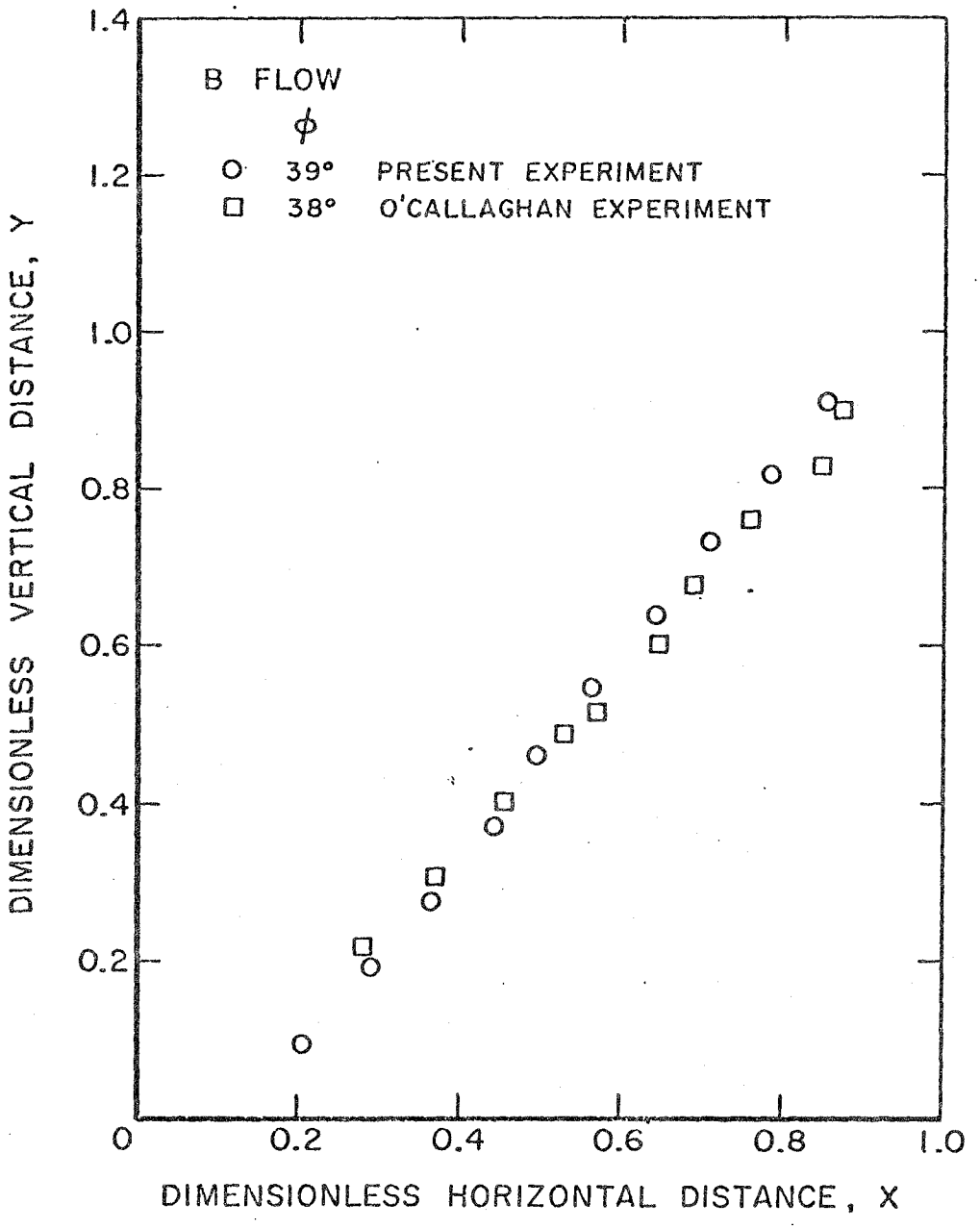

Figure 4.20 Comparison of the funnel shape of type B flow between O'Callaghan experiments ($\varphi = 38°$) and the present experiments ($\varphi = 39°$).

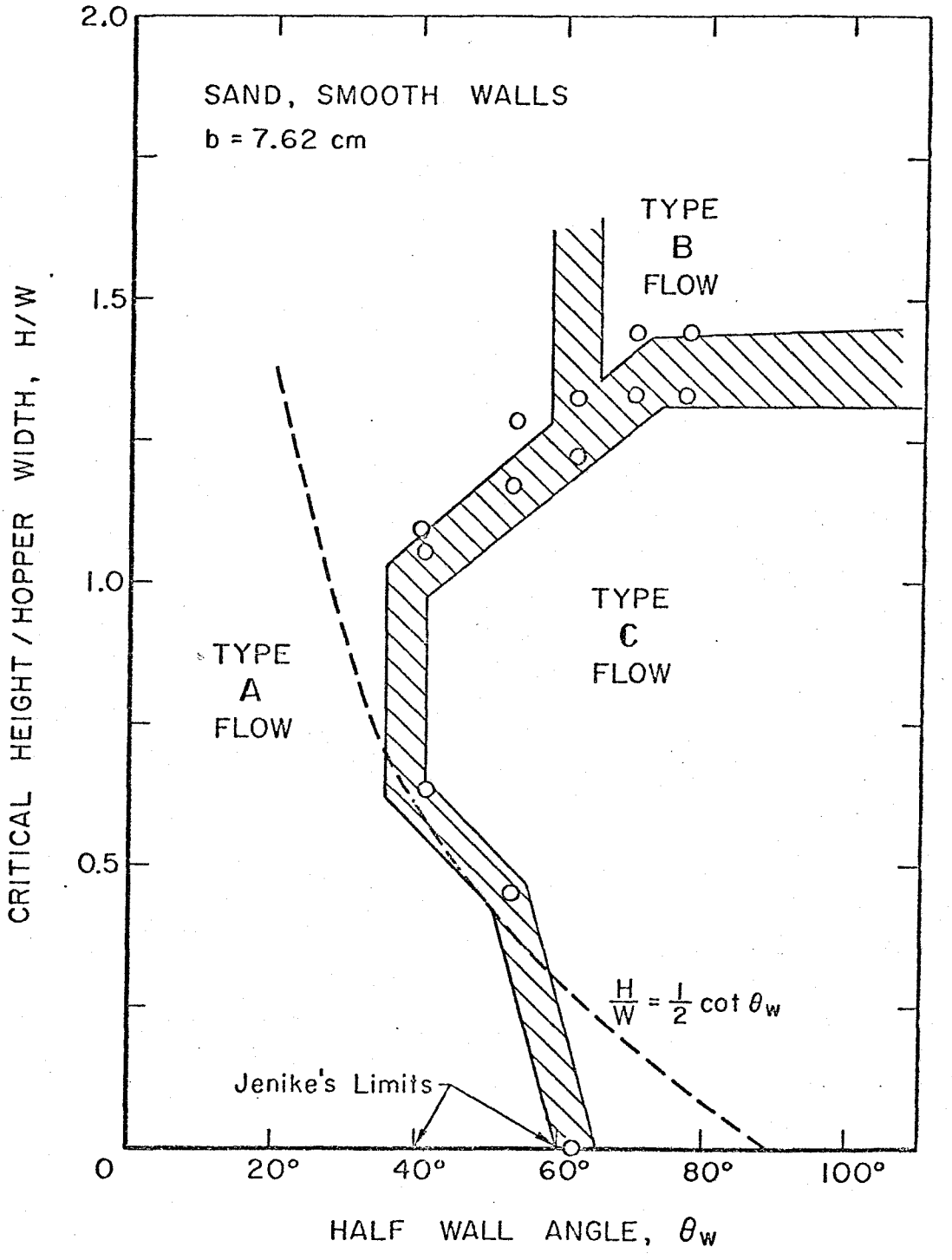

Figure 4.21 Maps of the different types of flow which exist as a function of the hopper geometry. The material is sand flowing in a smooth walled hopper with a thickness of 7.62 cm.

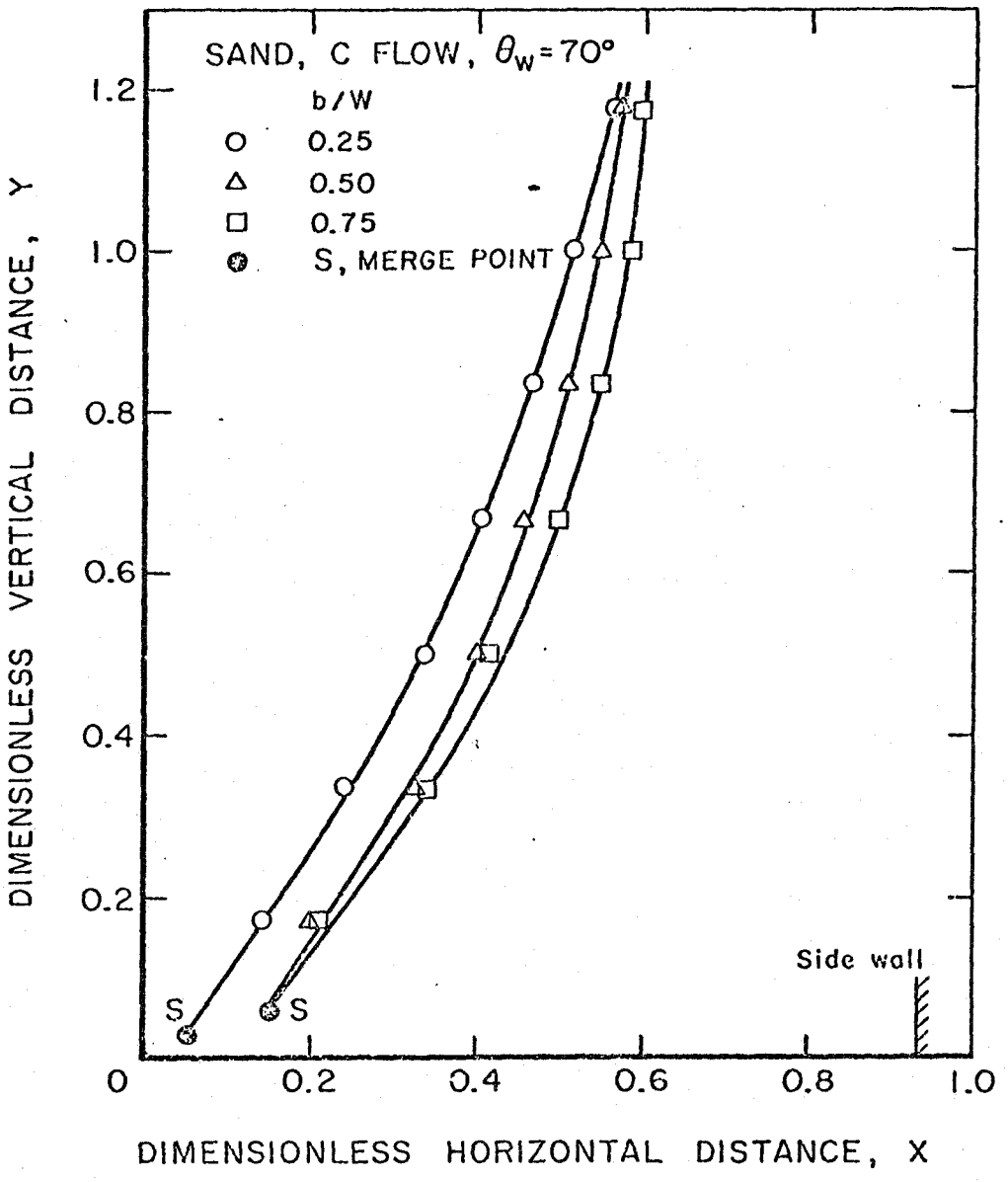

Figure 4.22 Funnel shape of type C flow for three different hopper thicknesses with fixed values of θ_w, H, W, D.

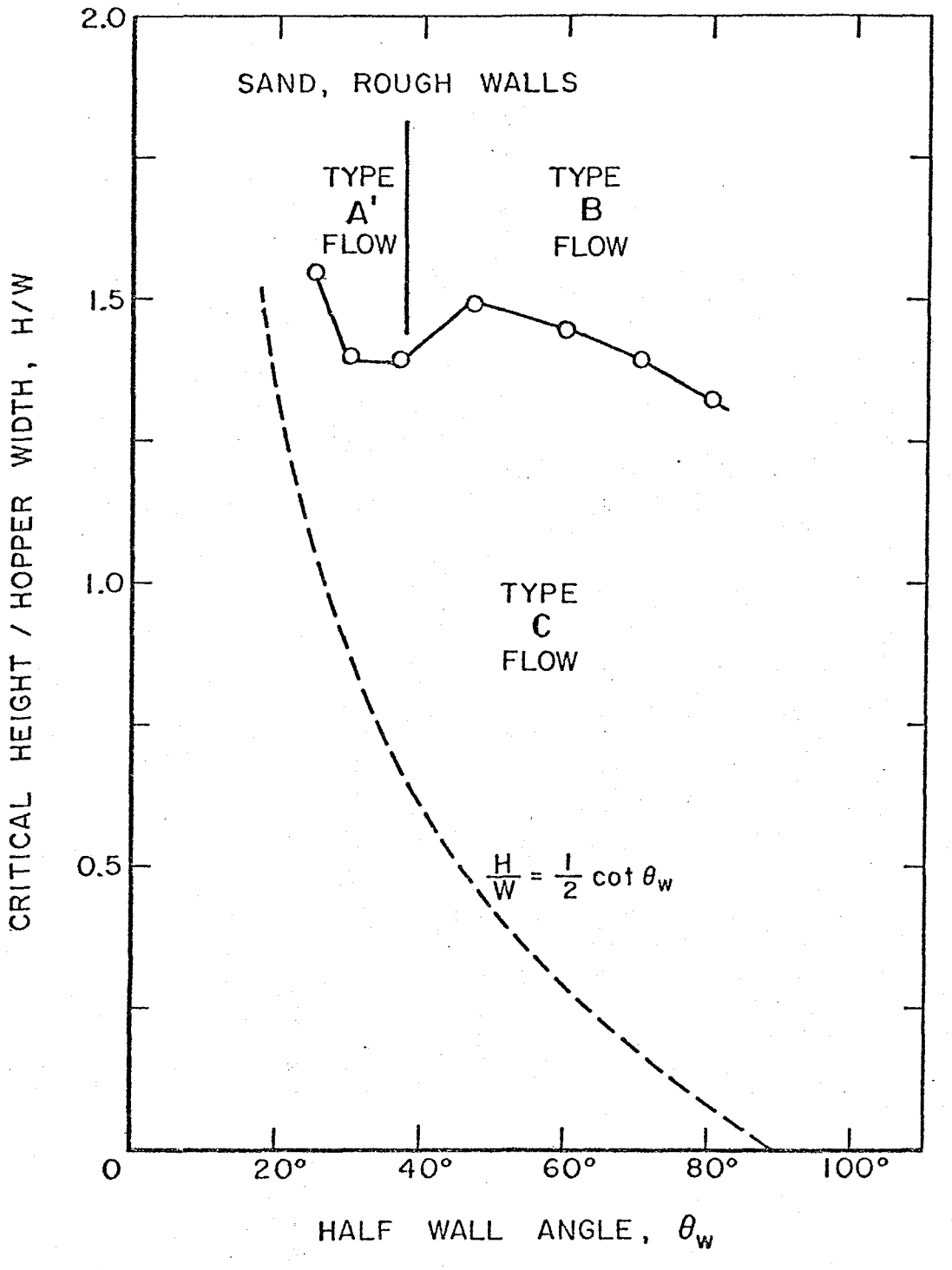

Figure 4.23 Map of the different types of flow which exist as a function of the hopper geometry. The material is sand flowing in a rough walled hopper with a thickness of 15.2 cm.

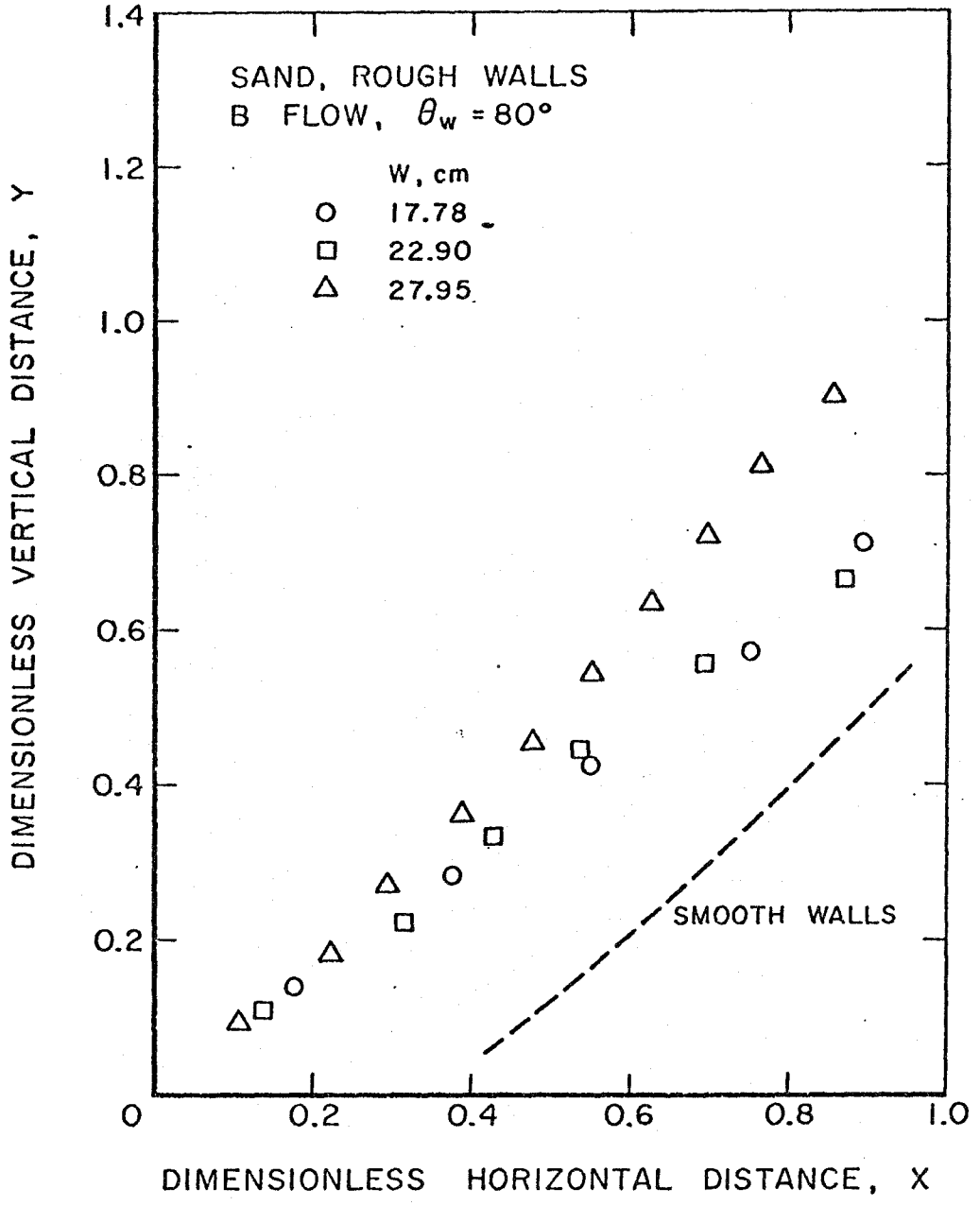

Figure 4.24 Funnel shape of type B flow in a rough walled hopper for various values of the width W of the vertical bin.

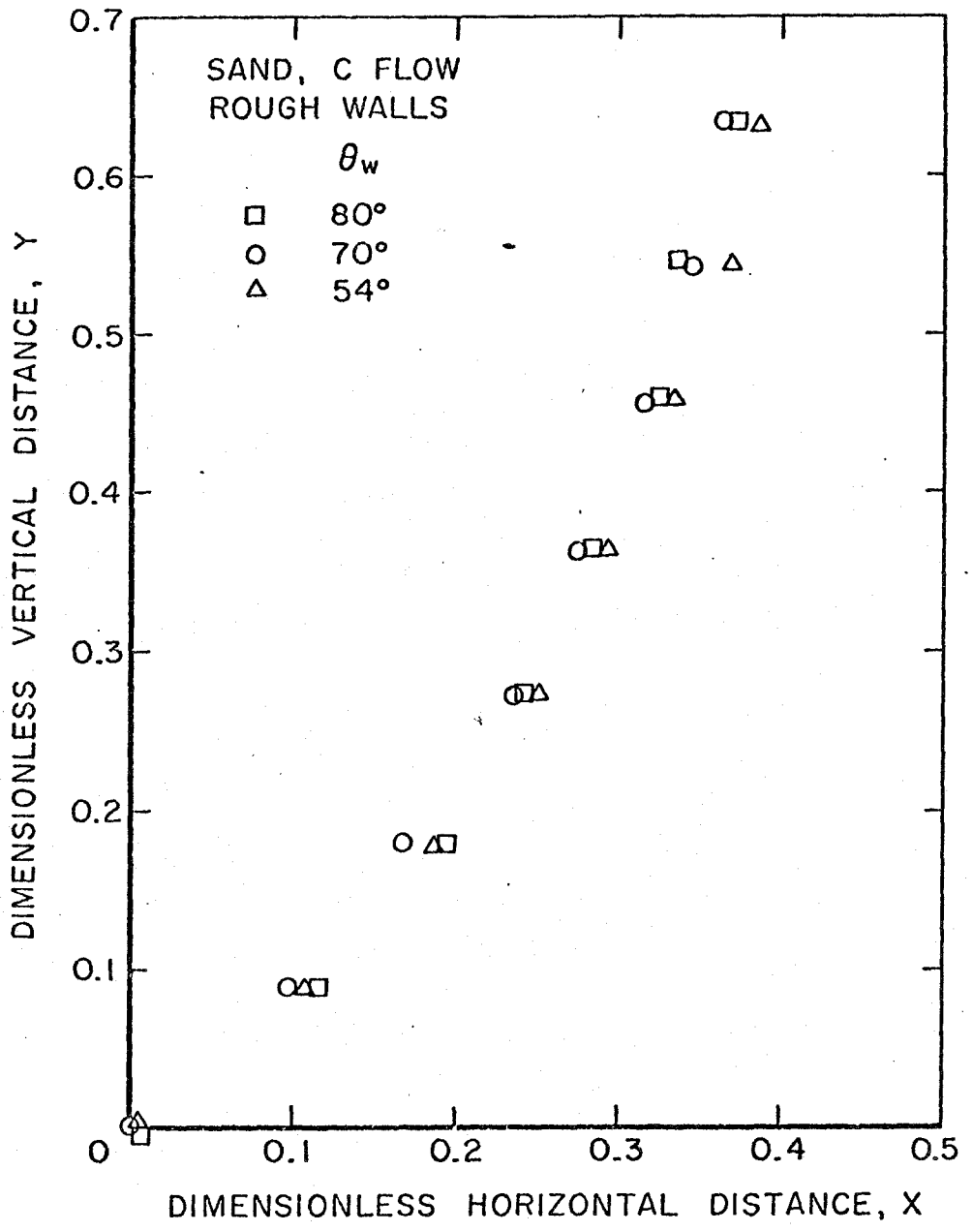

Figure 4.25 Funnel shape of type B flow in a rough walled hopper for various values of the hopper angle θ_w.

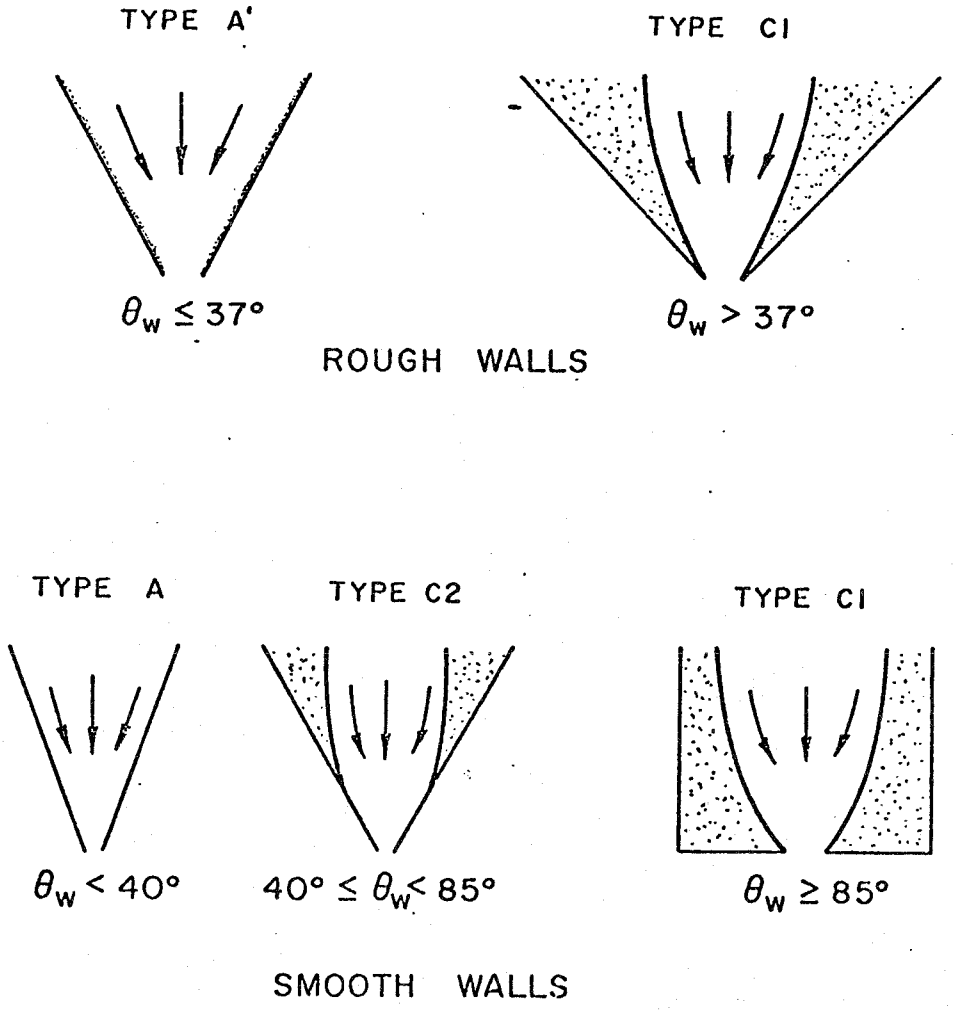

Figure 4.26 The different types of flow which exist as a function of the wall angle θ_w in hoppers with rough and smooth walls.

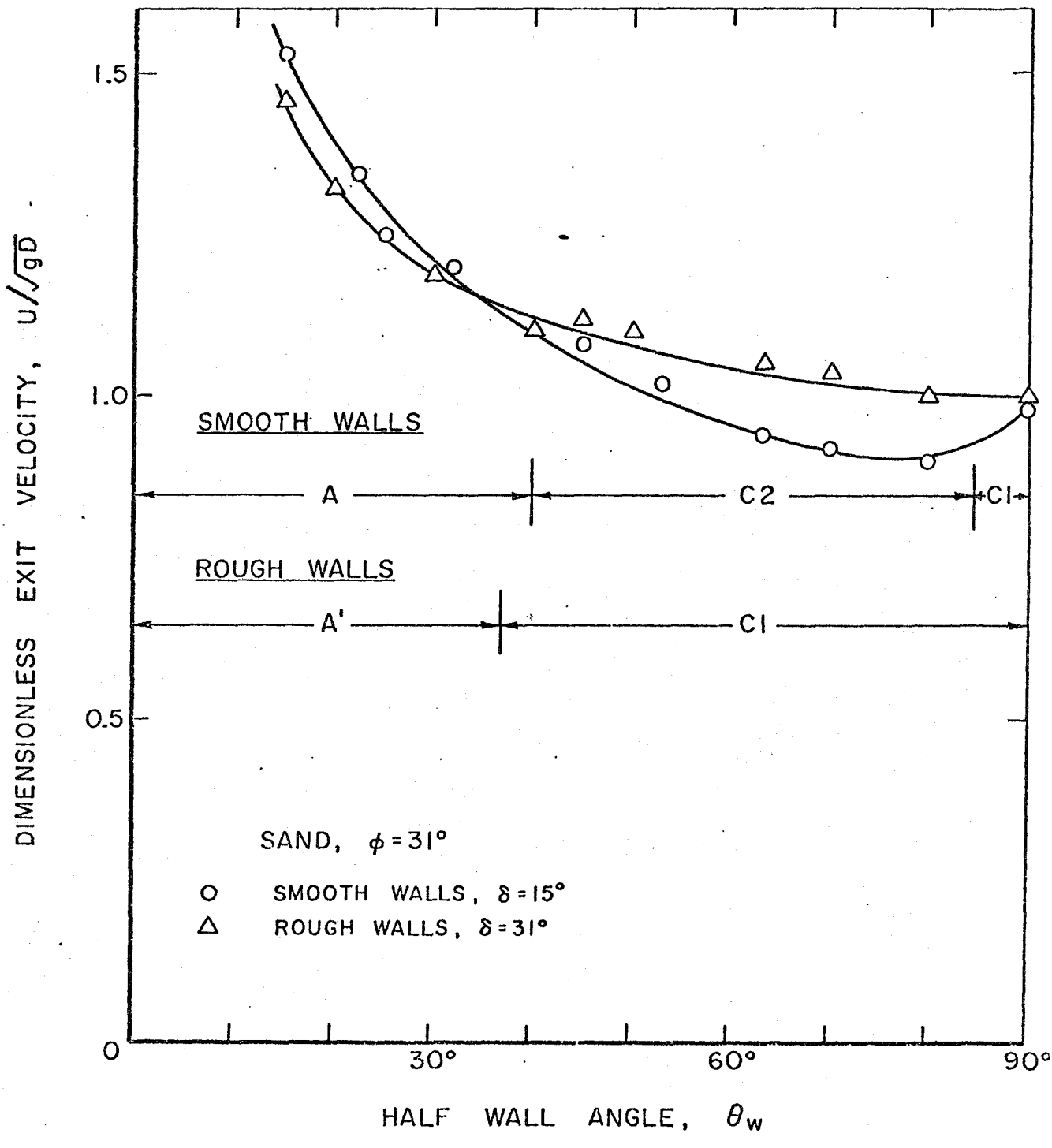

Figure 4.27 Comparison of the dimensionless mass flow rate from hoppers with smooth and rough walls. The material used is sand ($\varphi = 31°$, d = 0.5-1 mm).

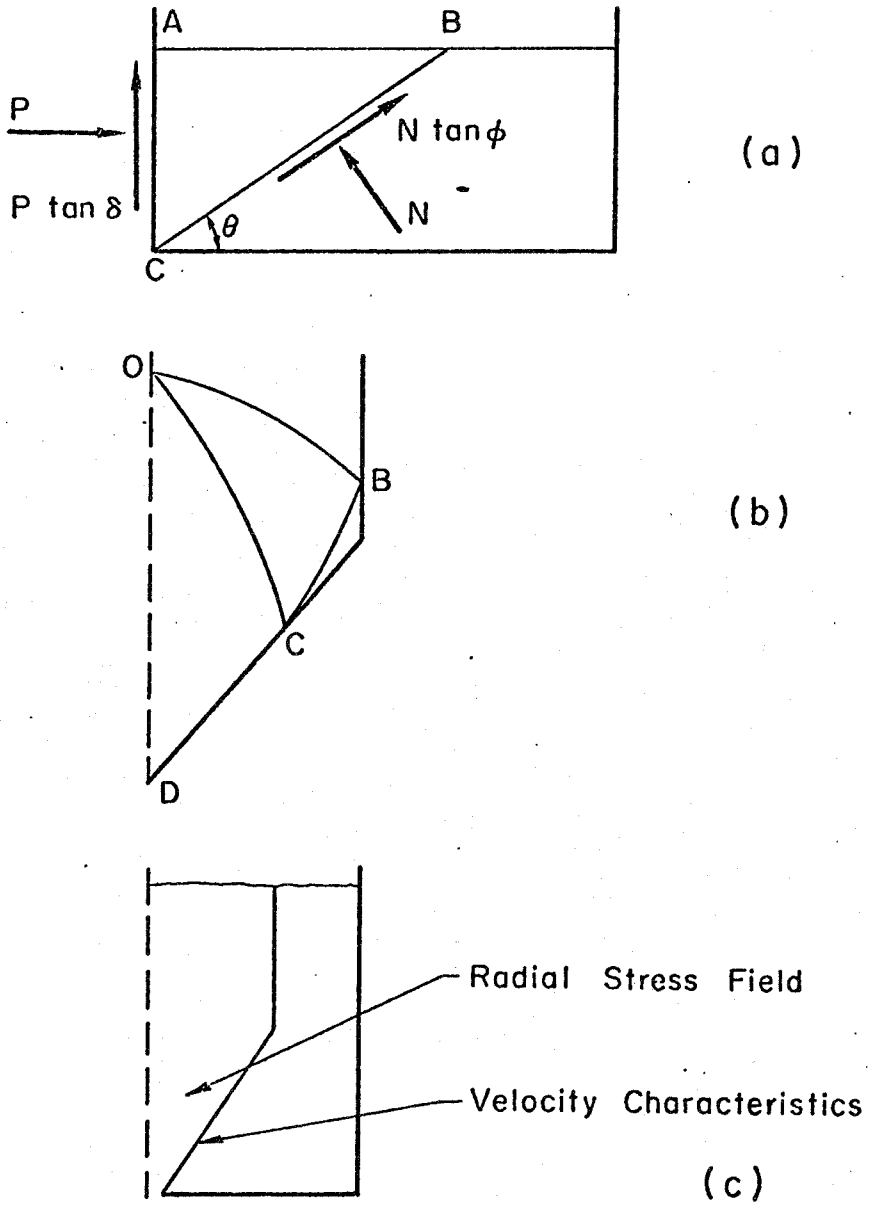

Figure 4.28 Geometries of the funnel flow field used by other investigators: Airy's solution (a), Gardner's solution (b), Guinta's solution (c).

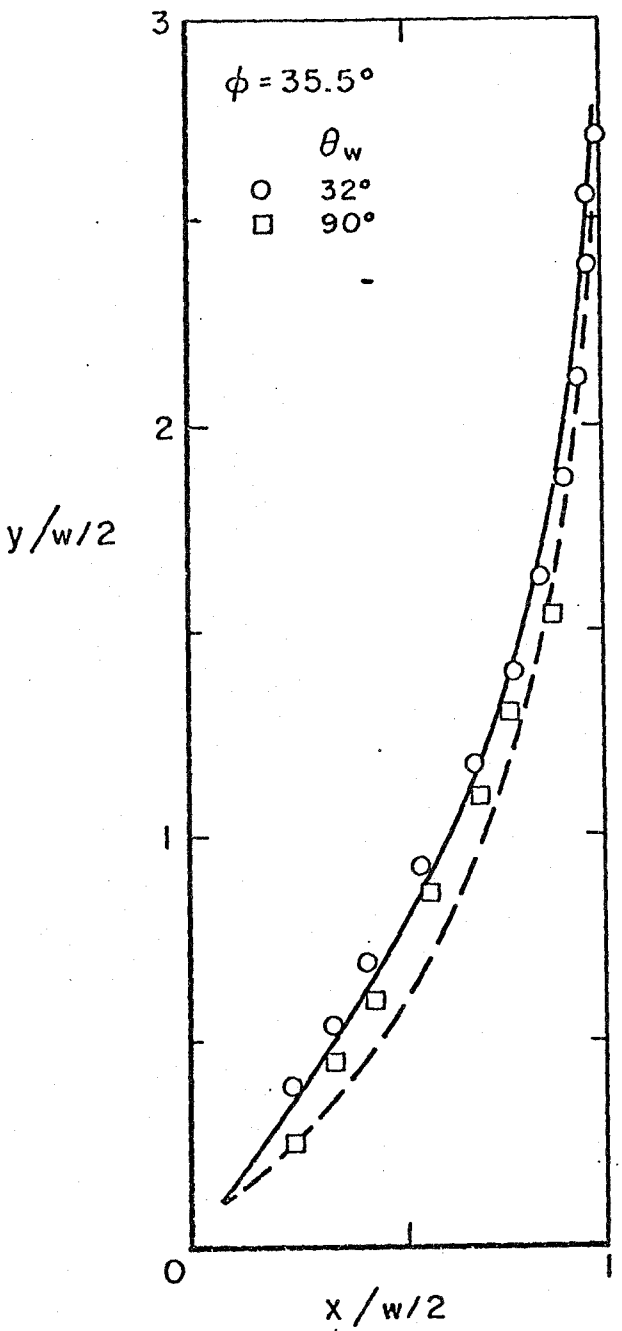

Figure 4.29 Comparison between Gardner's experimental and analytical results of the funnel boundary at two values of the hopper angles θ_w.

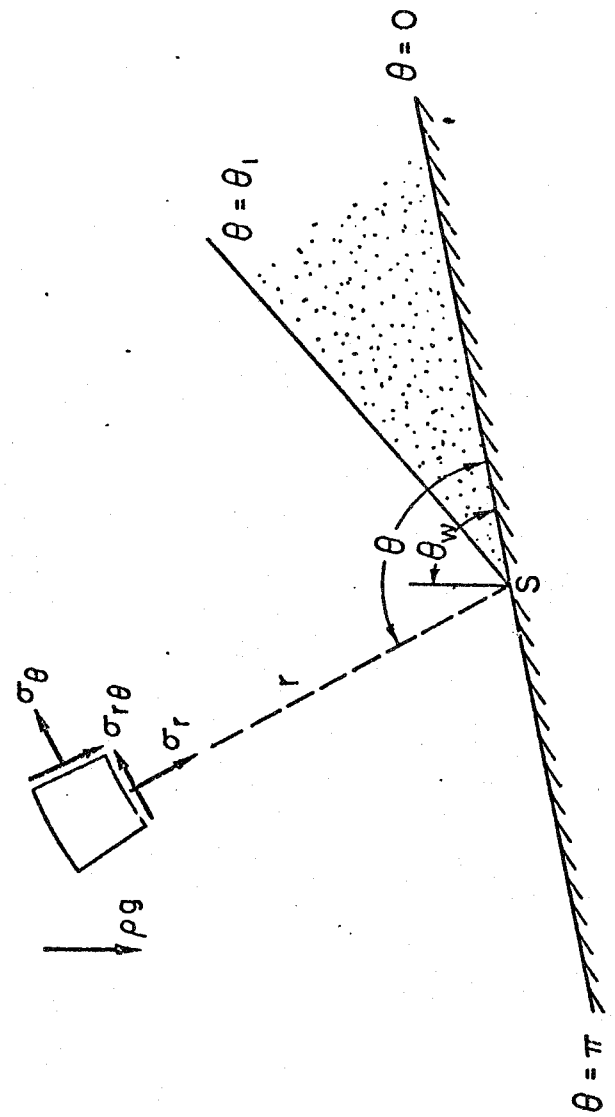

Figure 4.30 Geometry of the flow field near the merge point S. The material is flowing in region I. It is stagnant in region II.

CHAPTER 5

SUMMARY AND CONCLUSIONS

From this study of the flow of granular materials in hoppers, the following conclusions can be made:

First, the continuum model describes the flow of granular materials in a mass flow hopper fairly well. The computed results of the mass flow rate compare favorably with the experimental measurements. The solution also shows that the boundary conditions on the lower free surface at the hopper exit have to be specified with some care. For a consistent analytical approach the conditions have to be specified at a free surface which is initially unknown and must be determined from the stress-free condition.

Second, the flow field in a hopper with a vertical bin is quite complicated near the bin/hopper transition corner. The kinematics of the deformation there is a complicated one with material at different states of deformation being present. The flow field near the hopper exit is however, fairly uniform with the motion being mainly in the radial direction. It resembles closely the one being assumed in the analytical solution. This may explain the good agreement obtained between the analytical and experimental results.

Third, the occurence of funnel flow in hoppers is strongly affected by the presence of the vertical bin. The three types of flow in the hopper are identified and classified. The observations show that the ratio of the height of the material in the vertical bin to the width

of the bin (H/W) must be used in addition to the hopper angle θ_w in order to obtain a complete picture of the flow field. The boundary between the flowing and stagnant material is observed to depend mainly on the material properties. It is more or less independent of some hopper dimensions such as the hopper angle θ_w and the exit width D.

REFERENCES

1. Augenstein, D.A. and Hogg, R., "An Experimental Study of the Flow of Dry Powder over Inclined Surfaces", Powder Technology, Vol.19, No.2, 1978, p.205.

2. Beverloo, W.A., Leniger, H.A. and Van De Velde Jr., "The Flow of Granular Solids Through Orifices", Chemical Engineering Science, Vol.15, 1961, p.260.

3. Blair-Fish, P.M. and Bransby, P.L., "Flow Patterns and Wall Stresses in a Mass Flow Bunker", ASME Journal of Engineering for Industry, Vol.95, 1973, p.17.

4. Bosley, J., Schofield, C. and Shook, C.A., "An Experimental Study of Granular Discharge from Model Hoppers", Transaction of the Institution of Chemical Engineers, Vol.47, 1969, p.T147.

5. Bransby, P.L., Blair-Fish, P.M. and James, R.G., "An Investigation of the Flow of Granular Materials", Powder Technology, Vol.8, 1973, p.197.

6. Bransby, P.L. and Blair-Fish, P.M., "Wall Stress in Mass Flow Bunker", Chemical Engineering Science, Vol.29, 1974, p.1061.

7. Bransby, P.L. and Blair-Fish, P.M., "Deformation Near Rupture Surface in Flowing Sand", Geotechnique, Vol.25, 1975, p.384.

8. Bransby, P.L. and Blair-Fish, P.M., "Initial Deformation During Mass Flow From a Bunker: Observation and Idealization", Powder Technology, Vol.11, 1975, p.273.

9. Brennen, C. and Pearce, J.C., "Granular Material Flow in Two-Dimensional Hoppers", ASME Journal of Applied Mechanics, Vol.45, 1978, p.43.

10. Brown, R.L., "Minimum Energy Theorem for Flow of Dry Granules Through Apertures", Nature, London, Vol.191, 1961, p.458.

11. Brown, R.L. and Richards, J.C., Principles of Powder Mechanics, Pergamon Press, 1970.

12. Choda, A. and Willis, A.H., "Flow Regimes of Grains in Inclined Chutes", Transaction of the American Society of Agricultural Engineers, Vol.10, 1967, p.136.

13. Cowin, S.C., "A Theory for the Flow of Granular Materials", Powder Technology, Vol.9, 1974, p.61.

14. Cowin, S.C., "The Theory of Static Loads in Bins", ASME Journal of Applied Mechanics, Vol.44, 1977, p.409.

15. Connelly, L.M., "Wall Pressure and Material Velocity Measurements for the Flow of Granular Material Under Plane Strain Conditions", Mechanics Applied to the Transport of Bulk Materials, American Society of Mechanical Engineers, AMD, Vol.31, 1979, p.35.

16. Crewdson, B.J., Ormond, A.L. and Nedderman, R.O., "Air Impeded Discharge of Fine Particles from a Hopper", Powder Technology, Vol.16, 1977, p.197.

17. Cuttress, J.O. and Pulfer, R.F., "X-Ray Investigation of Flowing Powders", Powder Technology, Vol.1, 1967, p.213.

18. Davidson, J.F. and Nedderman, R., "The Hour-Glass Theory of Hopper Flow", Transaction of the Institution of Chemical Engineers, Vol.51, 1973, p.29.

19. De Josselin De Jong, G., "The Double Sliding, Free Rotating Model for Granular Assemblies", Geotechnique, Vol.21, 1971, p.155.

20. Deming, W.E. and Mehring, A.L., "The Gravitational Flow of Fertilizers and Other Comminuted Solids", Industrial and Engineering Chemistry, Vol.21, 1929, p.661.

21. Deutsch, G.P. and Clyde, D.H., "Flow and Pressure of Granular Materials in Silos", Proceeding ASCE – Engineering Mechanics Division, Vol.93, EM6, 1969, p.103.

22. Drescher, H. and De Josselin De Jong, G., "Photoelastic Verification of a Mechanical Model of the Flow of a Granular Material", Journal of the Mechanics and Physics of Solids, Vol.20, 1972, p.337.

23. Drescher, A., "An Experimental Investigation of Flow Rules for Granular Materials Using Optically Sensitive Glass Particles", Geotechnique, Vol.26, 1976, p.591.

24. Drescher, A., Cousens, T.W. and Bransby, P.L., "Kinematics of the Mass Flow of Granular Material Through a Plane Hopper", Geotechnique, Vol.28, 1978, p.27.

25. Drucker, D.C. and Prager, W., "Soil Mechanics and Plastic Analysis of Limit Design", Quarterly of Applied Mathematics, Vol.10, 1952, p.157.

26. Drucker, D.C., Gibson, R.E. and Henkel, D.J., "Soil Mechanics and Work Hardening Theories of Plasticity", Transactions, ASCE, Vol.122, 1957, p.338.

27. Eckhoff, R.K. and Leversen, P.G., "A Further Contribution to the Evaluation of the Jenike Method for Design of Mass Flow Hoppers", Powder Technology, Vol. 10, 1974, p. 51.

28. Enstad, G., "On the Theory of Arching in Mass Flow Hoppers", Chemical Engineering Science, Vol. 30, 1975, p. 1273.

29. Fowler, R.J. and Glastonbury, J.R., "The Flow of Granular Solids Through Orifices", Chemical Engineering Science, Vol. 10, 1959, p. 150.

30. Fung, Y.C., A First Course in Continuum Mechanics, Prentice Hall, Inc., 1969.

31. Gardner, G.C., "The Region of Flow When Discharging Granular Materials from Bins", Chemical Engineering Science, Vol. 21, 1966, p. 261.

32. Goodman, M.A. and Cowin, S.C., "A Continuum Theory for Granular Materials", Arch. Ration. Mech. Anal., Vol. 44, 1972, p. 249.

33. Goodman, M.A. and Cowin, S.C., "Two Problems in the Gravity Flow of Granular Materials", Journal of Fluid Mechanics, Vol. 45, Part 2, 1971, p. 321.

34. Giunta, J.S., "The Study of Flow Patterns of Granular Solids in Flat-Bottom Bins with Circular Openings", MS Thesis, University of Pittsburgh, 1966.

35. Hancock, A.W. and Nedderman, R., "Prediction of Stresses on Vertical Bunker Walls", Transaction of the Institution of Chemical Engineers, Vol. 52, 1974, p. 170.

36. Horne, R.M. and Nedderman, R., "Analysis of the Stress Distribution in Two-Dimensional Bins by the Method of Characteristics", Powder Technology, Vol. 14, 1976, p. 93.

37. Horne, R.M. and Nedderman, R., "An Analysis of Switch Stresses in 2-D Bunkers", Powder Technology, Vol. 19, 1978, p. 235.

38. Horne, R.M. and Nedderman, R., "Stress Distribution in Hoppers", Powder Technology, Vol. 19, 1978, p. 243.

39. Jenike, A.W. and Shield, R.T., "On the Plastic Flow of Coulomb Solids Beyond Original Failure", ASME Journal of Applied Mechanics, Vol. 26, 1959, p. 599.

40. Jenike, A.W., "Steady Gravity Flow of Frictional-Cohesive Solids in Converging Channels", ASME Journal of Applied Mechanics, Vol. 31, 1964, p. 5.

41. Jenike, A.W., Elsey, P.W., Woolley, R.H., "Flow Properties of Bulk Solids", Proceedings ASTM, Vol.60, 1960, p.1168.

42. Jenike, A.W., "Storage and Flow of Solids", Bulletin No.123, Utah Engineering Experiment Station, University of Utah, 1964.

43. Jenike, A.W., "Gravity Flow of Frictional Cohesive Solids – Convergence to Radial Stress Field", ASME Journal of Applied Mechanics, Vol.32, 1965, p.205.

44. Jenike, A.W., and Johanson, J.R., "Bin Loads", Proceedings ASCE – Structural Division, Vol.94, 1968, p.1011.

45. Jenike, A.W. and Johanson, J.R., "On the Theory of Bin Loads", ASME Journal of Engineering for Industry, Vol.95, 1973, p.1.

46. Jenike, A.W., Johanson, J.R. and Carson, J.W., "Bin Loads – Part 2: Concepts", ASME Journal of Engineering for Industry, Vol.95, 1973, p.1

47. Jenike, A.W., Johanson, J.R. and Carson, J.W., "Bin Loads – Part 3: Mass Flow Bins", ASME Journal of Engineering for Industry, Vol.95, 1973, p.6.

48. Jenike, A.W., Johanson, J.R. and Carson, J.W., "Bin Loads – Part 4: Funnel Flow Bins", ASME Journal of Engineering for Industry, Vol.95, 1973, p.13.

49. Jenkins, J.T., "Static Equilibrium of Granular Materials", ASME Journal of Applied Mechanics, Vol.42, 1975, p.603.

50. Jenkins, J.T. and Cowin, S.C., "Theories for Flowing Granular Materials", Mechanics Applied to the Transport of Bulk Materials, American Society of Mechanical Engineers, AMD, Vol.31, 1979, p.79.

51. Johanson, J.R., "Stress and Velocity Field in the Gravity Flow of Bulk Solids", ASME Journal of Applied Mechanics, Vol.31, 1964, p.499.

52. Johanson, J.R. and Colijin, H., "New Design Criteria for Hoppers and Bins", Iron and Steel Engineer, October 1964, p.85.

53. Johanson, J.R., "Method of Calculating the Rate of Discharge from Hoppers and Bins", Transaction SME, Vol.232, 1965, p.69.

54. Lakshman Rao, V. and Venkateswarlu, D., "Internal Pressure in Flowing Granular Materials from Mass Flow Hoppers", Powder Technology, Vol.11, 1975, p.133.

55. Lee, J., Cowin, S.C. and Templeton III, J.S., "An Experimental Study of the Kinematics of Flow Through Hoppers", Transaction of the Society of Rheology, Vol.18, 1974, p.247.

56. Levinson, M., Shmutter, B. and Resnick, W., "Displacement and Velocity Field in Hoppers", Powder Technology, Vol. 16, 1977, p. 29.

57. McCabe, R.P., "Flow Pattern in Granular Material in Circular Silos", Geotechnique Vol. 24, 1974, p. 45.

58. McDougall, I.R. and Knowles, G.H., "Flow of Particles Through Orifices", Transaction of the Institution of Chemical Engineers, Vol. 47, 1969, p. T73.

59. Mandel, J., "Sur les Equations D'écoulement des Sols Idéaux en Déformation Plane et le Concept du Double Glissement", Journal of the Mechanics and Physics of Solids, Vol. 14, 1966, p. 303.

60. Mandl, G. and Fernandez Luque, R., "Fully Developed Plastic Shear Flow of Granular Materials", Geotechnique, Vol. 20, 1970, p. 277.

61. Mehrabadi, M.M. and Cowin, S.C., "Initial Planar Deformation of Dilatant Granular Materials", Journal of the Mechanics and Physics of Solids, Vol. 26, 1978, p. 269.

62. Morrison, H.L. and Richmond, O., "Application of Spencer's Ideal Soil Model to Granular Materials Flow", ASME Journal of Applied Mechanics, Vol. 43, 1976, p. 49.

63. Morrison, H.L., "A One-Dimensional Analysis of Granular Flow in Bunkers", Chemical Engineering Science, Vol. 33, 1978, p. 241.

64. Novosad, J. and Surapati, K., "Flow of Granular Materials: Determination and Interpretation of Flow Patterns", Powder Technology, Vol. 2, 1968-1969, p. 82.

65. O'Callaghan, J.R., "Internal Flow in Moving Beds of Granular Materials", Journal Agr. Engng. Res., Vol. 5, 1960, p. 200.

66. Pariseau, W.G., "Gravity Flow of Ideal Plastic Materials Through Slots", ASME Journal of Engineering for Industry, Vol. 91, 1969 p. 414.

67. Pariseau, W.G., "Discontinuous Velocity Fields in Gravity Flow of Granular Materials Through Slots", Powder Technology, Vol. 3, 1970, p. 218.

68. Passman, S.L., "Mixtures of Granular Materials", International Journal of Engineering Science, Vol. 15, 1977, p. 117.

69. Passman, S.L. and Thomas, Jr., J.P., "On the Linear Theory of Flow of Granular Media", Developments in Theoretical and Applied Mechanics, Proceedings of the 9th SECTAM, 1978.

70. Pemberton, C.S., "Flow of Imponderable Granular Materials in Wedge Shape Channels", Journal of the Mechanics and Physics of Solids, Vol. 13, 1965, p. 351.

71. Pearce, J.C., "Mechanics of Flowing Granular Media", Ph.D. Thesis, California Institute of Technology, 1976.

72. Perry, M.G., Rothwell, E. and Woodfin, W.T., "Model Studies of Mass Flow Bunkers: II Velocity Distribution in the Discharge of Solids from Mass Flow Bunkers", Powder Technology, Vol. 14, 1976, p. 81.

73. Perry, M.G., "Pressure in Flowing and Static Sand in Model Bunkers", Powder Technology, Vol. 4, 1970, p. 89.

74. Roberts, A.W., "The Dynamics of Granular Materials Flow Through Curved Chutes", Mechanical and Chemical Engineering Transaction, Nov. 1967, p. 216.

75. Roberts, A.W., "An Investigation of the Gravity Flow of Non-Cohesive Granular Materials Through Discharge Chute", ASME Journal of Engineering for Industry, Vol. 91, 1969, p. 373.

76. Roberts, A.W. and Montagner, G.J., "Flow in a Hopper Discharge Chute System", Chemical Engineering Progress, Vol. 71, 1975, p. 71.

77. Roberts, A.W., "Optimum Chute Profile in Gravity Flow of Granular Materials: A Discrete Segment Solution Method", ASME Journal of Engineering for Industry, Vol. 97, 1975, p. 10.

78. Roscoe, K.H., "The Influence of Strain in Soil Mechanics", Geotechnique, Vol. 20, 1970, p. 129.

79. Rose, H.E. and Tanaka, T., "Rate of Discharge of Granular Materials from Bins and Hoppers", Engineer, London, Vol. 208, 1959, p. 465.

80. Rowe, P.W., "The Stress-Dilatancy Relation for Static Equilibrium of an Assembly of Particles in Contact", Proceedings of the Royal Society, Series A, Vol. 269, 1962, p. 500.

81. Savage, S.B., "The Mass Flow Rate of Granular Materials Derived from Coupled Velocity-Stress Field", British Journal of Applied Physics, Vol. 16, 1965, p. 1885.

82. Savage, S.B., "Gravity Flow of Cohesionless Bulk Solids in a Converging Conical Channel", International Journal of Mechanical Sciences, Vol. 9, 1967, p. 651.

83. Savage, S.B. and Yong, R.N., "Stress Developed by Cohesionless Granular Media in Bins", International Journal of Mechanical Sciences, Vol. 12, 1970, p. 675.

84. Savage, S.B., "Experiments on Shear Flow of Cohesionless Granular Materials", Proceedings of the U.S. Japan Seminar on Continuum Mechanical and Statistical Approaches in the Mechanics of Granular Media, Gakujutsu Bunken Fukyukai, Tokyo, Japan, 1978, p.241.

85. Savage, S.B., "Gravity Flow of Cohesionless Granular Materials in Chutes and Channels", Journal of Fluid Mechanics, Vol.92, Part I, 1979, p.53.

86. Savage, S.B. and Sayed, M., "Gravity Flow of Cohesionless Granular Materials in Wedge Shaped Hoppers", Mechanics Applied to the Transport of Bulk Materials, American Society of Mechanical Engineers, AMD, Vol.31, 1979, p.1.

87. Schofield, A. and Wroth, P., Critical State Soil Mechanics, McGraw Hill, London, 1968.

88. Scott, R.F., Principles of Soil Mechanics, McGraw Hill, 1963.

89. Shield, R.T., "Mixed Boundary Value Problems in Soil Mechanics", Quarterly of Applied Mathematics, Vol.11, 1953, p.61.

90. Shield, R.T., "Stress and Velocity Field in Soil Mechanics", Journal of Mathematics and Physics, Vol.33, 1954, p.144.

91. Shield, R.T., "On Coulomb's Law of Failure in Soils", Journal of the Mechanics and Physics of Solids, Vol.4, 1955, p.10.

92. Sokolovskii, V.V., Statics of Granular Media, Pergamon Press, London, 1965.

93. Spencer, A.J.M., "A Theory of the Kinematics of Ideal Soils Under Plane Strain Condition", Journal of the Mechanics and Physics of Solids, Vol.12, 1964, p.337.

94. Spencer, A.J.M and Kingston, M.R., "Plane Mechanics and Kinematics of Compressible Ideal Granular Materials", Rheologica Acta, Vol.12, 1973, p.194.

95. Spink, C.D. and Nedderman, R.M., "Gravity Discharge Rate of Fine Particles from Hoppers", Powder Technology, Vol.21, 1978, p.245.

96. Sullivan, W.N., "Heat Transfer to Flowing Granular Media", Ph.D. Thesis, California Institute of Technology, 1972.

97. Sundaram, V. and Cowin, S.C., "A Reassessment of Static Bin Pressure Experiments", Powder Technology, Vol.22, 1979, p.23.

98. Takagi, S., "Plane Plastic Deformation of Soils", Proceedings ASCE, Applied Mechanics Division, Vol.88, EM3, 1962, p.107.

99. Takahasi, K., "On the Dynamical Properties of Granular Mass", Geophysical Magazine, Vol. 11, 1937, p. 165.

100. Templeton, III J.S., "An Experimental Study of the Mechanics of Rupture Zones in the Gravity Flow of Granular Materials", The Effects of Void on Materials Deformation, American Society of Mechanical Engineers, AMD, Vol. 16, 1976.

101. Theimer, O.F., "Failures of Reinforced Concrete Grain Silos", ASME, Journal of Engineering for Industry, Vol. 91, 1969, p. 460.

102. Toyama, S., "The Flow of Granular Materials in Moving Beds", Powder Technology, Vol. 4, 1970-1971, p. 214.

103. Van Zanten, D. C. and Mooiji, A., "Bunker Design – Part 2: Wall Pressure in Mass Flow", ASME Journal of Engineering for Industry, Vol. 99, 1977, p. 815.

104. Van Zanten, D. C., Richards, P. C. and Mooiji, A., "Bunker Design– Part 3: Wall Pressures and Flow Patterns in Funnel Flow", ASME Journal of Engineering for Industry, Vol. 99, 1977, p. 819.

105. Walker, D.M., "An Approximate Theory for Pressure and Arching in Hoppers", Chemical Engineering Science, Vol. 21, 1966, p. 975.

106. Walker, D.M. and Blanchard, M.H., "Pressures in Experimental Coal Hoppers", Chemical Engineering Science, Vol. 22, 1967, p. 1713.

107. Walker, D.M., "A Basis for Bunker Design", Powder Technology, Vol. 1, 1967, p. 228.

108. Walters, J.K., "A Theoretical Analysis of Stresses in Silos with Vertical Walls", Chemical Engineering Science, Vol. 28, 1973, p. 13.

109. Walters, J.K., "A Theoretical Analysis of Stresses in Axially Symmetric Hoppers and Bunkers", Chemical Engineering Science Vol. 28, 1973, p. 779.

110. Wieghardt, K., "Experiments in Granular Flow", Annual Review of Fluid Mechanics, Vol. 7, 1975, p. 89.

111. Williams, J. C., "The Rate of Discharge of Coarse Granular Materials from Conical Mass Flow Hoppers", Chemical Engineering Science, Vol. 32, 1977, p. 247.

112. Wolf, E.H. and Hohenleiten, H. L., "Experimental Study of the Flow of Coal in Chutes at Riverside Generating Station", Transaction ASME, Vol. 67, 1945, p. 585.

113. Wolf, E.H. and Hohenleiten, H. L., "Flow of Coal in Hoppers", Mechanical Engineering, Vol. 70, April 1968, p. 313.

114. Wright, H., "An Evaluation of the Jenike Bunker Design Method", ASME, Journal of Engineering for Industry, Vol. 95, 1973, p. 48.

APPENDIX A

PHOTOGRAPHIC RECORDING OF THE THREE TYPES OF FLOW

The three types of flow are recorded photographically as shown in Fig. A. 1. Type A flow (Fig. A. 1a) is the mass flow regime. Types B and C flows (Fig. A. 1b, A. 1c) are the funnel flow regimes. They are classified according to the presence of stagnant material in the flow field. Figure A. 1d shows the type C2 flow where the merge point S is at some distance from the edge of the discharge opening.

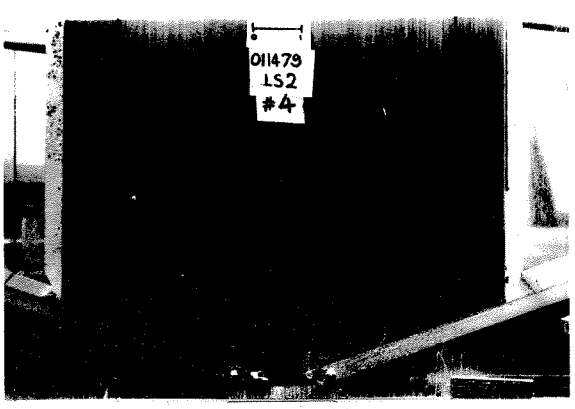

a

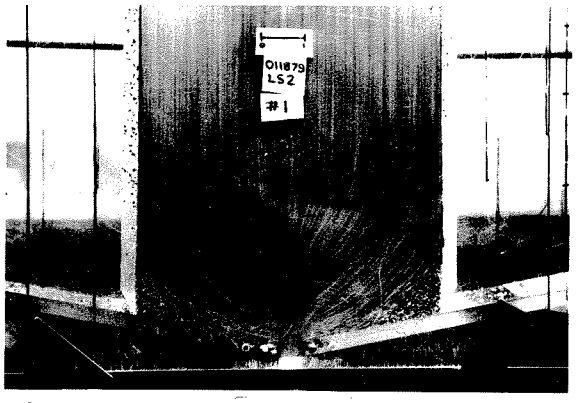

b

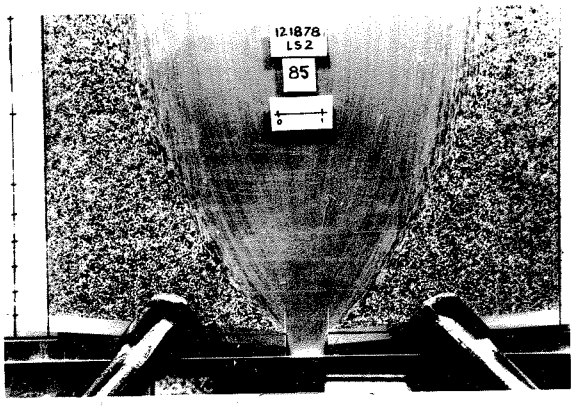

c

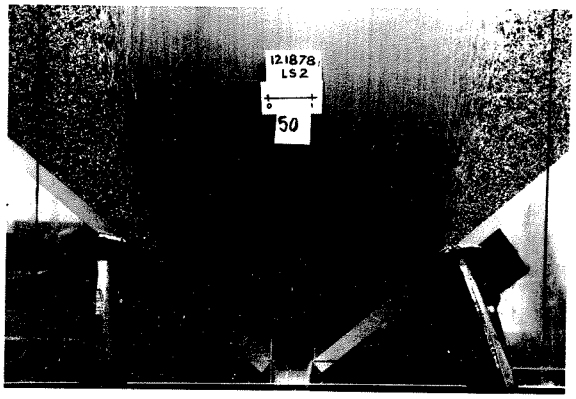

d

Figure A.1. Photographic examples of the flow patterns for the sand ($\varphi = 31^\circ$). The thickness, b, is 15.2 cm in all cases. The following are the values of θ_w, H, W, D (in cm): (a) 70°, 36.8, 22.9, 1.9 (b) 80°, 58.4, 17.8, 1.37 (c) 70°, 35.6, 30.5, 2.54 (d) 50°, 35.6, 30.5, 2.54.